

The Levantine Basin – a seismic investigation of the crustal structure and the evolution of the Messinian evaporites

Dissertation

zur Erlangung des Doktorgrades der Naturwissenschaften
im Department für Geowissenschaften der Universität Hamburg

vorgelegt von

Gesa Luise Netzeband

aus

Hamburg

Hamburg
2006

Als Dissertation angenommen vom Department für Geowissenschaften der
Universität Hamburg

Auf Grund der Gutachten von Prof. Dirk Gajewski
und Dr. Christian Hübscher

Hamburg, den 18. 4. 2006

Prof. Dr. Kay-Christian Emeis
Leiter des Departments für Geowissenschaften

A big thankyou to

Prof. Dirk Gajewski for the opportunity to write this thesis, for valuable suggestions and thought-provoking impulses.

Dr. Christian Hübscher, my supervisor, for the exciting project and for many fruitful discussions and great ideas. Special thanks for setting ambitious aims and for the full support at any time.

Dr. Karsten Gohl for introducing me to the world of refraction seismics and forward modelling and for an Antarctic Cruise packed with superlatives. Best ever...

Dr. Ekkehart Tessmer for the always reliable administration of the computer network.

Dr. Ali Dehghani, the center of gravity, for always providing the right tool and for many fabulous cruises together.

Dr. Jan Grobys (do you feel the pressure?), my scientific twin. Thank you for conquering the same fields with me.

Dr. Martin Bak Hansen for sharing office, schedule and coffee. We fought the same demons. Thanks for keeping me focussed.

Dr. Tina Kaschwich, Lady of Theory. Thanks for filtering the noise from daily life and for smoothing rough edges.

Dipl. Inf. Malte Vöge for assisting with modern data media (e.g. lending me your USB-stick) and for being good company across the corridor.

Dr. Daniela Kühn for being an infinite source of information.

Dipl. Geophys. „STIDO" Stefan Dümmling and Dr. Micky Yoon, heirs of my office, for coffee and football chats and for general encouragement.

Christel Mynarik, the soul of the institute.

the members of the IfG for scientific support and for the social activities e.g. our successful participation in the GeoKick Tournament. Olé, Olé, Olé!

my parents for everlasting support and love.

Jan, my beloved spouse, for constantly asking inconvenient questions and for proofreading the manuscript. But above all, my sincere thanks for your support, your unshakable confidence in me and your patience.

the DFG for supporting my project

the crews and scientists of Meteor 52/2 and Pelagia 228 - you did an excellent job!

Contents

| | | |
|----------|---|-----------|
| 1 | Introduction..... | 1 |
| 1.1 | Motivation..... | 1 |
| 1.2 | Present knowledge..... | 3 |
| 1.3 | Objective..... | 6 |
| 2 | Conceptual basics..... | 9 |
| 2.1 | Crust - structure and composition..... | 9 |
| 2.1.1 | General remarks on continental and oceanic crust..... | 10 |
| 2.1.2 | The evolution of ocean basins..... | 11 |
| 2.2 | Evaporites..... | 12 |
| 2.2.1 | Chemical composition and formation..... | 12 |
| 2.2.2 | Physical Properties..... | 13 |
| 2.2.3 | Thin-skinned tectonics or halotectonics..... | 14 |
| 3 | Data..... | 17 |
| 3.1 | Reflection seismics..... | 18 |
| 3.2 | Refraction seismics..... | 20 |
| 4 | The Levantine Basin - Crustal Structure and Origin..... | 25 |
| | Abstract..... | 25 |
| 4.1 | Introduction..... | 25 |
| 4.2 | Geological and geophysical setting..... | 27 |
| 4.3 | Previous work..... | 27 |
| 4.4 | New geophysical data..... | 30 |
| 4.4.1 | Seismic refraction data - acquisition..... | 30 |
| 4.4.2 | Seismic refraction data - processing and characteristics..... | 30 |
| 4.4.3 | Seismic reflection data - acquisition..... | 34 |
| 4.4.4 | Seismic reflection data - processing and characteristics..... | 34 |
| 4.4.5 | Gravity data..... | 36 |
| 4.5 | Modelling of refraction data..... | 36 |
| 4.5.1 | Resolution and uncertainty of the modelled velocity structure..... | 38 |
| 4.6 | Results..... | 41 |
| 4.6.1 | Profile 1..... | 41 |
| 4.6.2 | Profile 2..... | 42 |
| 4.6.3 | Gravity models..... | 43 |
| 4.7 | Discussion..... | 46 |
| 4.7.1 | Velocity distribution and crustal structure..... | 46 |
| 4.7.2 | β -factor..... | 51 |
| 4.7.3 | Implications..... | 51 |
| 4.8 | Conclusions..... | 53 |
| | Acknowledgements..... | 54 |
| 5 | The structural evolution of the Messinian Evaporites in the Levantine Basin..... | 55 |
| | Abstract..... | 55 |
| 5.1 | Introduction..... | 56 |
| 5.2 | Regional setting..... | 57 |
| 5.3 | Materials and methods..... | 61 |
| 5.4 | Results..... | 62 |
| 5.4.1 | Post-Messinian subsidence..... | 63 |
| 5.4.2 | Internal reflections..... | 63 |
| 5.4.3 | Marginal structures..... | 71 |
| 5.4.4 | Israeli Slump Complex..... | 75 |

| | | |
|----------|--|-----------|
| 5.4.5 | Mud Volcano | 76 |
| 5.4.6 | The basin | 78 |
| 5.5 | Discussion | 80 |
| 5.5.1 | Origin of the internal reflections | 80 |
| 5.5.2 | Syn-depositional evaporite deformation | 81 |
| 5.5.3 | Post-Messinian Deformation | 83 |
| 5.6 | Conclusions | 88 |
| | Acknowledgements | 90 |
| 6 | Conclusions..... | 91 |

1 Introduction

1.1 Motivation

The Levantine Basin is located in the southeastern Mediterranean Sea (Fig. 1.1). In this area the African, the Arabian, the Anatolian, and the Eurasian plates interact, forming a complex tectonic environment. The Levantine Basin and its margin are key areas for the understanding of the geodynamic evolution of the Eastern Mediterranean. From Early Triassic on, the Tethys was the major ocean of the world. The present Levantine margin was a Tethys margin of Pangea, although, naturally, they do not completely coincide (Fig. 1.2). Many plate tectonic reconstructions of this area have been developed, e.g. Stampfli and Borel (2002), Garfunkel (1998, 2004), and Robertson (1998). However, major geologic issues related to the Mesozoic and Cenozoic history of the area are still unsolved and the different models of the opening and closing of the Neo-Tethys partly contradict each other (Walley 1998).

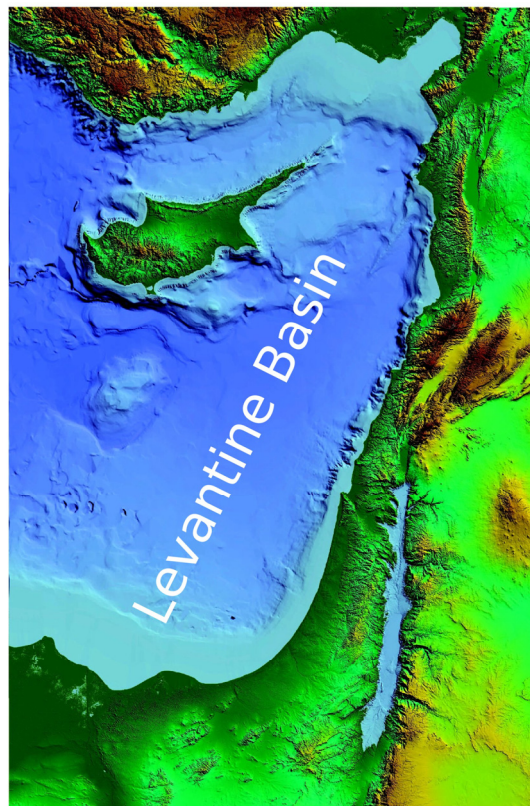


Figure 1.1 shaded relief bathymetry of the Eastern Mediterranean from the 50 m contours of Hall (1994) merged with the 3" Shuttle Radar Topographic mission (SRTM) land data. From Hall (2005).

While Robertson (1998) and Garfunkel (1998) date the initial rifting phase to the Permian, Ben-Avraham and Ginzburg (1990) and Hirsch (1984) postulate that the rifting set in during the Triassic. Ben-Avraham and Ginzburg (1990) and Garfunkel and Derin (1984) claim that the spreading axis was directed NE, whereas Garfunkel (1998) recognises a spreading axis in E - W direction. Robertson (1998) and Garfunkel and Derin (1984) agree that the spreading lasted from Late Triassic to Jurassic, while Hirsch (1984) postulates spreading was limited to the north of the Arabian plate, but there it continued until the Cretaceous.

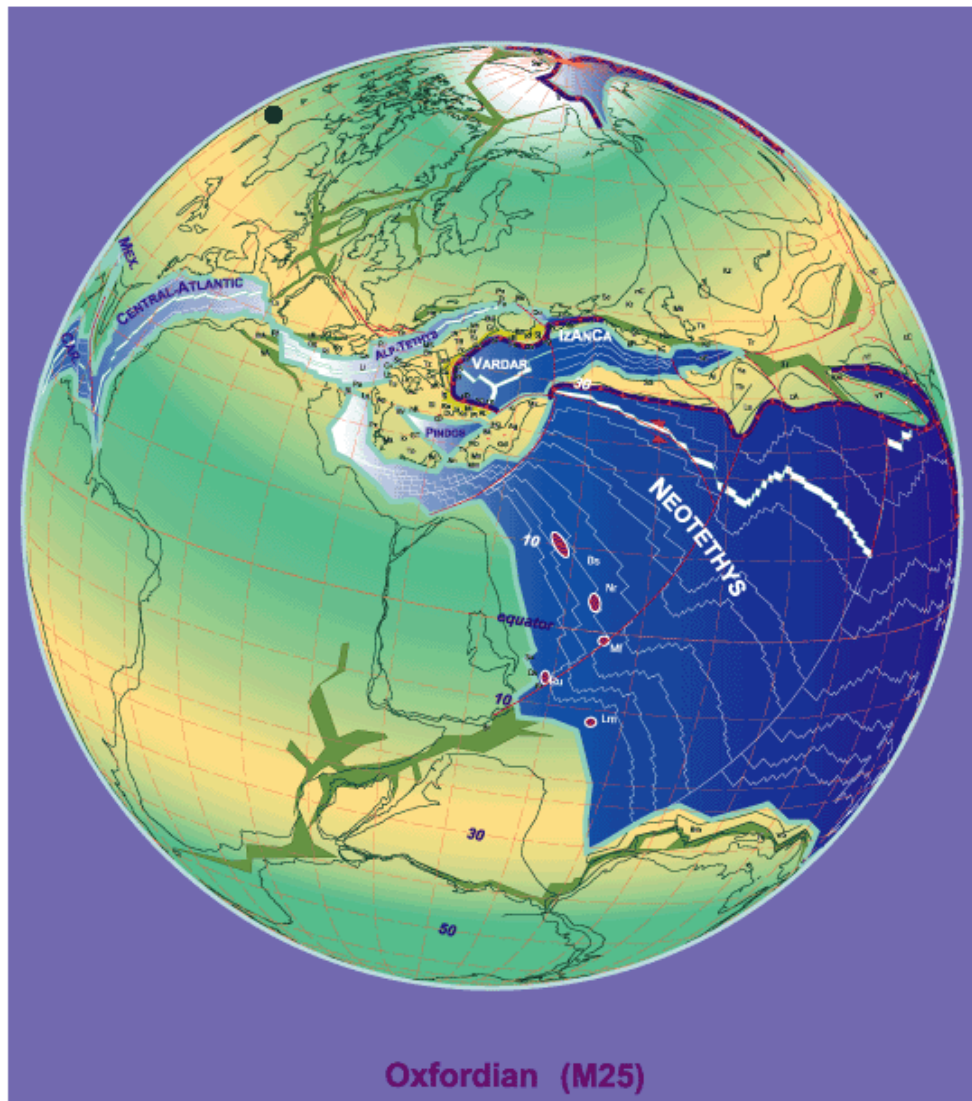


Figure 1.2 Paleo-reconstruction of the Tethys in the Triassic, after Stampfli and Borel (2002).

A central issue concerning the reconstruction of the Neo-Tethys is the nature and origin of the crust in the Levantine Basin. Was it rifted during the opening of the Tethys? Did seafloor spreading set in? Where would be the transition of continental to oceanic crust? Is there still oceanic crust in the basin or has it all been consumed by subduction at the Cyprus Arc? Recent publications state that the Cyprus Arc is in

transition from subduction to continent collision (e.g. Hall et al. 2005). This model contradicts most of the earlier publications which propose remnants of oceanic crust in the Levantine Basin. There are only few places in the world where a plate margin is in the process of changing from one kind of motion to another. The question of continental or oceanic crust in the Levantine Basin is therefore even more relevant. Geophysical investigations of this area have been hampered by the thick sediment cover on the basement in the basin (Fig. 1.3).

The younger history of the Levantine Basin was strongly influenced by the Messinian Salinity Crisis 5.9 - 5.3 Ma ago. 14 Ma ago the Mesozoic Neotethys lost its connection to the Indo-Pacific Ocean in Middle Miocene (Gvirtzman and Buchbinder, 1987). The water exchange was still ensured by the connection to the Atlantic Ocean. In Late Miocene (5.9 Ma ago) a combination of several circumstances such as tectonic uplift, sea level changes and climatic conditions caused a narrowing of the western connection to the Atlantic Ocean and initiated the Messinian Salinity Crisis (Hsü et al., 1973; 1978). The water shortage and the high evaporation rates in the Mediterranean climate resulted in a drop of the sea level. The subsequent rise in the salt concentration finally lead to precipitation. Up to 2 km of evaporites were deposited during that time. Whether there was a time when the Mediterranean Sea was completely dried up and the evaporites were subaerially exposed is not yet known. Druckman et al. (1995) show that the sea level in the Mediterranean had dropped about 800-1300 m. The huge masses of salt imply that the Mediterranean Sea cannot have been completely isolated from the Atlantic Ocean but that certain amounts of saltwater must have seeped continuously into the basin. The reflooding of the Mediterranean Sea by Atlantic waters must have been a rather sudden event that took place at about 5.3 Ma ago and lasted only for 1000-2000 years (Hsü et al., 1973).

The evaporites are buried by 0.5 km of sediments in the basin and 1 - 3 km on the shelf. Because of the young age of the evaporites and the tectonic inactivity of the area, only little tectonic overprint is expected on the Messinian evaporites. Therefore they are considered an excellent site to study early stages of salt tectonics.

1.2 Present knowledge

Previous studies in this area mostly focused on the Levantine margin and shelf areas (e.g. Almagor 1984, Druckman 1995, Ben-Gai et al. 2005). Until 2002, only two wide angle seismic experiments penetrating the crust with a total of three lines had been conducted in the basin in 1979 and 1989 (Makris 1983, Ben-Avraham 2002) (Fig. 1.4). Their results primarily show a continuous lower crustal layer and an upper crust, which pinches out offshore the Israeli margin. From these models they deduced that the pinchout represents the transition of continental to oceanic crust. Since their study consisted of comparatively few receivers and the models are rather simple, a new approach to analyse the crust in the Levantine Basin employing contemporary methods was necessary. Makris et al. (1983) and Ben-Avraham et al. (2002) constructed their

models from a very restricted amount of data with a large receiver spacing. Velocity gradients within the individual layers were not considered. Also, no assessment of uncertainties or resolution of the modelling results was given.

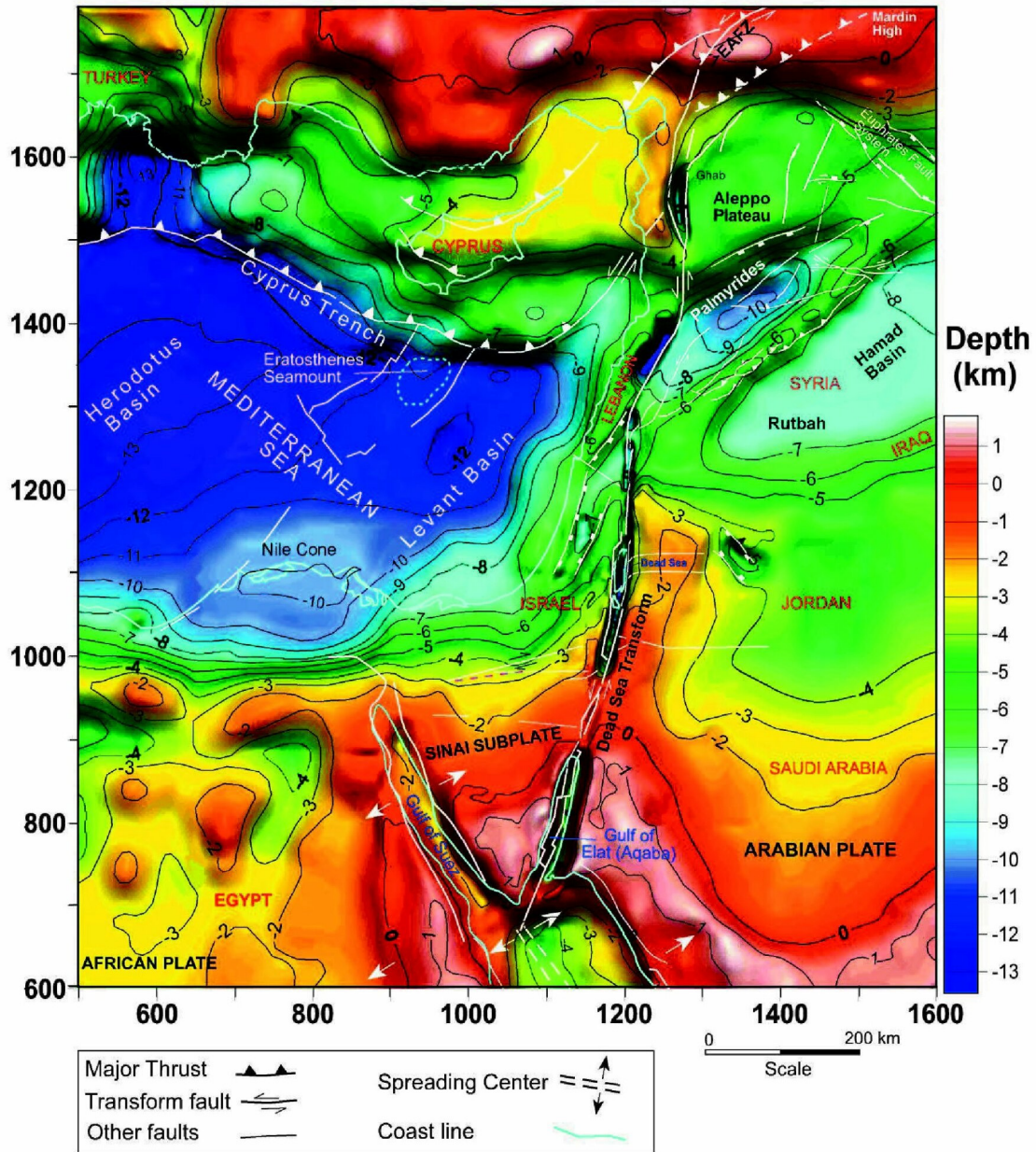


Figure 1.3 Top of basement map after Rybakov and Segev (2004)

In the 70s and 80s of the last century, the eastern Levantine Basin has been recognized as a world class site to investigate lateral salt tectonics, which includes significant lateral salt flow and complex deformation of the sedimentary overburden (e.g., Garfunkel et al., 1979; Almagor, 1984, Garfunkel, 1984; and others). The Messinian evaporites and their origin were the focus of two Deep Sea Drilling Project (DSDP) legs (Hsü et al., 1973, 1978) and numerous other studies (e.g. Cohen 1993,

Clauzon et al. 1996, Gradmann et al. 2005). A subdivision into upper and lower evaporites was observed especially in seismic data from the western Mediterranean Sea (Hsü et al., 1978), and presumably represents a massive layer of halite and another of carbonate and gypsum. This layering is generated by a certain precipitation sequence which results from changing sea water concentrations. Deposition of carbonates and sulfates, which present the minor part of the sea water mineral content, is succeeded by deposition of ductile halite and may re-occur when the concentrated sea water mixes with fresh sea water (Cohen, 1993). The development of such a tripartition of evaporites depends on several other factors (water depth, erosional conditions, water supply, etc.) and has been recorded from the western Mediterranean Sea (Réhault et al., 1984). Gradmann et al. (2005) have found that the basinal Messinian evaporites in the Levantine Basin consist of several seismically transparent units separated by continuous internal reflections. A distinction between an upper, brittle evaporite layer, and a lower, ductile layer was postulated.

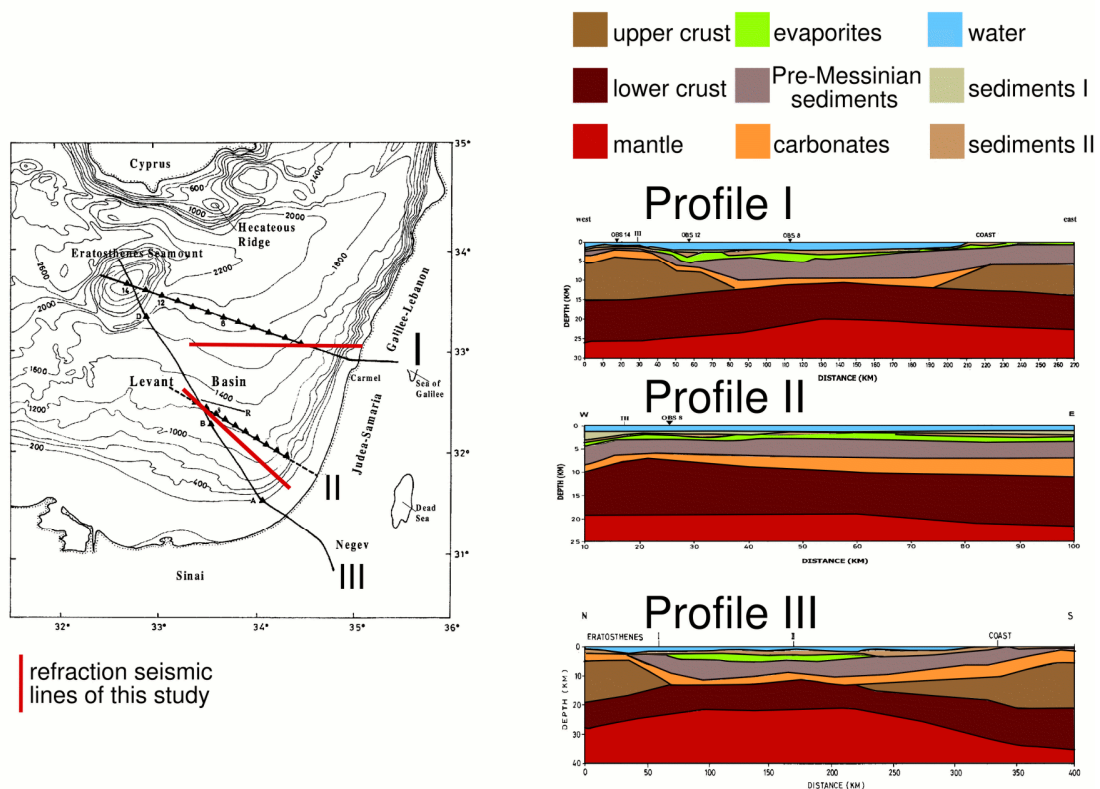


Figure 1.4 Compilation of velocity models of the Levantine Basin based on previous seismic studies in the area (Makris et al. 1983, Ben-Avraham et al. 2002).

Mud volcanoes, pockmarks and cold seeps have been observed in the Levantine Basin (Dimitrov and Woodside 2003, Loncke et al. 2004, Coleman and Ballard 2001). The understanding of the interaction of fluids and evaporites has been limited to locations where the evaporite layer has been significantly thinned or is entirely absent. However, salt is permeable for fluids if the fluid pressure is above the lithostatic

pressure (J. Urai, pers. comm.). Fluid migration through a solid sequence of Messinian evaporites has already been proposed by Gradmann et al. (2005).

1.3 Objective

The objective of this thesis is the thorough understanding of the formation processes in the Levantine Basin. The question about the nature and origin of the crust is closely related to the question of active subduction at the Cyprus Arc, which is a key factor in the analysis of the present plate tectonic regime. For the analysis of the crustal structure two refraction seismic lines were used. The data quality was significantly better than in previous studies and the receiver spacing was much smaller. Modern modelling techniques have been applied including forward and inverse modelling, which allowed the consideration of velocity gradients within the model. An assessment of uncertainties of the traveltimes picks and a discussion of the resolution of the modelling results provide an evaluation of the reliability of the model.

The multichannel reflection seismic lines cover the centre of the basin in E – W, SE – NW and S – N direction, which allows an assessment of the orientation of salt movements in the basin, in addition to the analysis of the processes on the slope. The sound data quality provides a high resolution of Plio-Quaternary structures and the evaporite layer, and the good image of the base of the evaporite layer enables a clear distinction between salt tectonic and plate tectonic processes. My analysis of these data reveals that the deformation within the Messinian evaporites and the Plio-Quaternary overburden is influenced by salt tectonic as well as plate tectonic processes. Based on a complete investigation of the Levantine Basin from the crust to the uppermost sediments, further constraints on the geodynamic setting are found, the superposition of salt and plate tectonics will be analysed, and the understanding of deposition and deformation of evaporite layers in general can be improved.

This work is structured as follows:

In this chapter a general introduction to the survey area and its special characteristics are given. The motivation of this work and the present state of knowledge are outlined.

In chapter 2 conceptual basics of the earth's crust and of evaporites are described. The fundamental differences between oceanic and continental crust are presented, and the evolution process of oceanic crust is resumed. The chemical composition and the physical properties of evaporites, especially halite, are specified and the principles of modern salt tectonics are summarized.

In chapter 3 the data base of this study is outlined. The properties of the multichannel reflection seismic data are described and an example of the data processing is shown. An example of the refraction seismic data is also given, along with screenshots of the software used for picking and modelling.

Chapter 4 and 5 consist of original articles which have been submitted to scientific journals:

Chapter 4, 'The Levantine Basin - Crustal Structure and Origin' (G. L. Netzeband, K. Gohl, C. P. Hübscher, Z. Ben-Avraham, G. A. Dehghani, D. Gajewski, P. Liersch, accepted by *Tectonophysics*, January 2006) deals with the question of continental or oceanic crust in the Levantine Basin. It contains details of the processing and modelling of the refractions seismic data and the gravity modelling, and presents the interpretation of the results in the geodynamic context of the evolution of the Neo-Tethys and the Mediterranean.

Chapter 5, 'The structural evolution of the Messinian Evaporites in the Levantine Basin' (G. L. Netzeband, C. P. Hübscher, D. Gajewski, submitted to *Marine Geology*, December 2005) deals with the interpretation of the multichannel reflection seismic lines. New insights into the deposition of the evaporites have been gained. The impact of the changes in the geodynamic setting in the past 5 Ma on the evaporite layer and the sediment overburden are analysed. Evidence of active plate tectonics has been found, and a mud volcano in an unusual setting, above a thick evaporite layer, has been observed.

Chapter 6 presents the conclusions gained from my thesis and their implications for the understanding of the geodynamic evolution in the eastern Mediterranean Sea, for the salt tectonics in this area and for evaporite deposition and deformation in general.

2 Conceptual basics

This chapter describes the principle basics of the earth's crust and of evaporites.

2.1 Crust - structure and composition

The earth's crust is the outermost solid layer, separated from the mantle by the Mohorovičić discontinuity (Moho). The Moho is defined by a rapid increase in p-wave velocity from about 6.9 - 7.3 km/s in the lower crust to 7.9 - 8.2 km/s in the upper mantle (Berckhemer 1990).

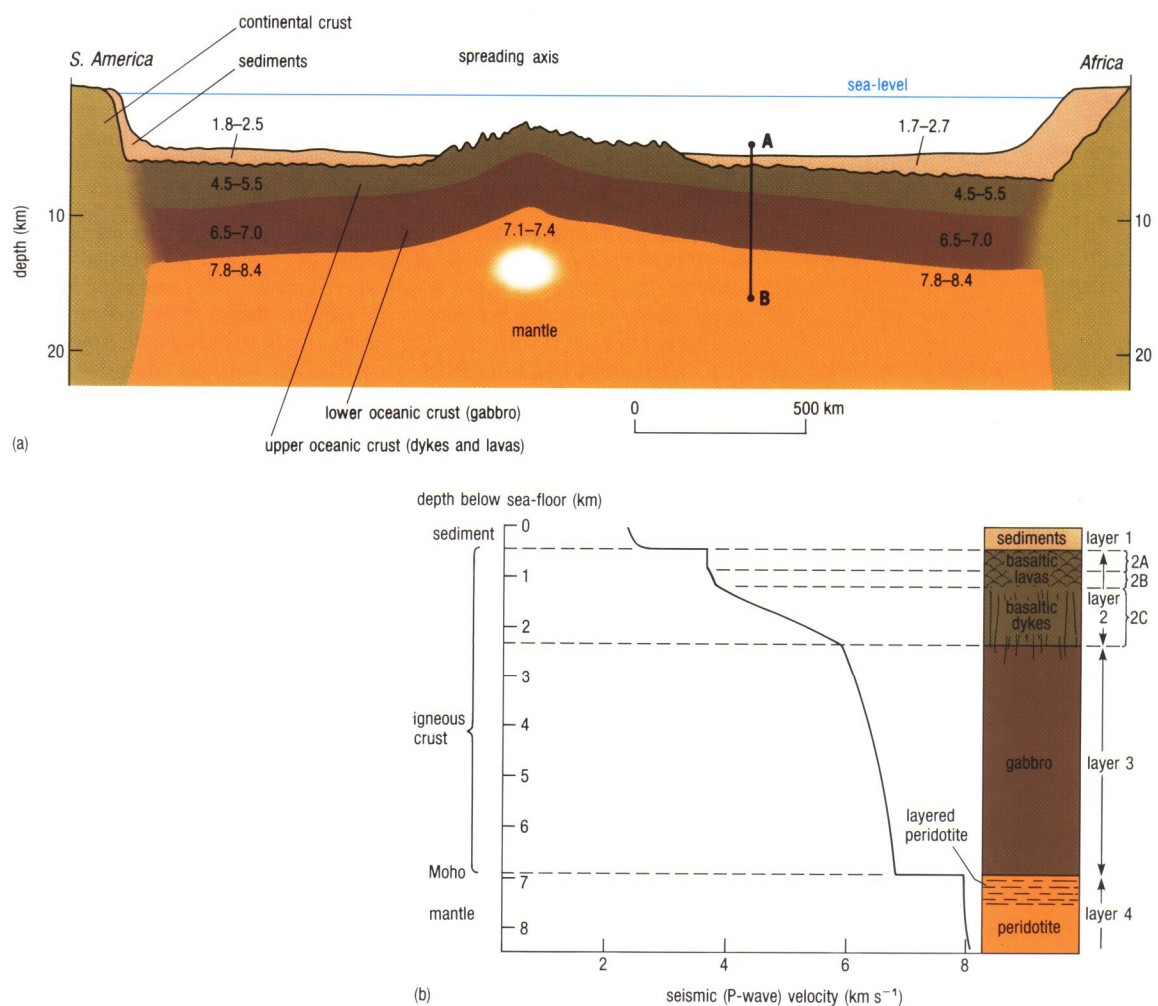


Figure 2.1 Schematic image of a typical oceanic crust. From Wright and Rothery (2001).

2.1.1 General remarks on continental and oceanic crust

Oceanic crust is generally composed of a gabbro layer with a p-wave velocity of 6.7 - 7.1 km/s, covered by basaltic sheeted dyke complexes and pillow lavas with approx. 4.5 - 5.5 km/s (Berckhemer 1990). Both layers are usually characterised by a large velocity gradient (Wright and Rothery 2001). The total thickness of normal oceanic crust is usually between 6 and 7 km (Fig. 2.1).

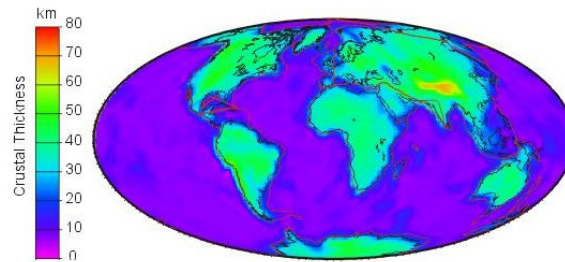


Figure 2.2 Global map of crustal thickness (after Cadek and Martinec 1991).

Continental crust is much more various. On average, it is composed of two or three layers with a p-wave velocity of 6.5 - 6.9 km/s. The middle crust and upper crust can be more variable or even entirely absent. Velocities of the middle crust vary between 5.8 km/s and 6.5 km/s, velocities of the upper crust can range between 5.1 and 6.4 km/s. Berckhemer (1990) gives average values for the upper and lower crust as 5.8 - 6.2 km/s and 6.6 - 7.0 km/s. The Moho depth of continental crust can be as much as 70 km under a young mountain range such as the Himalaya, but is generally between 30 and 40 km (Fig. 2.2).

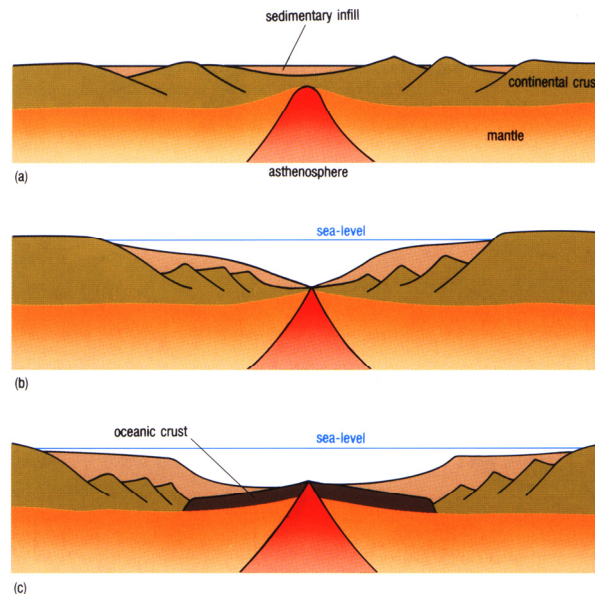


Figure 2.3 Schematic drawing of a rifting process. From Rothery and Wright (2001).

2.1.2 The evolution of ocean basins

Ocean basins grow from an initial rift, which develops along the line of continental separation. During crustal extension, the ductile lower part of the crust is stretched, but the brittle upper part is rifted (Fig. 2.3).

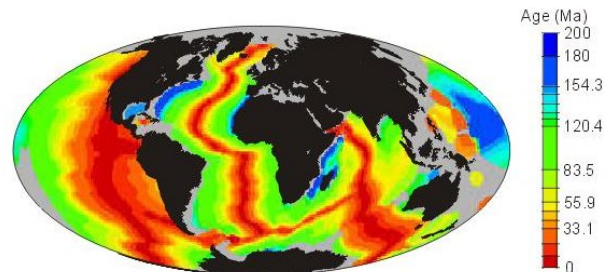


Figure 2.4 Global map of crustal age. After Müller et al. (1997):

Blocks of crust slide down fault planes, and sediments accumulate in the lakes and valleys which occupy the resulting depressions. When separation occurs, basaltic magma rises to fill the gap between the two continental blocks and a new spreading axis is formed. At this spreading axis, new oceanic crust is generated. With spreading rates of 1 - 20 cm/year, a total volume of 16 - 26 km³ of oceanic crust is produced per year at oceanic ridge systems. As the oceanic crust is both thinner and denser than the continental crust, it lies below sea level. Depending on the spreading rate, the age of the oceanic crust increases with distance from the spreading axis (Fig. 2.4). The oldest oceanic crust found in any major ocean is about 180 Ma.

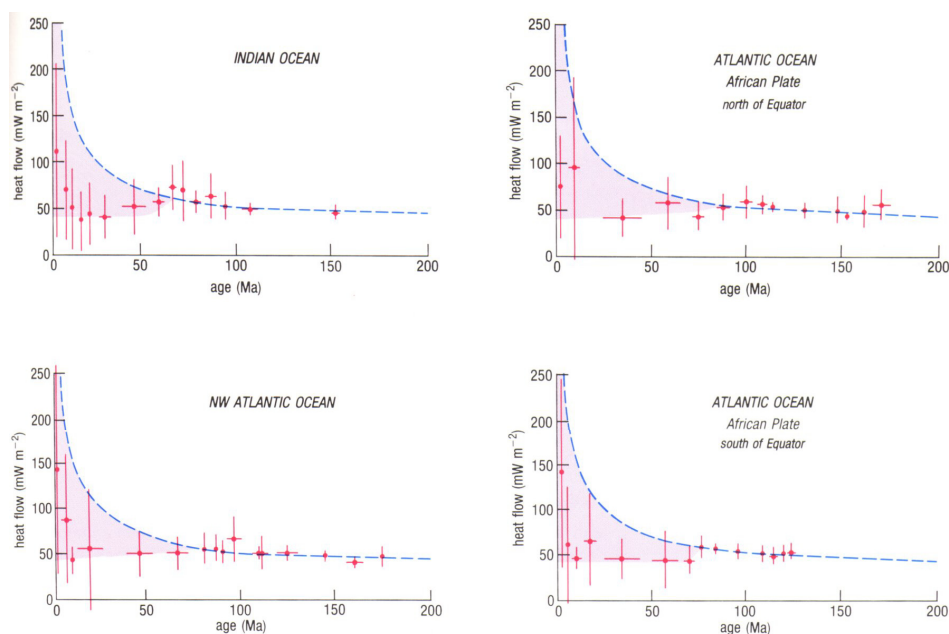


Figure 2.5 Theoretical curves (dashed blue lines) of heat flow in crust of different age and observed heat flow values (red dots with error bars). From Rothery and Wright (2001).

Along spreading axes, temperatures and heat flow values are higher than in any terrestrial hydrothermal system. According to Pollack et al. (1993), the average heat flow value of oceanic crust formed in the Quaternary is 140 mW/m^2 . With passing time, the heat flow decreases exponentially down to 51 W/m^2 for oceanic crust of Late Jurassic age (Fig. 2.5). In comparison, the average heat flow value of continental crust given by Sclater et al. (1980) is 57 W/m^2 .

2.2 Evaporites

Marine evaporites are of great importance in geology and the oil industry, and play an important role in the study of the Levantine Basin.

2.2.1 Chemical composition and formation

Evaporites are defined as rocks that were originally precipitated from a saturated surface or near surface brine by solar evaporation (Warren 1999). Among the wide range of chemically precipitated salts the following are of special geological interest: halite (NaCl), gypsum ($\text{CaSO}_4 \cdot 2\text{H}_2\text{O}$) and anhydrite (CaSO_4).

During the process of evaporation, crystals form at the air-brine interface, grow until they are too heavy to be supported by surface tension and then sink. Two types of brines are produced by evaporation of seawater, NaCl and MgCl-SO_4 brines. Up to a salinity of 330 ‰ (fraction in volume) the NaCl brines dominate, at higher salinities MgCl-SO_4 brines prevail, because the Na^+ ions are already precipitated. Thus, the prevailing cation changes from Na^+ to Mg^{2+} while the dominant anion is always Cl^- .

Beds of evaporites are usually decimetres to meters thick. They quickly accumulate and form units of hundreds of meters in relatively short time. The halite body in the Afar Deep, in Ethiopia, for example is up to 1 km thick and was deposited in less than 10.000 years. No other type of sediment, carbonate of silicoclastics can accumulate as rapidly as an evaporite salt bed (Warren, 1999).

Evaporites can be deposited in marine, non-marine or hybrid conditions. In the case of the Messinian evaporites in the Levantine Basin the prevailing conditions were marine. Normal seawater is dominated by Na^+ and Cl^- ions with lesser amounts of SO_4^{2-} , Mg^{2+} , Ca^{2+} , K^+ , CO_3^{2-} , HCO_3^- . It has a density of 1.03 g/cm^3 and a salinity of $35 \pm 2 \text{ ‰}$. According to Einsele (2000), in a closed sea-water basin, the first minerals which precipitate from the solution when the salinity increases to 40 - 60 ‰ and the density rises to 1.10 g/cm^3 are alkaline earth carbonates such as CaCO_3 (aragonite). These conditions are called mesohaline. With a further increase in salinity to 130 - 160 ‰ and in density to 1.13 g/cm^3 , the penesaline stage, gypsum ($\text{CaSO}_4 \cdot 2\text{H}_2\text{O}$) and anhydrite (CaSO_4) precipitate. For the precipitation of halite (NaCl) a salinity of 340 - 360 ‰ with a density of 1.22 g/cm^3 is required, and finally, when the density reaches

1.3 g/cm³, potassium and magnesium salts precipitate. This stage is called supersaline, by then the viscosity of the brine is that of liquid honey. The supersaline stage is rarely reached, because of the influence of humid air layers providing some sort of fresh water supply. In this marine, closed sea-water basin, the deposition pattern of the evaporites forms a so-called 'bull's eye', i.e. the poorly soluble evaporites, carbonates and calcium sulphates (gypsum and anhydrite), occupy the margin, while the most soluble evaporites are found in the centre of the basin (Einsele 2000) (Fig. 2.6).

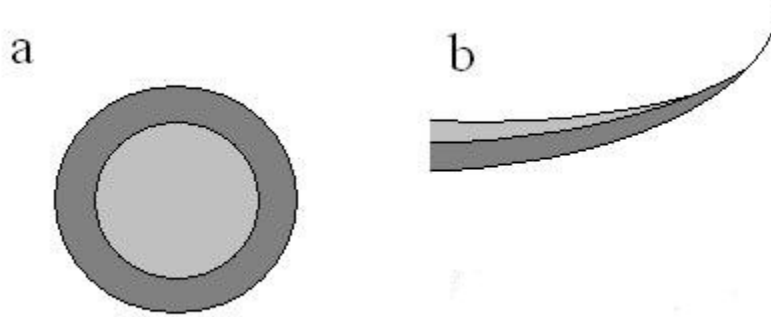


Figure 2.6 Schematic drawings of deposition patterns of evaporites in a closed sea-water basin under marine conditions after Einsele (2000). The dark grey areas represent the poorly soluble evaporites, e.g. gypsum and anhydrite, the light grey areas the well soluble halite. a) The 'bull's eye' pattern from bird's eye view, b) cross-section of a 'bull's eye'.

2.2.2 Physical Properties

Evaporites differ from other types of sediments in many aspects. They can form pressure seals because of their lack of permeability. The vertical escape of compaction and thermobaric fluids is blocked, and the pore fluid pressure is increased below the evaporitic seal. Sediments beneath an evaporite layer are usually overpressured, which means that the pore pressure exceeds the hydrostatic pressure.

While halite (NaCl) is almost incompressible down to depths of 6 - 8 km and has a constant density of 2.2 g/cm³ regardless of the depth, most other types of sediments initially have a lower density when they are deposited and gain a higher density than salt during the compaction process. The level of neutral buoyancy, when salt and surrounding sediments have the same density, is approx. 1 km burial depth. In hydrologically open compaction systems, this is also the depth in which the deposited gypsum (CaSO₄ · 2H₂O) is transformed into anhydrite (CaSO₄), discharging water.

Another characteristic of halite is its high thermal conductivity. The conductivity of halite is 7.3 W/m°C at 0 °C and approx. 4 W/m°C at 400 °C, compared to e.g. the conductivity of shales with 1.8 W/m°C at 0 °C and 1.5 W/m°C at 400 °C (Fig. 2.7). The effect of a salt bed is therefore a lower temperature gradient within the salt layer and a lower temperature of the sediments below the salt.

An important feature of halite is its viscosity. With 10^{18} Pa·s under dry conditions and 2 to 4 orders of magnitude less under wet conditions the viscosity of halite is 4 to 5 orders of magnitude higher than that of clays, shales or sand. Because of this viscosity salt shows extreme weakness to geologic strain rates. An evaporite layer cannot drag or stretch the overburden, but rather acts as a lubricant which decouples the overburden from the basement. Therefore basement structures cannot always be traced through an evaporite layer, and deformation of the overburden of a salt layer does not necessarily originate in the basement (Warren 1999).

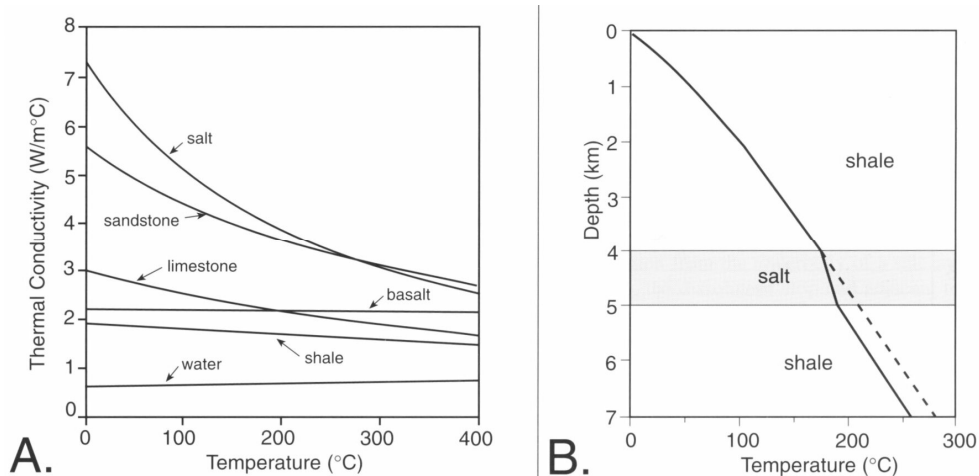


Figure 2.7a. Thermal conductivity of different materials vs. temperature. Note the high conductivity of salt. b. Illustration of the effect of a salt layer on the temperature below. From Warren (1999).

The seismic velocity of evaporites is generally higher than that of the sediment overburden. Halite has a p-wave velocity of 4.2 km/s, anhydrite of 4.9 km/s, compared to e.g. sands and clays with 1.5 - 2.5 km/s (Berckhemer, 1990). This causes a high acoustic impedance contrast, a high reflection coefficient, and a reduced transmission coefficient. Therefore the top of the evaporite layer is usually well recognized, whereas the signal penetration below the evaporites is limited.

2.2.3 Thin-skinned tectonics or halotectonics

Salt tectonics (halotectonics) played a major role in the development and application of exploration geophysics and geology in the past century. Until the 1970s, mainly vertical salt movements were studied, e.g. the evolution of salt domes (Trusheim 1957, Trusheim 1960). Salt and its overburden were described as two viscous fluids with different densities. Jackson (1995) suggested the term "fluid era" for this period. In the 1990s many researchers realized that salt tectonic related structures and salt domes could not sufficiently be explained by buoyancy of fluids alone (Worrel and Snelson 1989, Cobbold and Szamarti 1991, Vendeville and Jackson 1992a, b). Schultz-Ela et al. (1993) showed that buoying salt can only pierce a relatively thin overburden. This

overburden is now considered as a solid layer that reacts to stress by fracturing, and according to Jackson (1995) this marks the begin of the “brittle era”.

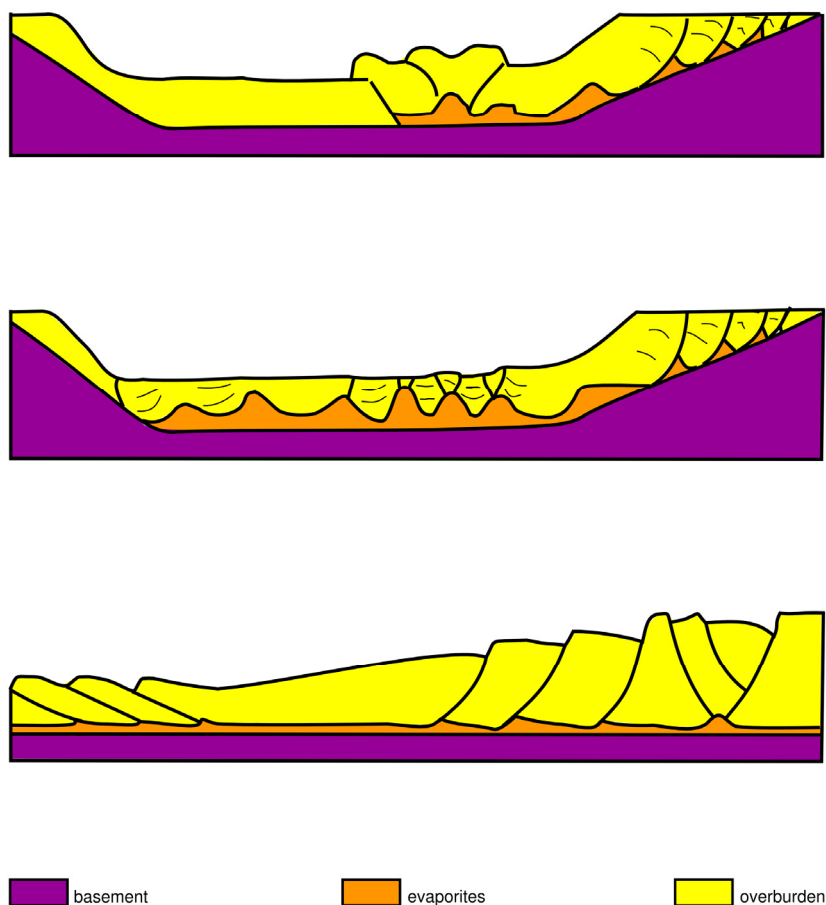


Figure 2.8 Illustration of gravity gliding without backstop (top), gravity gliding with backstop (middle) and gravity spreading (bottom). After Letouzey et al. (1995).

Not only vertical but also lateral salt movements can now be explained (Vendeville and Cobbold, 1987). Thin-skinned tectonics are caused by a viscous salt layer, which decouples near surface stress from deeper regional stress fields. Vendeville and Jackson (1992a, b) investigated the rise and fall of diapirs in (thin-skinned) extensional settings and showed that the regional stress field and differential load are the main forces effecting salt diapirism.

In the beginnings of the ‘brittle era’, the eastern Levantine Basin was recognized as a world class site to investigate this kind of lateral salt tectonics, which includes significant lateral salt flow and complex deformation of the sedimentary overburden (e.g., Garfunkel et al. 1979, Almagor 1984, Garfunkel 1984, and others). Lateral displacements were studied by analogue, later also by numerical modelling (Gemmer et al. 2004). Letouzey et al. (1995) developed an analogue model of gravity gliding in a basin (Figure 2.8). As already suggested by Humphris (1978) and Martin (1978), the slope of a margin or simply the differential load of a seaward prograding shelf (gravity

spreading) causes the overburden to move basinwards leaving extensional structures such as listric normal faults and rotated blocks along the slope. The mobile salt layer also flows basinwards along with the overburden. The extension on the slope corresponds to accumulation of the overburden in a compressional zone basinward. Depending on the distance between the extensional zone and the backstop at the end of the basin, a transitional zone of mere translation of the sediment package may occur (Crans et al. 1980, Letouzey et al. 1995) (Fig. 2.8). Gradmann et al. (2005) have refined this model by dividing the evaporite body into two layers, a brittle upper layer and a ductile lower layer (Fig. 2.9).

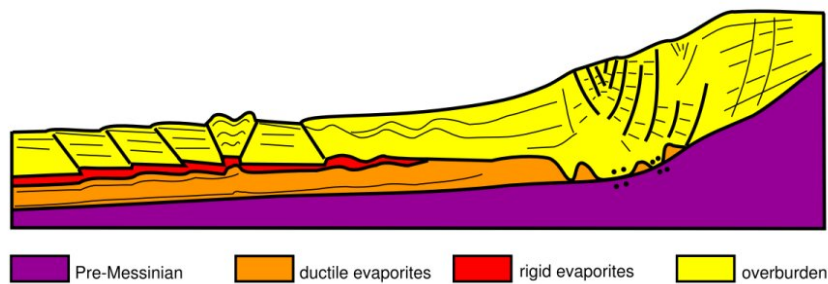


Figure 2.9 Modification of Letouzey's Model of gravity gliding including a layer of rigid evaporites. After Gradmann et al. (2005).

3 Data

This study is based on 2 refraction seismic profiles with 20 stations each and 56 multichannel reflection seismic (MCS) lines (Fig. 3.1). The two refraction seismic lines and 44 MCS lines were recorded in 2002 during the cruise M52/2 with the research vessel RV METEOR, another 12 MCS lines in 2004 during the cruise PE228 with the Dutch research vessel RV PELAGIA. Gravity measurements were continuously recorded on all lines during the cruise M52/2.

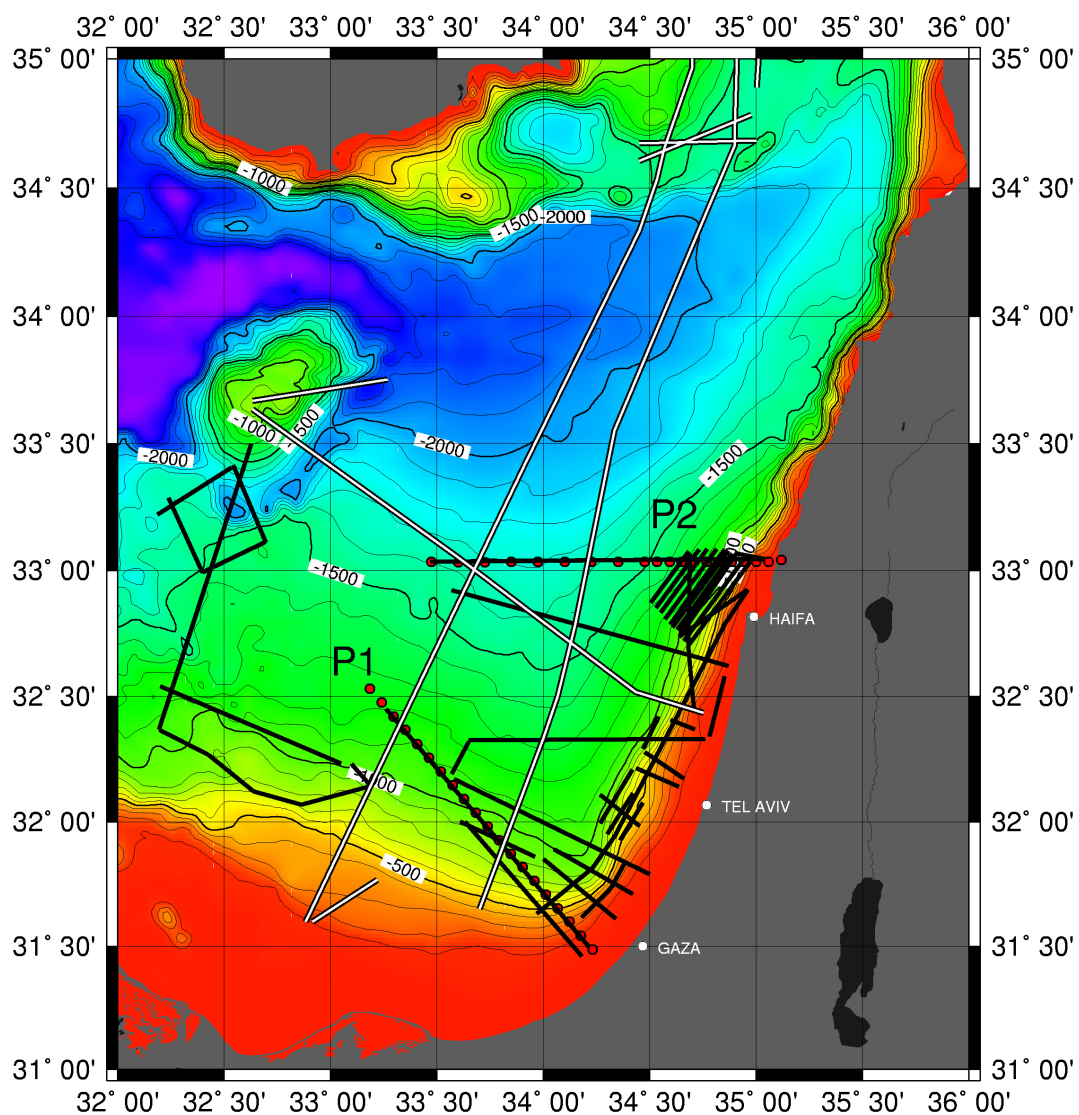


Figure 3.1 Bathymetric map of the survey area. Red dots mark the position of the ocean bottom hydrophones, black-and-white lines indicate the multichannel seismic lines of the M52/2 cruise in 2002, blue lines mark the multichannel seismic lines of the PE228 cruise in 2004.

3.1 Reflection seismics

All MCS lines were recorded with a streamer of 600 m active length. All lines recorded in 2002, except for HH02-07 and HH02-19, which were shot simultaneously with the refraction seismic lines, were also recorded with a second streamer of 150 m active length. The longer streamer provided velocity information, while the shorter streamer offered a better image quality. Both streamers comprised 24 channels with a group distance of 6.25 m and 25 m and a maximum offset of 190 m and 700 m, respectively. The sampling rate was 1 ms. During the cruise M52/2, with the exception of HH02-07 and HH02-19, a GI-Gun cluster (2 x 205/105 in³) was used as a source (Table 3.1). For HH02-07 and HH02-19 the source consisted of two small airgun clusters: one cluster with two GI-Guns, each with a volume of 105 in³ operated in the harmonic mode, and the other cluster consisting of one GI-Gun with 205/105 in³ operated in the airgun mode and a G-Gun of 380 in³ (6 l). During the cruise PE 228 the source consisted of 2 G-Guns with 380 in³ (6 l) or alternatively of 2 GI-Guns with a volume of 105 in³. The shot spacing was 25 m (10 s).

| | HH02-07 and HH02-19 | HH02-lines | HH04-lines |
|-----------------|---|-----------------------------|--|
| cruise | M52/2 | M52/2 | PE228 |
| streamer | 600m | 150m & 600m | 150m & 600m |
| source | 2xGI, 105 inch ³ , 1xGI, 205/105 inch ³ 1xG, 380 inch ³ | 2xGI, 105 inch ³ | 2xG, 380 inch ³ or 2xGI, 105 inch ³ |

Table 3.1 Assembly of acquisition parameters

During the processing, the recordings were assorted to their common midpoint (CMP) with a CMP spacing of 6.25 m and 12.5 m, then stacked and bandpass filtered with passing frequencies between 10 and 150 Hz. Finally, in order to remove velocity effects in the undulations of the lower reflections, i.e. velocity pull-ups or -downs, the lines HH02-01, HH02-07, HH02-19, HH04-06, and HH04-08 were time and depth migrated. Therefore a stacking velocity analysis was carried out on every 100th CMP in supergathers of 5 - 9 CMPs with the software package geodepth by Paradigm). With increasing horizon depth more CMPs were stacked into the supergather. The resulting velocity field was then used for the pre-stack time migration and stacking (Fig. 3.2). Then an interval velocity analysis followed, and with the resulting velocity field (Fig. 3.3) a Kirchhoff pre-stack depth migration was carried out (Fig. 3.4). The interval velocities of Post-Messinian sediments and evaporite layers were 2.0 ± 0.2 km/s and 4.2 ± 0.3 km/s (Fig. 3.3). The offset-target ratio was not optimal with a target depth of 4 km (base of the evaporites) and a maximum offset of 700m. Therefore the interval velocities were not used for the interpretation, only for the depth migration.

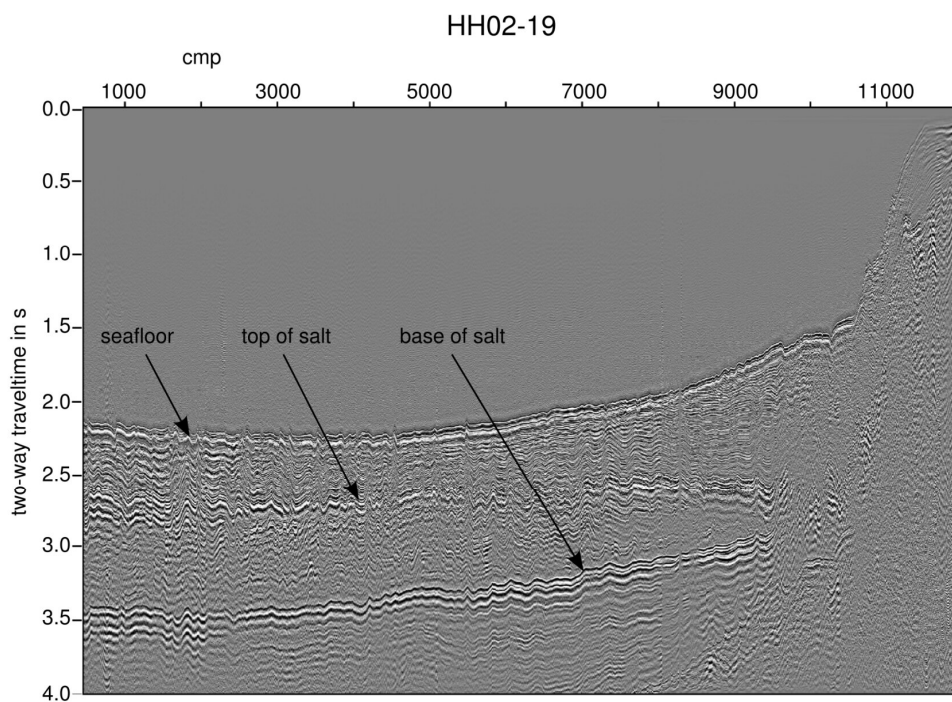


Figure 3.2 Time migrated section of line HH02-19. Note the main reflections from the seafloor, the top of the evaporite layer, and the base of the evaporite layer. The image of the base of the evaporites is extraordinarily good. The time difference between the seafloor and the top of the salt is about 0.7 s, the time difference between the top and the bottom of the salt is about 0.8 s.

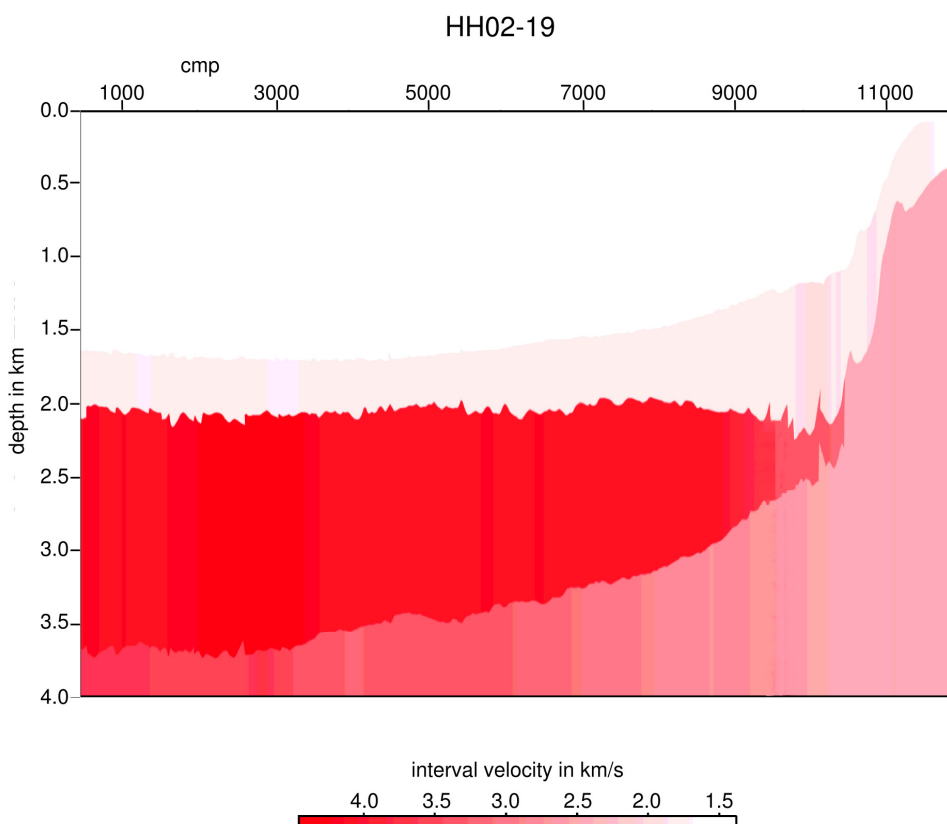


Figure 3.3 Interval velocity field of line HH02-19. This velocity model was used for the depth migration with *geodepth*. Note how the velocity increases at the boundary of the sediments and the evaporites. Also note the velocity inversion at the base of the evaporites.

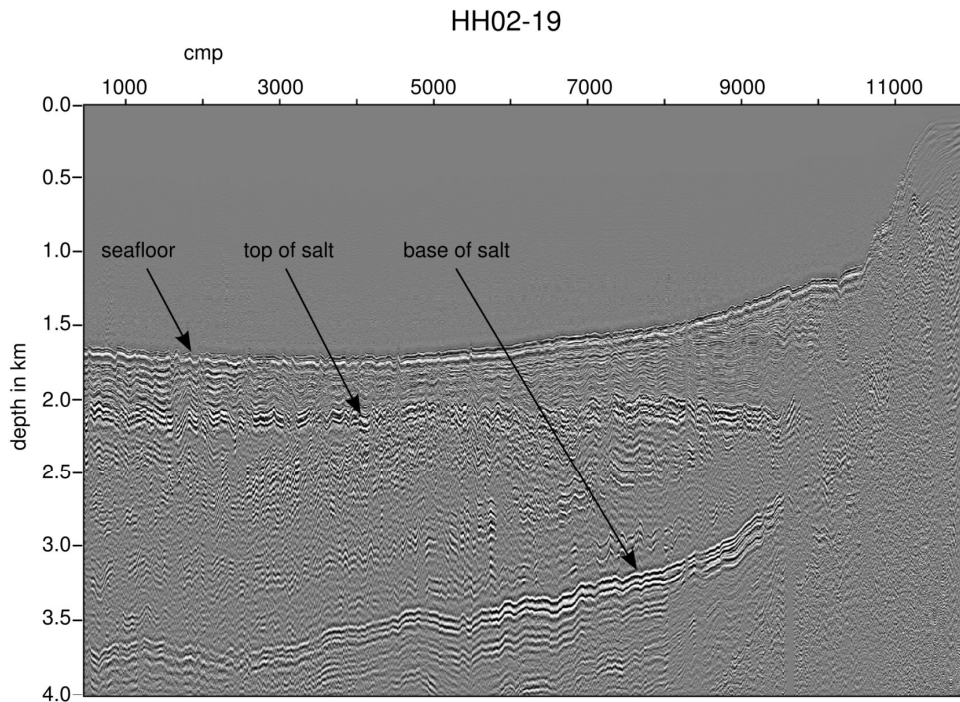


Figure 3.4 Depth migrated section of line HH02-19. The remaining undulations in the base of the evaporite layer can be considered to be real. The thickness of the sediment layer is about 0.5 km, while the thickness of the salt is 1.5 km.

3.2 Refraction seismics

On the refraction seismic line P1, 20 ocean bottom hydrophones (OBH) were deployed over a distance of 150 km. The second line, P2, consists of 19 OBH deployed along 158 km. In the prolongation of line P2, a seismic station was set up onshore ($33^{\circ} 02.508 \text{ N} / 35^{\circ} 07.167 \text{ E}$, Fig. 3.1). All of the instruments on line P2 recorded data, although the recording of the station onshore only showed one phase. On line P1 five OBHs (1, 2, 8, 12, and 19) failed and two more (6 and 14) showed only the direct wave, because of insufficient amplification. The sampling rate of the OBHs was 4 ms, that of the onshore station 5 ms. Two to three 321-Bolt-Airguns were used as source with a shot spacing of 125 m (60s).

After adapting the proper geometry, the seismic refraction data were loaded into the interactive picking program *ZP* by Barry Zelt (<http://www.soest.hawaii.edu/users/bzelt/zp/zp.html>). After application of a bandpass filter with passing frequencies of 3 - 25 Hz and a 1 s automatic gain control (AGC) the different arrivals were picked (Fig. 3.5). *ZP* allows the assignment of phase numbers during the picking process and visualizes the picks of different phases with different colours (Fig. 3.5). The picks were then used for forward modelling with the software package *rayinvr* of Zelt and Smith (1992) (Fig. 3.6). The depth migrated images of line

HH02-07 and HH02-19 served as starting models for the upper layers. Depending on the S/N-ratio and the phase correlation quality, uncertainty values were assigned to the traveltimes picks. The traveltimes are fitted within these uncertainties, and the resolution and the misfit of the model are calculated accordingly.

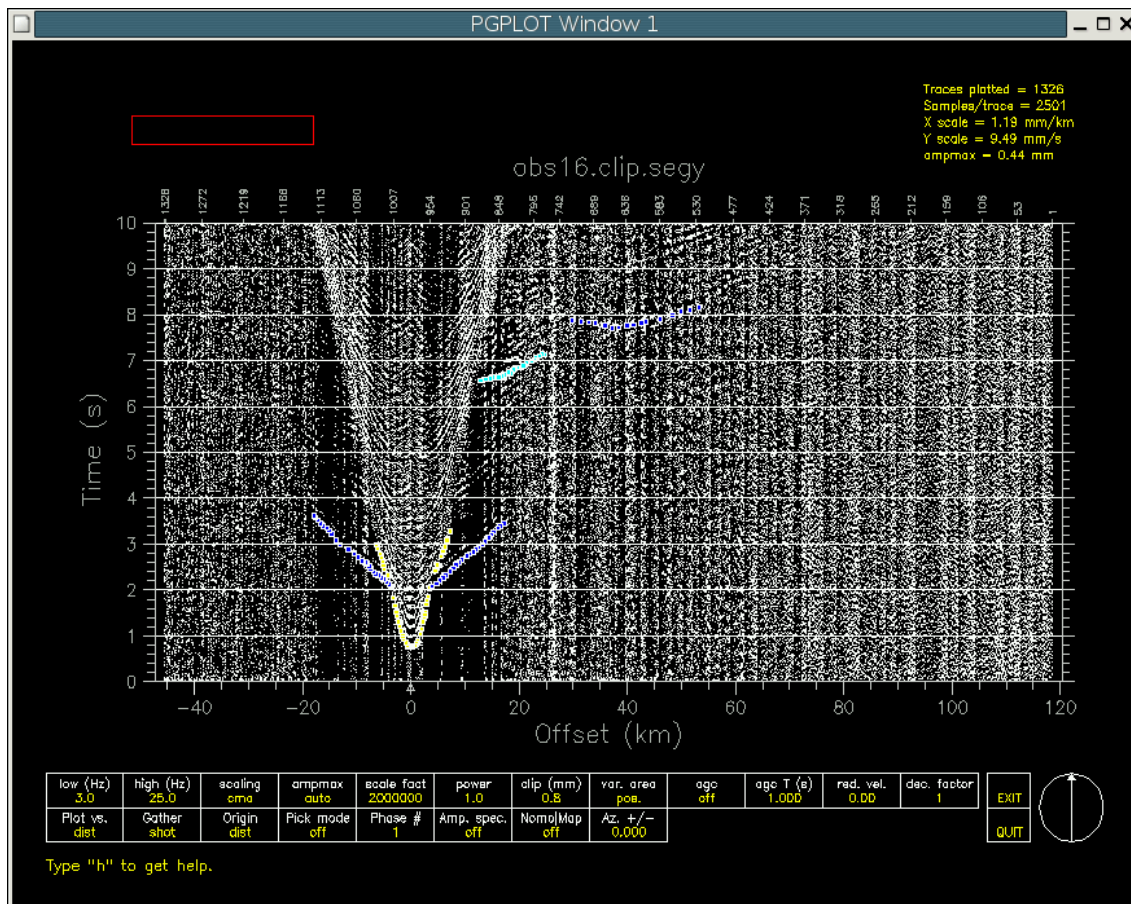


Figure 3.5 Screenshot of ZP, showing OBS 16 of line P01, and the picked phases in different colours.

The layer boundaries and velocities of the velocity-depth model are defined at nodes. At these nodes the depth, the velocities above and below the node are specified. Between the nodes of one layer, the velocity and depth values are linearly interpolated. The initial velocity-depth model was now modified until the modelled traveltimes would fit the picked traveltimes. For the modification of the velocity-depth model the graphical, interactive velocity model editor *vmed*, also by Barry Zelt, was used (<http://www.soest.hawaii.edu/users/bzelt/vmed/vmed.html>) (Fig. 3.7). The modelling was carried out layer by layer. Velocity and depth nodes were held fixed, when the next, deeper layer was modelled. As a consequence, the uncertainties increase with depth. Insertion of more nodes yields improved traveltimes fits. But the more nodes are added to the model, the less constrained they are. Exceptions are nodes which are confined by the depth migrated MCS data, e.g. at the base of the salt layer. The final models of both

lines were derived by application of the inversion method of *rayinvr*.

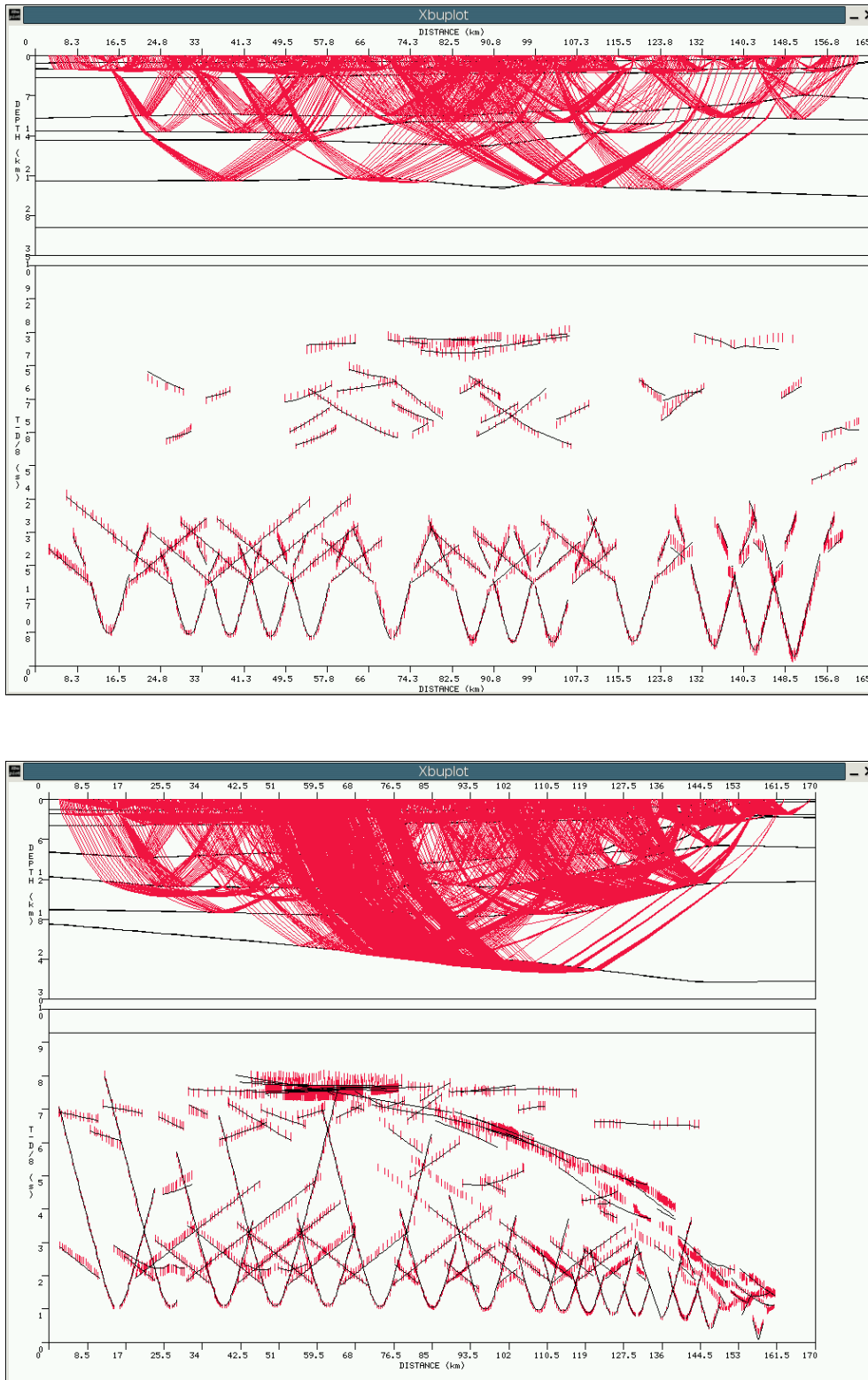


Figure 3.6 Screenshots of raytracing with *rayinvr* (model of line P1 above, model of P2 below). Rays are shot through the models in the upper part of the windows, and the observed and calculated traveltimes are displayed in the lower part of the windows.

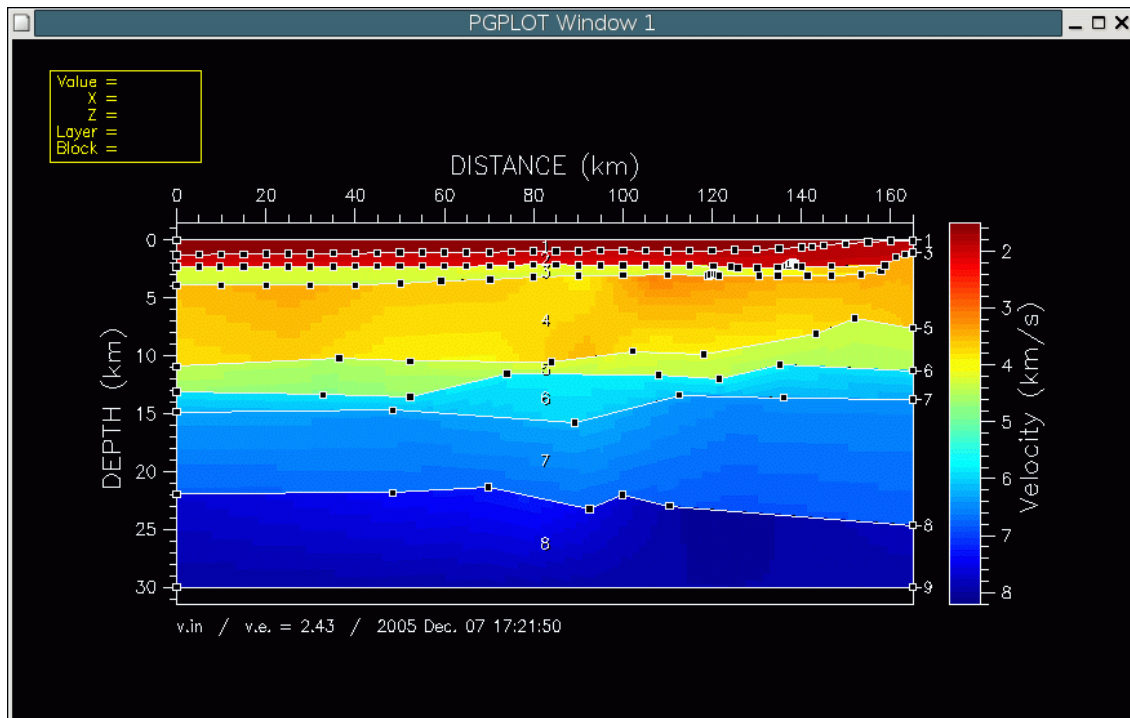


Figure 3.7 Screenshot of the graphical, interactive velocity model editor *vmed*. Here, the model of P1 is displayed. The black dots mark the nodes which define the model. One or more nodes can be selected and their depths and velocities above and below can be modified, either manually or with the mouse.

4 The Levantine Basin - Crustal Structure and Origin

(G. L. Netzeband, K. Gohl, C. P. Hübscher, Z. Ben-Avraham, G.A. Dehghani, D. Gajewski, P. Liersch, accepted by Tectonophysics)

Abstract

The origin of the Levantine Basin in the Southeastern Mediterranean Sea is related to the opening of the Neo-Tethys. The nature of its crust has been debated for decades. Therefore we conducted a geophysical experiment in the Levantine Basin. We recorded two refraction seismic lines with 19 and 20 ocean bottom hydrophones, respectively, and developed velocity models. Additional seismic reflection data yield structural information about the upper layers in the first few km. The crystalline basement in the Levantine Basin consists of two layers with a P-wave velocity of 6.0 - 6.4 km/s in the upper and 6.5 - 6.9 km/s in the lower crust. Towards the centre of the basin the Moho depth decreases from 27 to 22 km. Local variations of the velocity gradient can be attributed to previously postulated shear zones like the Pelusium Line, the Damietta-Latakia-Line and the Baltim-Hecateus Line. Both layers of the crystalline crust are continuous and no indication of a transition from continental to oceanic crust is observed. These results are confirmed by gravity data. A comparison with other seismic refraction studies in prolongation of our profiles under Israel and Jordan and in the Mediterranean Sea near Greece and Sardinia reveal similarities between the crust in the Levantine Basin and thinned continental crust, which is found in those regions. The presence of thinned continental crust under the Levantine Basin is therefore suggested. A β -factor of 2.3 - 3 is estimated. Based on these findings we conclude that seafloor spreading in the Eastern Mediterranean Sea only occurred north of the Eratosthenes Seamount, and the oceanic crust was later subducted at the Cyprus Arc.

Keywords: Levantine Basin, refraction seismics, crustal structure, gravity

4.1 Introduction

The early evolution of the Levantine Basin in the South-eastern Mediterranean Sea is closely related to the history of the Neo-Tethys. Determining whether the crust in the basin is continental or oceanic is crucial for the reconstruction of the Neo-Tethys opening and the position of its spreading axes. Whereas the continental character of the crust under the Eratosthenes Seamount and Cyprus is undisputed (Garfunkel, 1998,

Hirsch, 1984, Makris et al. 1983, Robertson 1998a), the nature of the crust underlying the Levantine Basin is still a matter for debate. Many authors, e.g. Ginzburg and Ben-Avraham (1987) and Ben-Avraham et al. (2002) postulate old oceanic crust under the basin, with the age varying from Triassic (Freund et al. 1975) to Cretaceous (Dercourt 1986). According to these theories the Eratosthenes Seamount was separated from the African margin in the Permian (Garfunkel 1998) along with other continental fragments (Ben-Avraham and Ginzburg 1990) and migrated northwards, where it presently collides with Cyprus (Robertson 1998b) with an annual collision rate of approx. 1cm/yr (Albarello et al. 1995, Kempler and Garfunkel 1994). Other authors claim that the crust under the Levantine Basin is continental (Hirsch 1984, Hirsch 1995, Woodside 1977, Vidal et al. 2000a) and argue that it was part of the Triassic African-Arabian plate system (Hirsch 1984).

Several plate tectonic reconstructions have been developed, differing in aspects as the origin of the crust under the Levantine Basin, the age of this crust, the location of the spreading axes and how far the Neo-Tethys was opened before subduction set in (Hirsch 1995, Garfunkel 1998, Robertson 1998, Stampfli and Borel 2002). Hirsch (1995) draws the Triassic Neo-Tethys with a width in N-S direction of approx. 700 km north of Arabia, and shows the African-Arabian margin including the area of the present Levantine Basin covered by a shallow sea. In the Jurassic, according to that study, the Tethys reaches a width of 2400 km and is in the Late Cretaceous reduced to approx. 200 km in the area of the present Mediterranean Sea. Garfunkel (1998) postulates rifting between Israel and the Eratosthenes Seamount as early as in the Permian. In the Late Triassic two rifting axes are described by Garfunkel (1998), one east and one west of the Eratosthenes, and a spreading axis north of the seamount, perpendicular to the rifting. Robertson (1998) dates the rifting phase that separated the Eratosthenes from the Levant margin to the Late Triassic, assuming oceanic crust in the Levantine Basin only north of 32°30' N (present day coordinates). Stampfli and Borel (2002) show an elaborate global scale plate reconstruction focussing on the Tethys area, giving a general idea of the Paleozoic and Mesozoic plate movements, but the development of the Levantine Basin in particular is not resolved. Mascle et al. (2000) found evidence for a Levantine-Sinai continental microplate extending from the Red Sea to roughly 35°N including the Eratosthenes Seamount and bounded to the east by the Dead Sea Transform Fault, and identified this microplate as a fragment of the African craton.

Two refraction seismic studies were previously conducted to analyse the crustal structure in the Levantine Basin (Makris et al. 1983, Ben-Avraham et al. 2002) consisting of three profiles (Fig. 4.1). Further deep seismic studies were carried out onshore by Ginzburg et al. (1979), Ginzburg et al. (1994), El-Isa et al. (1987) and recently the DESERT2000 project (Weber et al. 2004), providing information on the crustal structure under Israel, Jordan and the Sinai-Peninsula.

In 2002 a multidisciplinary cruise (the GEMME-Project, M52/2) was carried out with the R/V Meteor in order to unravel the nature and origin of the crust under the Levantine basin. A grid of reflection seismic lines and two new refraction seismic lines

with a close receiver spacing were recorded along with gravity measurements and echosounder (Parasound) data. The crustal structure along these refraction lines will be the topic of this study.

4.2 Geological and geophysical setting

The Eastern Mediterranean and with it the Levantine Basin is a relic of the Mesozoic Neo-Tethys Ocean (Robertson and Dixon 1984, Stampfli and Borel 2002, Garfunkel 2004). The Levantine Basin is confined by the Israeli and the Egyptian coasts, Cyprus, and the Eratosthenes Seamount (Fig. 4.1). In the Miocene, the so-called 'Messinian salinity crisis' was initiated by the disconnection of the Mediterranean from the Atlantic. This was caused by a combination of tectonic uplift and sea level changes (Hsü et al., 1973; 1978) and led to a drop of sea level, a rise in salt concentration and finally to precipitation (e.g. Gradmann et al. 2005). The evaporite layer deposited during that time in the Levantine Basin is up to 2 km thick.

The basin has undergone significant subsidence for more than 100 Ma (Mart 1982, Almagor 1993, Tibor et al. 1992, Vidal et al. 2000a), over 2 km since Pliocene (Mart 1982) and is still subsiding (Tibor et al. 1992). The basement is buried under up to 14 km of sediments (Ben-Avraham et al. 2002). The slope on the shelf steepens from 4° off Sinai to over 10° off northern Israel (Mart 1984). Faults trending NE-SW have been observed onshore (Mart 1982) and offshore (Neev et al. 1976, Abdel Aal 2000, Farris et al. 2004). A fold belt, which extends from the Western Desert of Egypt through Sinai into the Palmyra folds of Syria has been termed the Syrian Arc (Walley 1998). In its central segment, at the latitudes of Israel and Lebanon, it strikes NNE-SSW. The Pelusium Line (Fig. 4.1), a prominent fault line, runs ca. 35 - 50 km offshore subparallel to the Israeli coastline (Neev et al. 1976, Neev 1975 and 1977, Mart 1982, Hirsch 1995). The Pelusium line represents the western edge of the Syrian Arc fold belt. The evolution of this regional compressional tectonic feature began in the Late Cretaceous and continued until the Early-Middle Miocene (Gardosh and Druckmann 2006, Walley 1998). Its evolution was related to the closure of the Neo-Tethys (see Garfunkel 1998 and 2004 for comprehensive summaries).

4.3 Previous work

There has been a number of geophysical studies of the Levantine Basin. Three seismic refraction lines were recorded (Ben-Avraham et al. 2002) (Fig. 4.1), two in 1989 (Ben-Avraham et al. 2002), one in 1979 (Makris et al. 1983, Ginzburg and Ben-Avraham 1987). On these lines about 10 receivers per line were used, therefore receiver spacing was at least twice as wide as in our study.

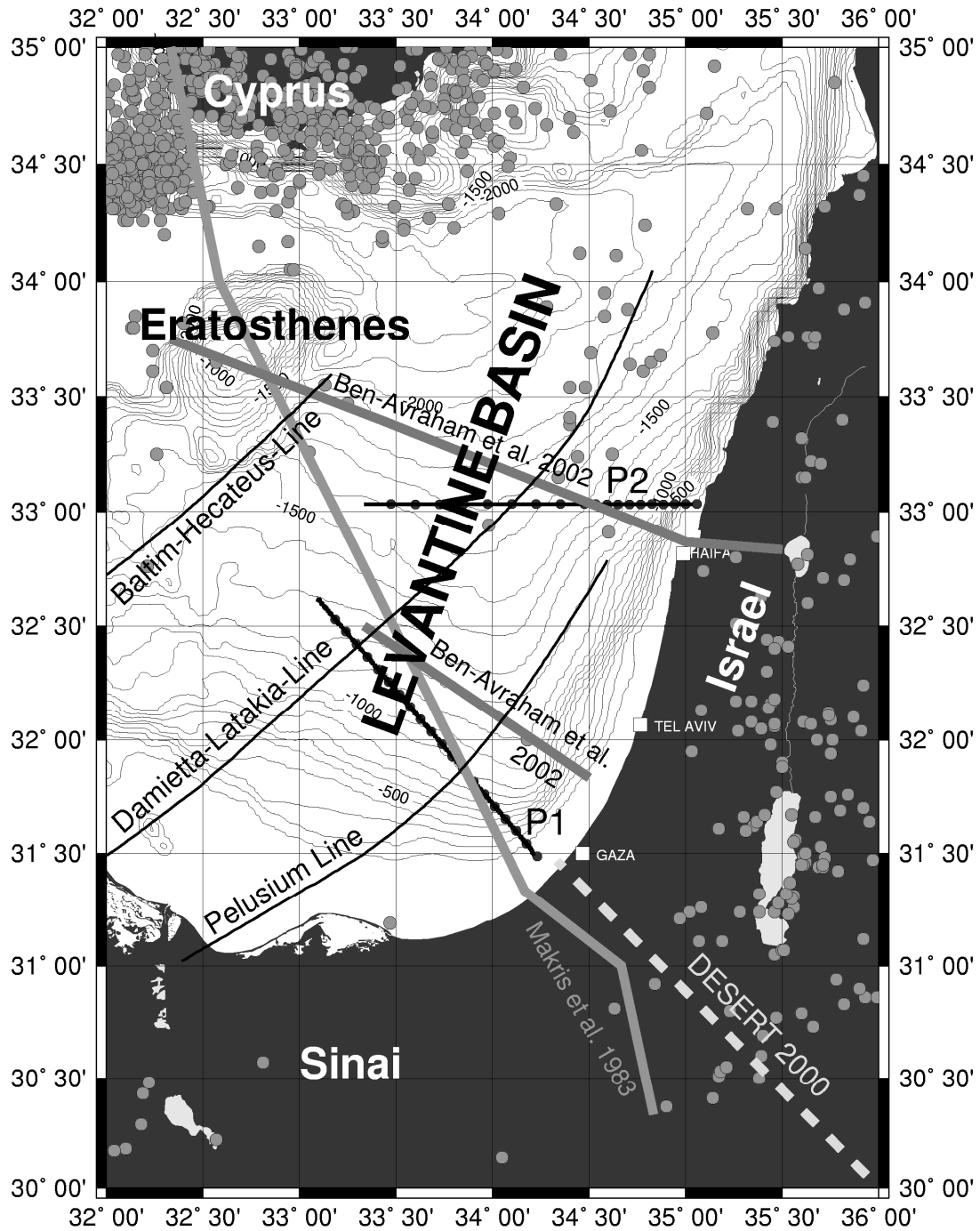


Figure 4.1 Map of the Levantine Basin. Thick solid lines mark the locations of profiles P1 and P2, with solid black circles indicating the positions of the OBH. The shear zones Pelusium Line, Damietta-Latakia-Line, and Baltim-Hecateus-Line are shown after Neev et al. (1976). Grey circles mark hypocenters of earthquakes since 1973 according to the US Geological Survey. Previous refraction seismic lines in the Levantine Basin are marked as light grey lines.

The models of these refraction seismic lines show a Moho depth of 20 - 25 km. A single crustal layer of 6.7 km/s was observed and interpreted as oceanic crust. Two crustal layers were observed under Israel, with a P-wave velocity of 6.7 km/s in the lower crust and the velocity in the upper crust varying from 6.3 km/s under northern Israel to 6.0 km/s in the south. The pinchout of the upper crust was located 20 km offshore on the northern profile and 100 km offshore on the southern line and interpreted as the transition zone between continental and oceanic crust. On all these lines, accompanying gravity and magnetic models were compiled, which were based on the refraction seismic models and showed matching results. Deep seismic experiments analysing the crust under Israel, Negev and Jordan have been carried out by Ginzburg et al. (1979), Ginzburg et al. (1994), El-Isa et al. (1987) and recently in the frame of the DESERT2000 project (Weber et al. 2004) (Fig. 4.1) and show a crustal thickness under Judea of less than 30 km, thinning to the north to slightly over 20 km under Galilee-Lebanon, and thickening to the south and east up to 40 km beneath Negev and Jordan. The mantle depth under the Eratosthenes Seamount has been modelled to 28 km. An analysis of the magnetic field of the Levantine Basin by Ben-Avraham and Makris (1986) revealed no elongated alternating magnetic anomalies typical of oceanic crust. The authors nevertheless maintained their idea of oceanic crust and offered two explanations of the missing anomalies: 1) The crust could have been created in an era without polarity reversals. 2) The magnetic anomalies could have been destroyed by later crustal deformation. Woodside (1977) analysed the gravity and magnetic field of the Eastern Mediterranean Sea, but came to a different conclusion: He states that there is evidence for the northward continuation of crustal structure from northern Egypt into the Eastern Mediterranean Basin and concludes that the crust under the Levantine Basin represents the thinned margin of the African plate. Hirsch (1995) and Vidal (2000a, 2000b) show reflection seismic lines which image the basin structure down to the basement. Both locate the top of the basement at ca. 12 km on average, and agree that the basement is not flat but faulted with displacements of up to 500 m. Based on the reflective character of the basement, the structure of the top basement unconformity and the large thickness of Mesozoic sediments, Vidal et al. (2000a) favour the hypothesis of considerably attenuated continental crust in the Levantine Basin.

Above the basement, the depositional sequences have been identified as Cretaceous-Jurassic, Paleogene-Neogene, Messinian, and Pliocene-Holocene (Vidal et al. 2000b, Abdel Aal et al. 2000). The Cretaceous-Jurassic unit above the basement has been interpreted as a carbonate sequence with a P-wave velocity of 4.5 km/s (Ben-Avraham et al. 2002). The layer above represents Post-Cretaceous to Pre-Messinian sediments with a velocity of 3.8 - 4.0 km/s (Vidal et al. 2000a), accumulated in 60 Ma during the subsidence of the basin. The Messinian sequence consists of Messinian evaporites, precipitated during the Messinian Salinity Crisis. This sequence is characterised by a high velocity of more than 4.0 km/s (Mart and Ben-Gai 1982), and the reflections marking top and bottom of this layer have been termed M- and N-Reflection, respectively (Ryan et al. 1970). On top of the Messinian evaporites, Nile sediments have been deposited since the re-flooding of the Mediterranean (Mart 1982).

4.4 New geophysical data

The data of this study were collected during the cruise M52/2 with the German research vessel RV METEOR in 2002 (Pätzold et al. 2003).

4.4.1 Seismic refraction data - acquisition

Two seismic refraction lines were acquired (Fig. 4.1). On line P1, the number of 20 ocean bottom hydrophones (OBH) were deployed over a distance of 150 km, line P2 consists of 19 OBH deployed along 158 km. In the prolongation of line P2, a seismic station was set up onshore ($33^{\circ} 02.508$ N / $35^{\circ} 07.167$ E). All of the instruments on line P2 recorded data, but on line P1 five OBHs (1, 2, 8, 12, and 19) failed and two more (6 and 14) showed only the direct wave, because of insufficient amplification. The sampling rate of the OBHs was 4 ms, that of the onshore station 5 ms. Two 32l-Bolt-Airguns were used as source with a shot spacing of 125 m (60s).

4.4.2 Seismic refraction data - processing and characteristics

Prior to analysis, the seismic refraction data were re-positioned and processed with a bandpass filter passing frequencies of 3 - 25 Hz. On some stations signals were enhanced by application of a 1 s automatic gain control (AGC). Generally, data quality suffered from harsh weather conditions, from the thick sedimentary layer in the Levantine Basin, because it absorbs a significant amount of seismic energy, and also from the Messinian salt layer, where a great part of the seismic energy is refracted. Predictive deconvolution did not help much in signal enhancement (Fig. 4.2a), i.e. although it makes the appearance of the modified signals is slightly clearer, the arrivals cannot be traced significantly farther than before the deconvolution. At greater offsets, where a wrap-around of the direct wave of the previous shot appeared, an F-K-filter was applied in order to reduce the amplitudes of the wrap-around. Nevertheless, new arrivals were not revealed (Fig. 4.2b).

Figures 4.3a-c show the recordings of station 07 in the centre of line P1, and stations 17 and 18 on line P2 on the shelf end. In the near offsets of Fig. 4.3a, steep reflections from the top of the evaporite layer (PeP) can be observed, but the first arrivals belong to turning waves within this layer (Pe). The Pe arrivals are very prominent all along the line, they are observed at each station, as well as the PeP. Later arrivals on Fig. 4.3a are reflections from the top of the carbonate layer (PcarbP), which are observed on 8 other stations as well, and from the top of the upper crust (PcuP), which are also seen on a number of other recordings. A weak Moho reflection (PmP) appears at an offset of 40 km at 8 s. 5 stations recorded PmP arrivals. A Pn phase consisting of waves turning within the upper mantle was detected at 4 stations. Internal crustal reflections, named PclP, were observed on only 2 stations, OBH 09 and OBH 17.

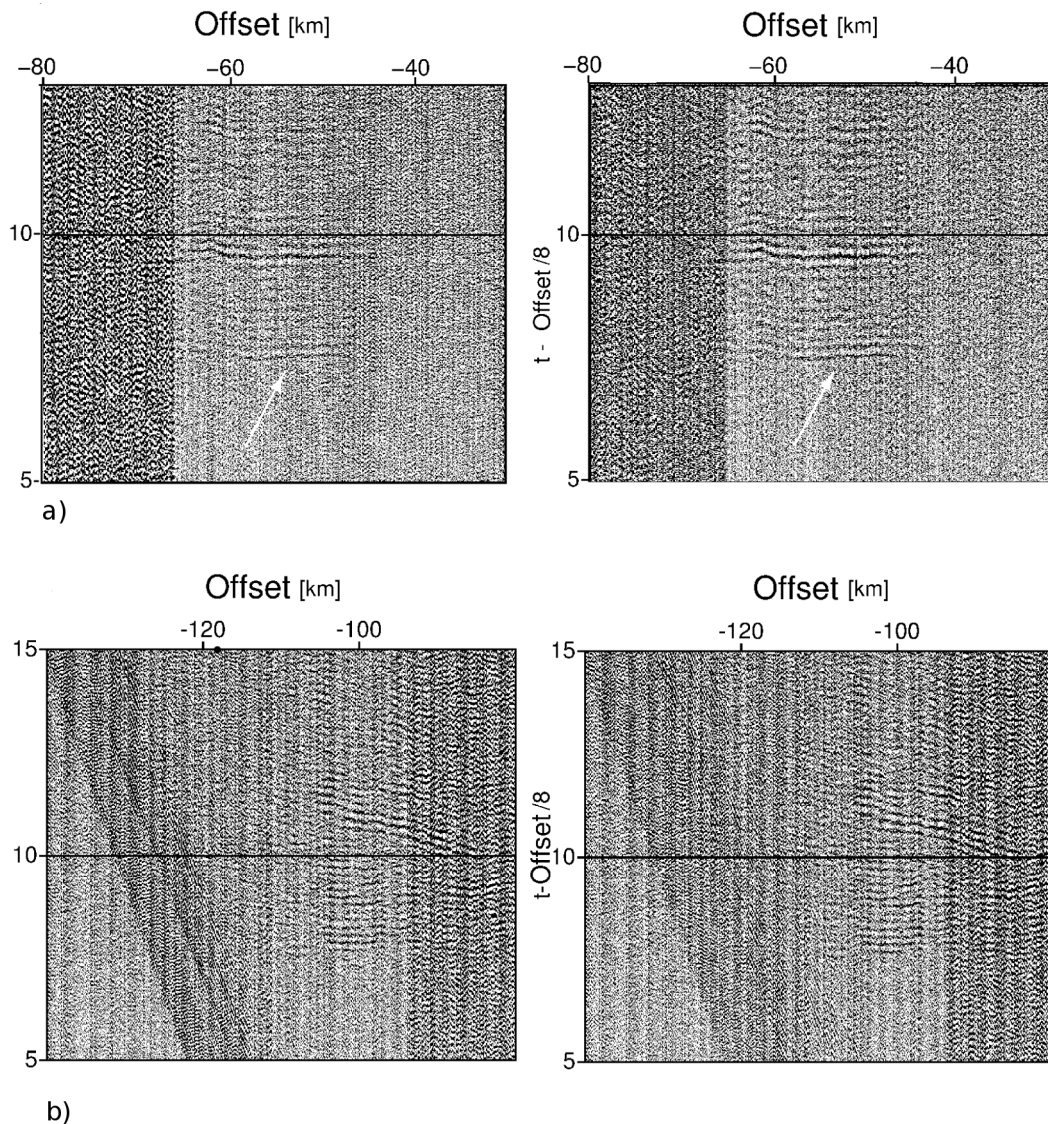


Figure 4.2 Example of predictive deconvolution and F-K-filtering. a) The left figure shows a section of the recording of OBH 09, P2 after bandpass filtering (3-25 Hz), showing the Moho refraction. The right figure shows the result after deconvolution. The signal is only slightly enhanced. b) The left figure shows a section of the recording of OBH 18, P2, after bandpass filtering (3-25 Hz) showing the Moho refraction. The right figure shows the result of the F-K-filtering. The wrap-around is significantly reduced, but new arrivals are not revealed.

At OBH 17 on line P2 (Fig. 4.3b) PeP arrivals, and turning waves from both sediment blocks, Ps1 and Ps2, are observed. From an offset of 40 km the refraction of the upper crust, Pcu, can be seen, and at 60 km the refraction of the upper crust, Pcl, appears. At an offset of approx. 75 km the Pn, turning waves of the upper mantle, arrive. At OBH 18 (Fig. 4.3c) the PeP and Pe arrivals are not observed, the Pe arrivals start at OBH 16 and are present on all other stations basinwards. The PeP only appear

OBH 7, Profile 1

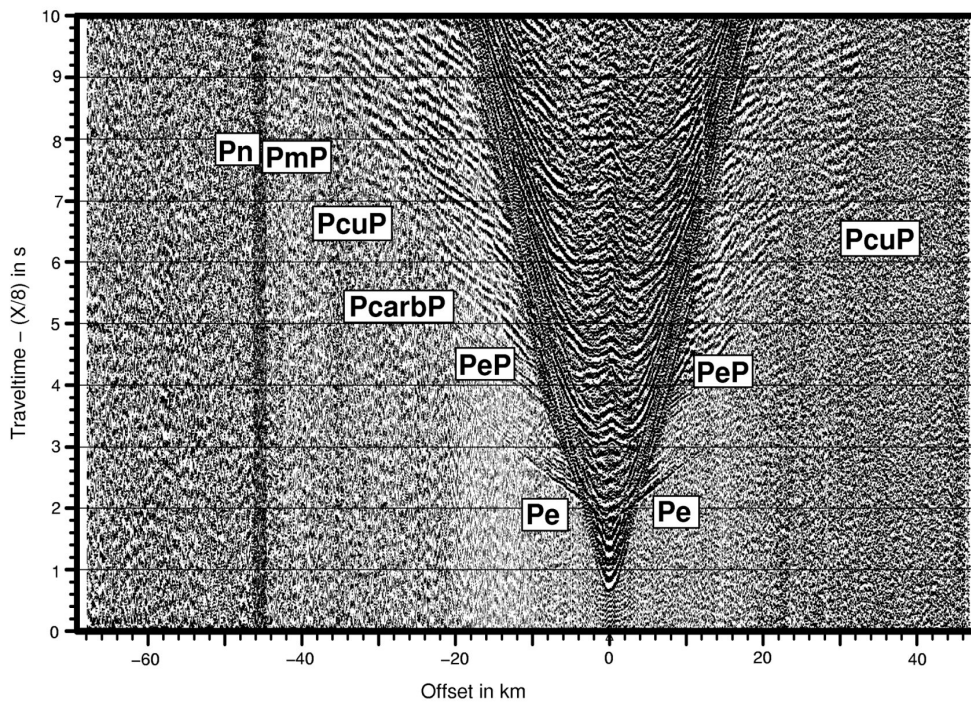


Figure 4.3 a) Recording of OBH 07, P1. The observed arrivals are marked. PeP - reflection from the top of evaporites, Pe - refraction at evaporite layer, PcarbP - reflection from the top of the carbonate layer, PcuP - reflection from the top of the upper crust, PmP - Moho reflection, Pn - Moho refraction.

OBH 17, Profile 2

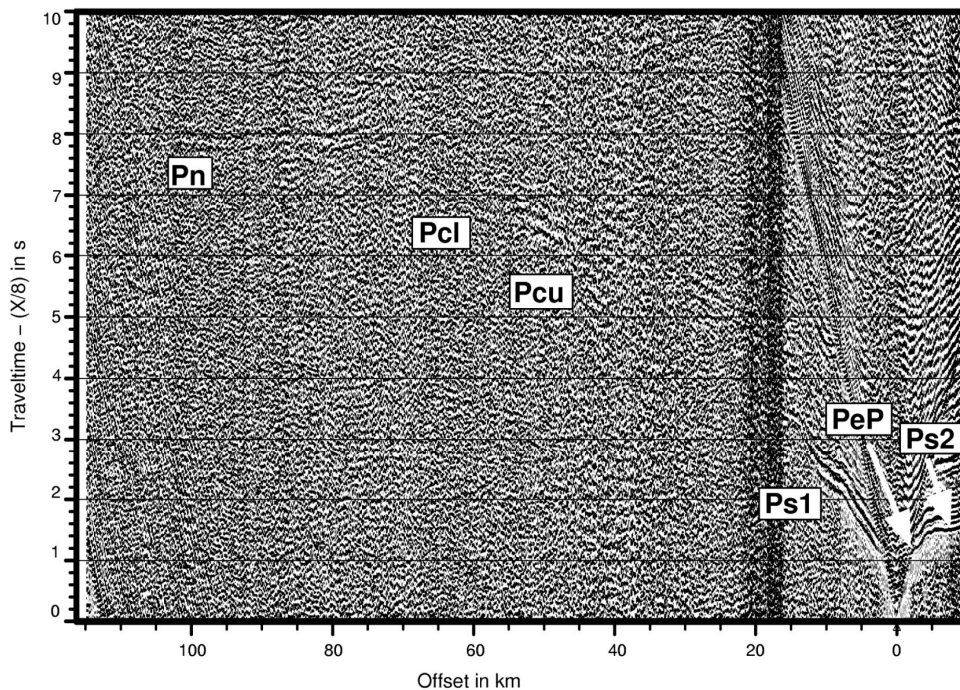


Figure 4.3 b) Recording of OBH 17, P2. The observed arrivals are marked. PeP reflections from the top of the evaporites, Ps1P- and Ps2P- reflection from the top of the second layer of Pre-Messinian sediments, Pcu - refraction from the upper crust, Pcl - refraction from the lower crust, Pn - Moho refraction.

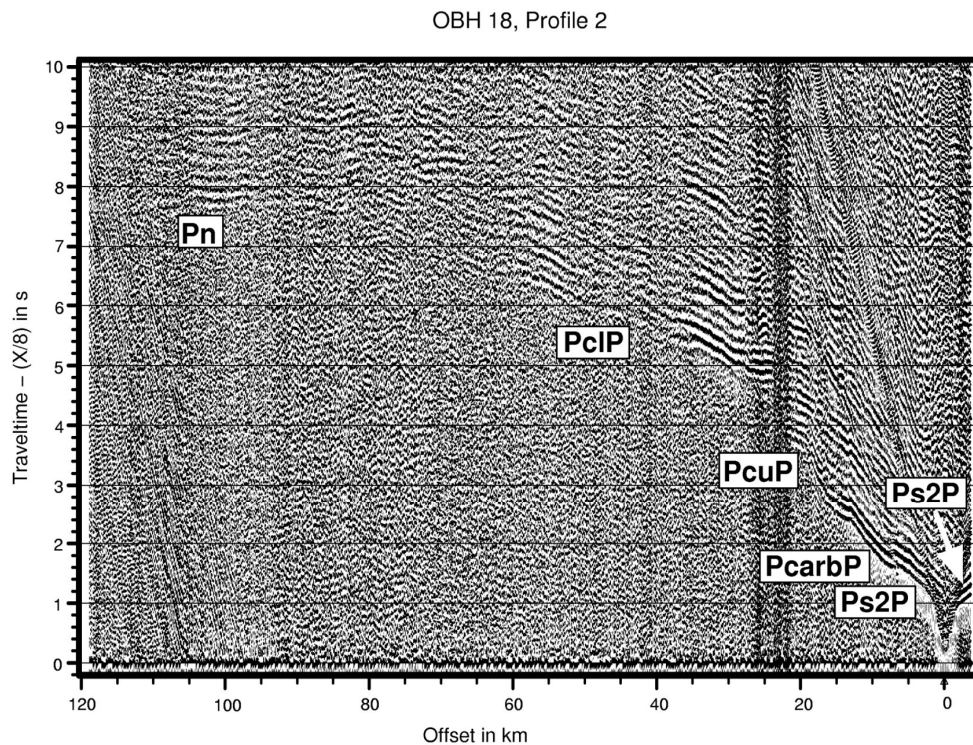


Figure 4.3 c) Recording of OBH 18, P2. The observed arrivals are marked. Ps2P - reflection from the top of the second layer of Pre-Messinian sediments, PcarbP - reflection from the top of the carbonate layer, PcuP - reflection from the top of the upper crust, PclP - reflection from the top of the lower crust, Pn - Moho refraction.

on some stations on the slope, on OBH 14, 16, and 17. On line P2 two Pre-Messinian sediment layers are found and the first arrivals at near offsets of Fig. 4.3c are reflections from the base of the upper sediment layer (Ps2P). Reflections from the upper sediment layer (Ps1P), and turning waves within these layers (Ps1,Ps2) are only observed on a few stations on the slope owing to the limited extent of the lower sediment layer and its relatively small thickness on the shelf. The reflection of the top of carbonates (PcarbP) marks the next arrival at 12 km offset. This reflection is observed on 7 more stations, diving waves of the carbonate layer (Pcarb) are not recorded on OBH 18, but on 3 other OBH. At 20 km the PcuP can be identified on Fig. 4.3c and farther away the PclP arrival. At an offset of about 80 km turning waves of the upper mantle arrive (Pn). Pcu, Pcl, and PmP are not be observed on OBH 18. PcuP, Pcu, and PclP are represented on 8, 7, and 6 stations, respectively, PmP and Pn on 6, respectively 5. Ray coverage of Pcu and PclP arrivals on line P2 are shown in Fig. 4.4.

The onshore station only recorded signals up to 15 km offset, and only one phase that was identified as PcarbP. There is a lateral transition zone of the marine carbonate layer into a layer of sandstones (Garfunkel 2004) near the coast, but since this transition could not be resolved on either line, this arrival on the seismic section is treated as a reflection from the top of the carbonate layer.

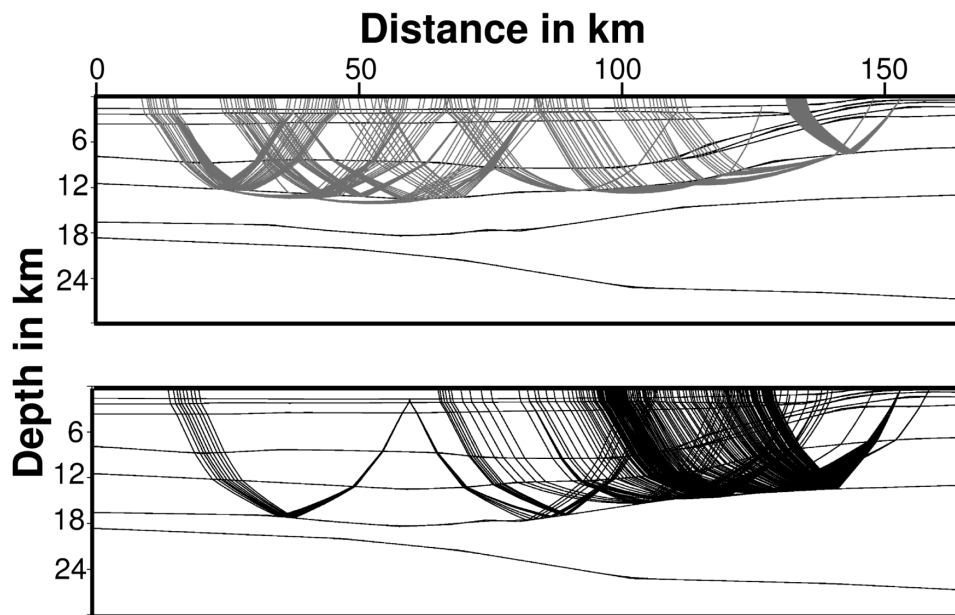


Figure 4.4 Example of ray coverage of the upper crust on P2. The upper image shows the refractions within the upper crust recorded by 7 stations, the lower image shows reflections from the top of the lower crust recorded by 6 stations.

4.4.3 Seismic reflection data - acquisition

During the cruise M52/2, the amount of 44 multichannel seismic reflection lines were recorded, two of these coincide with the refraction profiles, line HH02-07 runs along refraction line P1, and HH02-19 runs parallel to P2. Both were recorded with two streamers of 150 m and 600 m active length, respectively. Both streamers comprised 24 channels with a group distance of 6.25 m and 25 m, respectively, and a maximum offset of 190 m and 700 m, respectively. Both recorded with a sampling rate of 1 ms. The source consisted of two small clusters: one with two GI-Guns, each with a volume of 105 in³ operated in the harmonic mode, and the other cluster consisting of one GI-Gun with 205/105 in³ operated in the airgun mode and a G-Gun of 380 in³ (6 l). The shot spacing was 25 m (10 s). The airgun array was designed for maximum signal strength accepting a reduced primary to bubble ratio.

4.4.4 Seismic reflection data - processing and characteristics

The recordings of both streamers were CMP-sorted with a CMP spacing of 6.25 m and 12.5 m, respectively, then stacked and bandpass filtered with passing frequencies between 6 and 160 Hz. Only to the recordings of the longer streamer further processing was applied. A stacking velocity analysis was carried out on every 100th CMP

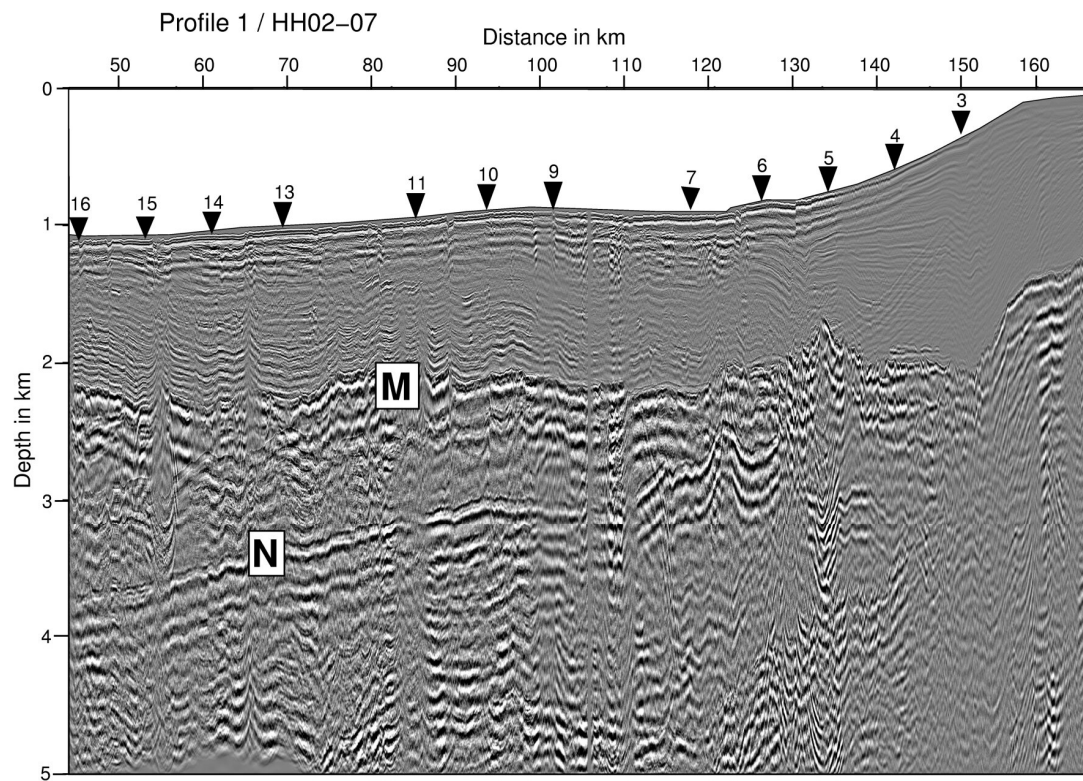


Figure 4.5 Model based depth migrated section of HH02-07 parallel to P1. Average interval velocities used for the migration were 2.0 km/s for the Plio-Quaternary sediments and 4.2 km/s for the salt layer. M marks the top and N the base of evaporites. Black triangles show the positions of the OBH on line P1.

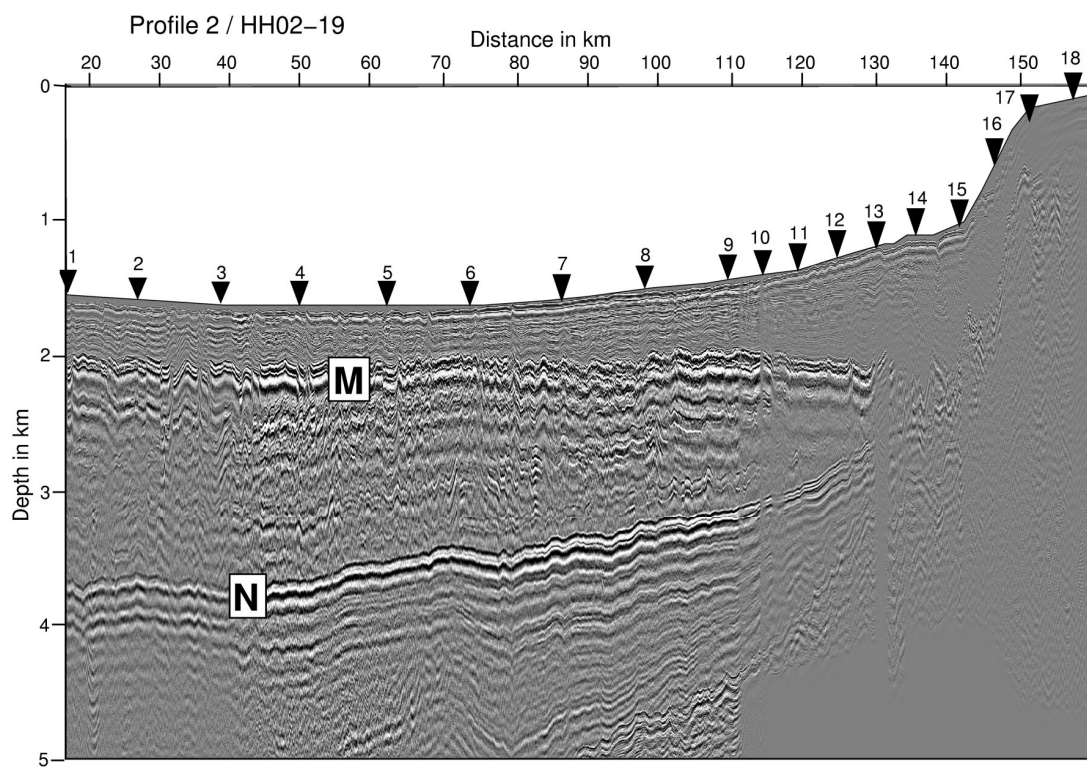


Figure 4.6 Model based depth migrated section of HH02-19 parallel to P2. Average interval velocities used for the migration were 2.0 km/s for the Plio-Quaternary sediments and 4.2 km/s for the salt layer, as on HH02-07. M marks the top and N the base of evaporites. Black triangles show the positions of the OBH on line P2.

in supergathers of 5 - 9 CMP. The deeper the analysed horizon, the more CMPs were combined to the supergather. The resulting velocity field was smoothed and the data were time-migrated and stacked accordingly. Afterwards, an interval velocity analysis was carried out and a model based depth migration accomplished. Average interval velocities of Post-Messinian sediments and evaporite layer were 2.0 km/s and 4.2 km/s, respectively. Figs. 4.5 and 4.6 show the depth migrated images of lines HH02-07 and HH02-19, respectively. On both images the top (M-reflection) and the base (N-reflection) of the salt layer are clearly visible. The M-reflection displays a rough surface owing to salt movement and compression (Gradmann et al. 2005), but the N-reflection which represents the Pre-Messinian seafloor is smooth. On line HH02-07, which corresponds to line P1, the sediment thickness of roughly 1 km is almost constant in the basin. N rises gently towards the shelf, but is severely contorted between km 105 and the salt pinchout. Near the location of OBH 05, a structure can be observed that affects both top and base of the evaporites, N is bent downwards and M upwards. The pinchout of the evaporites is not very distinct, but probably near the position of OBH 03. On line HH02-19 (Fig. 4.6) corresponding to line P2, the sediment layer is significantly thinner. It is only about 0.5 km thick and shows a clear thickening on the bottom of the slope. The salt layer is slightly thicker than on line HH02-07 and does not exhibit any significant contortion of N. The pinchout is even more disguised than on line HH02-07, but is assumed to occur near the location of OBH 15.

4.4.5 Gravity data

Gravity data were continuously recorded along the entire ship track in the research area, thus also along the two refraction lines. Gravity values were measured with the Gravity Meter System KSS30/31 and instantly converted into free-air anomaly values.

4.5 Modelling of refraction data

On line P1 13 stations were used for raytracing, on P2 all 19 stations were suitable for the modelling. The land station at the end of line P2 was also included. The modelling was performed with the software package *rayinvr* of Zelt and Smith (1992). The depth migrated images of lines HH02-07 and HH02-19 served as starting models for the uppermost sediments and the top and base of the salt layer. Suitable uncertainty values (error bars) were assigned to all the traveltimes: Depending on the S/N-ratio and the phase correlation quality, uncertainties between 0.020 s and 0.125 s were assigned (Table 1). First a forward modelling technique was applied, in which the modelling took place layer by layer. Velocity and depth nodes were held fixed when the next, deeper layer was modelled. Improved traveltimes fits come with the addition of nodes in the model. However, because of the sparse ray coverage in some areas it was also an aim not to over-fit the model by adding too many nodes that would be poorly

constrained. Excepted were nodes that were confined by the depth migrated MCS data, e.g. the undulation in the top of salt layer at approx. 135 km and in the base of this layer at about 120 km. The final models of both lines were derived by application of the

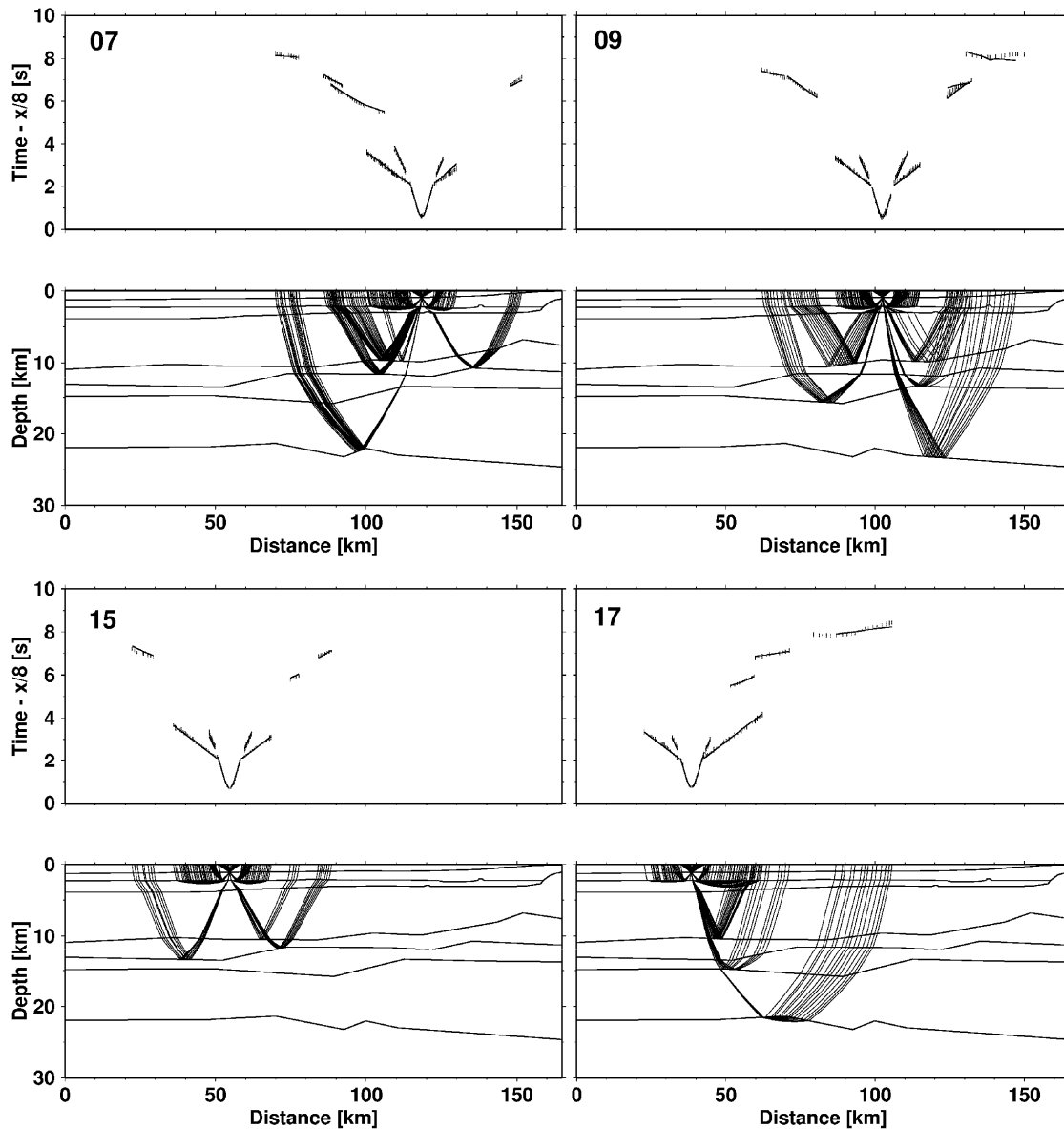


Figure 4.7 Examples of raytracing along Profile P1 from stations 07, 09, 15, 17. These stations cover different parts of the model. The upper parts show the observed and calculated P-wave arrivals. The error bars indicate the assigned error to the picked traveltimes. Solid lines show the traveltimes calculated using the final velocity model shown in Fig. 4.11. The lower parts are respective paths of rays calculated by rayinvr.

inversion method of *rayinvr*. Raytracing examples of 4 stations of each line are shown in Figures 4.7 and 4.8. They show the good fit of the observed and calculated traveltimes and the generally dense sampling by the rays.

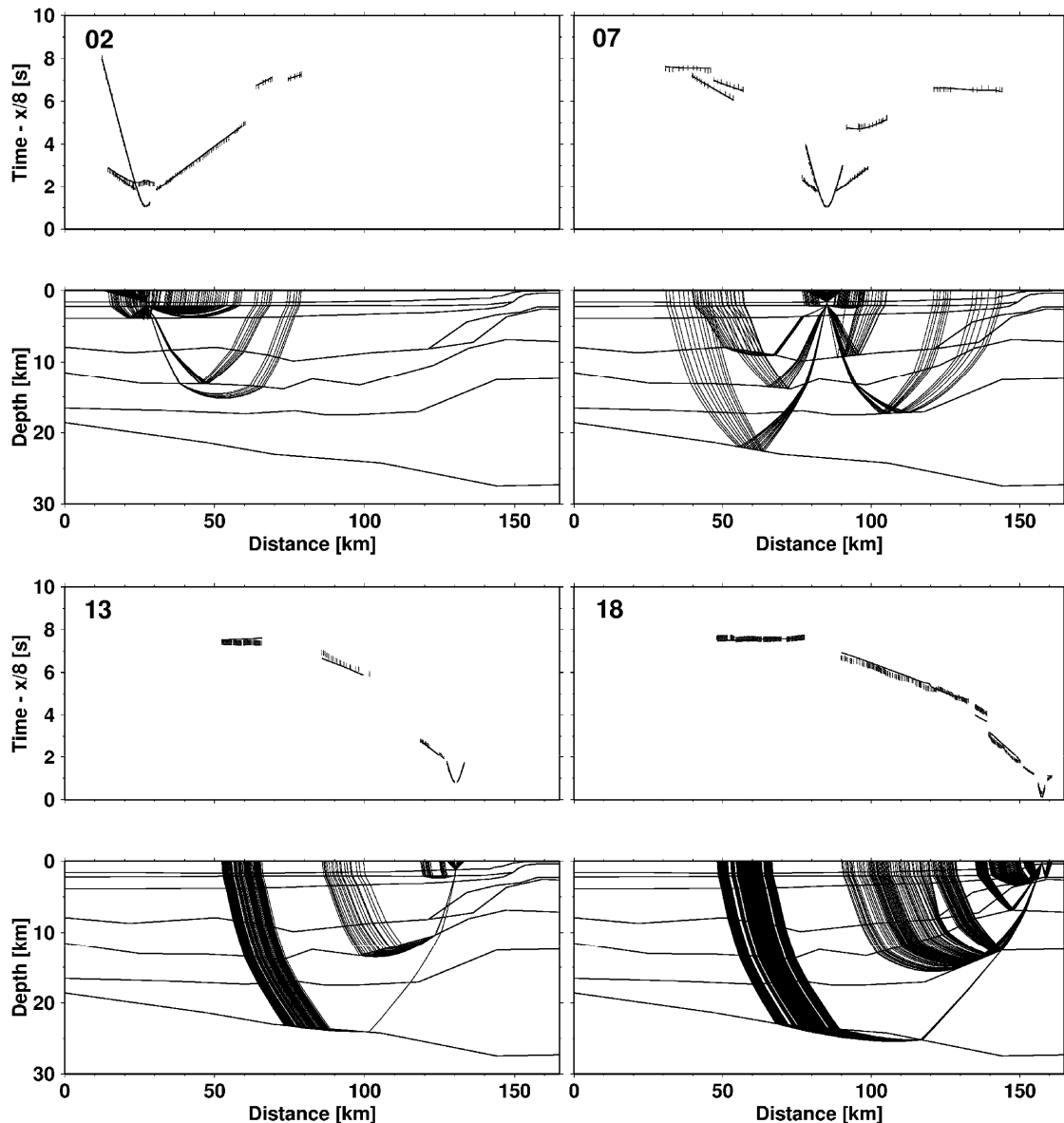


Figure 4.8 Examples of raytracing along Profile P2 from stations 02,07,13,18. The upper parts again show the observed and calculated P-wave arrivals. The error bars indicate the error assigned to the picked traveltimes. Solid lines show the traveltimes calculated using the final velocity model shown in Fig. 4.12. The lower parts are respective paths of rays calculated by rayinvr.

4.5.1 Resolution and uncertainty of the modelled velocity structure

The reliability of the final velocity structure is expressed in the resolution calculated by the inversion algorithm of *rayinvr* (Zelt and Smith 1992). This quantitative approach is based on the relative number of rays which determine the parameterization of the model, i.e. the velocity nodes. According to Zelt and Smith (1992) resolution values of 0.5 or greater are considered to be well resolved. A resolution is calculated for each velocity node in the final model and then interpolated into a 2.5 x 0.25 km grid (Figures 4.9 and 4.10), velocity and boundary uncertainties were fixed at 0.2 km/s and

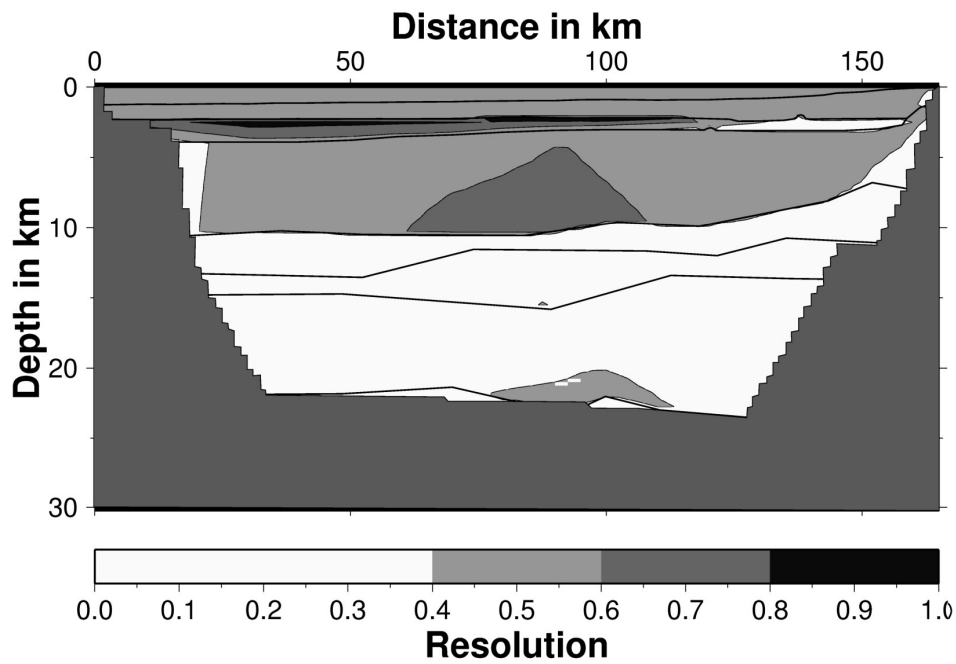


Figure 4.9 Resolution of final P-wave velocity model of P1 calculated by rayinvr. Resolution is shown in grayshade intervals. The resolution values represent the values of the main diagonal of the resolution matrix of the p-wave velocity depth model. Maximum resolution is represented by the value of 1. Smaller values denote a spatial averaging of the true earth by a linear combination of model parameters. (Zelt 1999). According to Zelt and Smith (1992), resolution values greater than 0.5 are considered well-resolved and reliable, although this is only an empirical value.

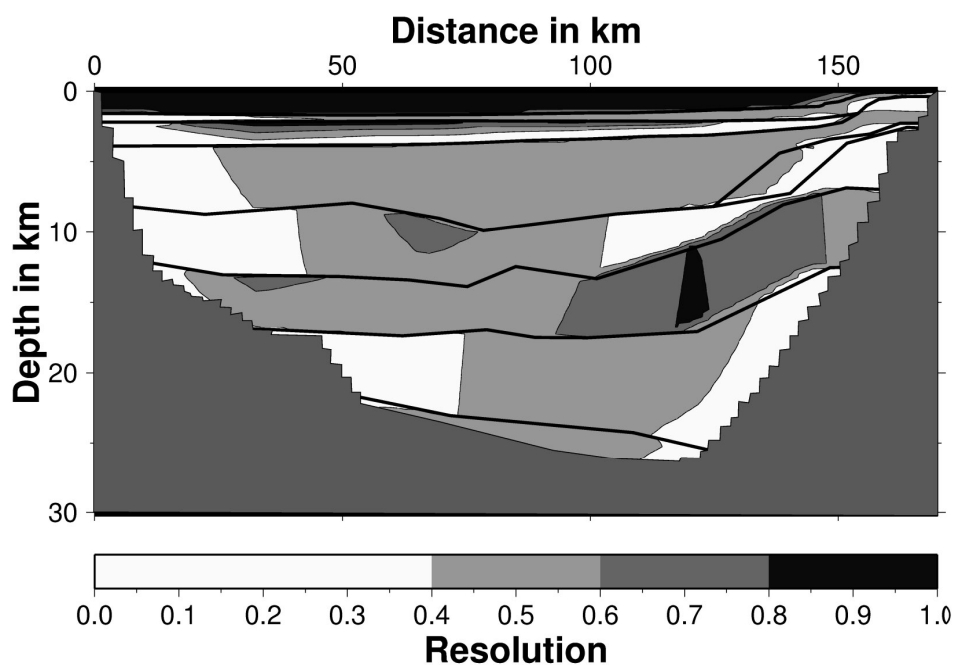


Figure 4.10 Resolution of final P-wave velocity model of P2 calculated by rayinvr. Resolution is shown in grayshade intervals. See fig. 4.9 for explanation.

| Line P1 | | | | |
|----------------|-------------|-----------------|-----------------------|----------|
| Phase | Points used | Uncertainty [s] | Traveltime misfit [s] | χ^2 |
| Pw | 430 | 0.020 – 0.125 | 0,079 | 2,087 |
| PeP | 276 | 0.020 – 0.125 | 0,094 | 1,502 |
| Pe | 553 | 0.035 – 0.125 | 0,070 | 1,145 |
| PcarbP | 139 | 0.035 – 0.075 | 0,056 | 0,826 |
| PcuP | 109 | 0.035 – 0.080 | 0,084 | 1,196 |
| PclP | 28 | 0.050 – 0.100 | 0,089 | 0,988 |
| PmP | 87 | 0.035 – 0.100 | 0,085 | 0,864 |
| Pn | 56 | 0.050 – 0.125 | 0,077 | 0,800 |
| Entire model | 1678 | - | 0,078 | 1,389 |

| Line P2 | | | | |
|----------------|-------------|-----------------|-----------------------|----------|
| Phase | Points used | Uncertainty [s] | Traveltime misfit [s] | χ^2 |
| Pw | 754 | 0.050 – 0.100 | 0,080 | 2,353 |
| PeP | 18 | 0.035 – 0.100 | 0,133 | 2,391 |
| Pe | 708 | 0.035 – 0.125 | 0,073 | 1,043 |
| PsuP | 63 | 0.035 – 0.125 | 0,113 | 2,297 |
| Psu | 5 | 0,100 | 0,164 | 3,359 |
| PslP | 190 | 0.035 – 0.125 | 0,091 | 1,112 |
| PcarbP | 80 | 0.050 – 0.125 | 0,204 | 6,247 |
| Pcarb | 45 | 0.075 – 0.125 | 0,149 | 1,758 |
| PcuP | 161 | 0.035 – 0.125 | 0,222 | 5,305 |
| Pcu | 63 | 0.050 – 0.125 | 0,121 | 0,988 |
| PclP | 222 | 0.075 – 0.125 | 0,154 | 1,591 |
| Pcl | 27 | 0.050 – 0.125 | 0,178 | 2,727 |
| PmP | 112 | 0.050 – 0.125 | 0,198 | 2,636 |
| Pn | 317 | 0.050 – 0.125 | 0,145 | 1,837 |
| Entire model | 2765 | - | 0,123 | 2,059 |

Table 4.1 Table showing the number of used points, the uncertainty values, the rms-traveltime misfits, and the χ^2 -normalized misfit parameters of each line, itemised after the individual phases.

0.5 km, respectively. The resulting calculated resolution of the model of profile P1 is shown in Fig. 4.9. It reveals a moderate resolution down to the top of the carbonate layer, but poor resolution below, except for a small part of the lower crust. One way to enhance resolution is to limit the number of nodes, but since the number of velocity nodes in both crustal layers and the carbonate layer was already reduced to five, the resolution of this model could not be improved any further. The resolution of the model of profile P2 is shown in Figure 4.10. Here, the resolution is satisfying throughout the model, with the exception of the edges and a part of the carbonate and the lower sediment layer.

Further constraints on the reliability of the velocity models are given by the rms-traveltime misfits and the χ^2 -normalized misfit parameters provided by *rayinvr*. The number of used picks, the rms-traveltime misfit and the χ^2 -values are given in Table 4.1. An χ^2 -value equal to 1 indicates that the data are fitted within their assigned uncertainties. χ^2 -values smaller than 1 refer to the presence of structures in the model not required by traveltime picks. This occurs mainly at the PmP and Pn of line P1

because of the small number of picks. According to Zelt and Smith (1992) small-scale heterogeneous structures and significant out-of-plane structural and velocity variations can increase χ^2 . According to Hirsch (1995) and Vidal et al. (2000a and b), the basement and the carbonate layer up to the Neogene sediments are noticeably faulted with significant vertical displacements. Such displacements cannot be resolved and lead to an increased χ^2 . Considering this the values in this study can be regarded as acceptable. Generally, stations on the slope produce higher misfits than stations in the basin. On P2, the highest χ^2 -values are reached at OBH 15 with 4.085, but most of the stations (01, 02, 03, 04, 05, 06, 07, 10, 11, 12, 13, 19 and the land station) achieve a χ^2 -value under 2.3.

4.6 Results

4.6.1 Profile 1

The model (Fig. 4.11) shows a layer of Plio-Quaternary sediments of 1.9 - 2.1 km/s above the evaporite layer with 4.3 - 4.4 km/s, as has already been shown on the MCS-lines. Under these layers, older sediments from Jurassic to Miocene are located with velocities of 3.5 - 3.9 km/s. These sediments lie on a layer of 4.4 - 4.8 km/s, respectively, which has been observed before (Ben-Avraham et al. 2002) and has been identified as marine carbonates that are interbedded among sandstones near the shelf (Garfunkel 2004). Two crustal layers are present throughout the model, the upper crust with 6.0 - 6.2 km/s, the lower crust with 6.4 - 6.8 km/s. The Moho lies at a depth of 22 - 23 km and the velocity of the uppermost mantle is determined on 7.8 km/s.

Small bulges are located in the top of the evaporite layer at 138 km and in the base at 120 km. These are below the resolution limit, but have been observed on the MCS line and included in the model. The bulge in the top of salt may be related to salt tectonics, but the one at the base of salt is an indication of deeper tectonic activity. The Pre-Messinian sediments show a change of velocity at 90 and 110 km, and at 25 km. At 25 km the velocity of the entire sediment package is reduced by ca. 200 m/s, while at 110 km only the upper section is involved, the velocity at the base of the sediments is not affected. The velocity variation at 90 km also involves the whole layer. Here the velocity gradient is significantly changed, the velocity stays almost constant from the top to the base of this layer. The carbonate layer and the crust, exhibiting an otherwise uniform velocity distribution, also comprise a zone of reduced velocity at 90 km. Thus this zone of reduced velocity extends from a depth of 4 km down to the Moho at 23 km. The gravity model shows a steep decline of the Moho under the shelf.

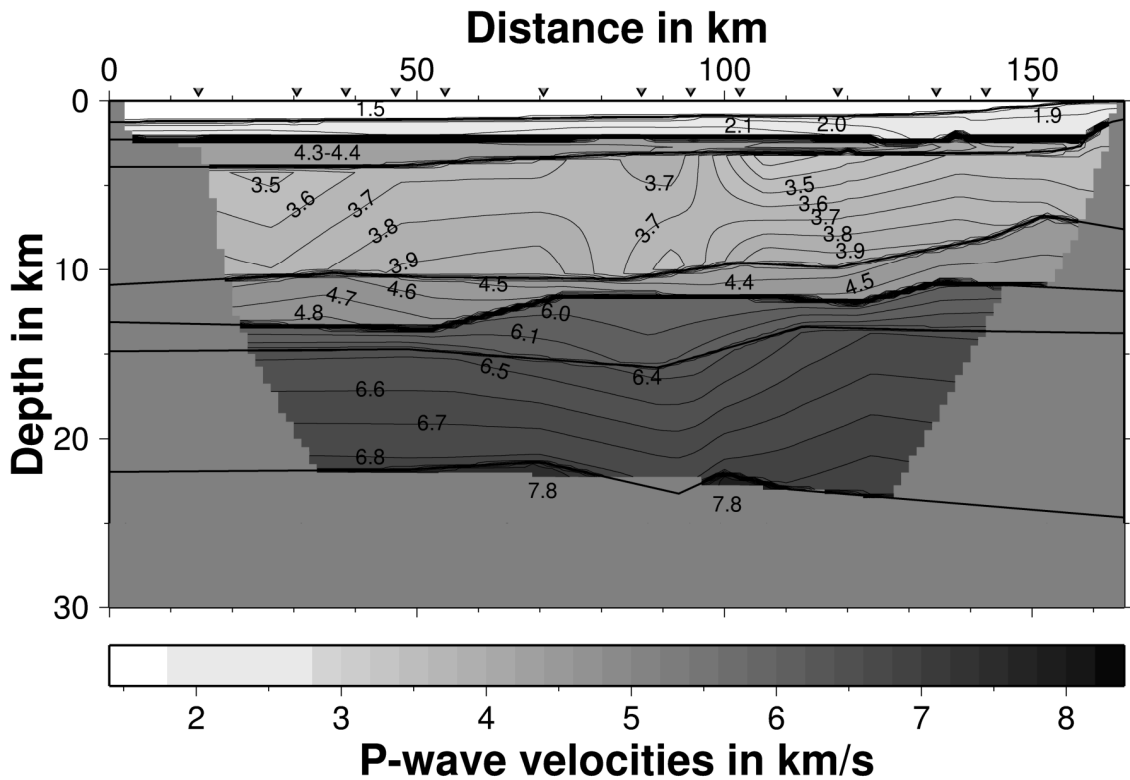


Figure 4.11 Final velocity model of line P1. Velocities (in km/s) are indicated by greyscale and contour lines where constrained by ray coverage. Thick black lines represent layer boundaries. Triangles mark the positions of the OBH.

4.6.2 Profile 2

The model of P2 (Fig. 4.12) shows a very similar layering to the model of P1. The Pre-Jurassic sediments have a slightly higher P-wave velocity of 3.7 - 4.4 km/s with a steeper velocity gradient. P2 also contains a second sediment layer of 4.5 - 4.6 km/s that forms a wedge at the bottom of the slope. The velocity of the carbonate layer is also higher with 4.6 - 4.9 km/s. Both crustal layers that appear in line P1, the upper crust with a velocity of 5.7 - 6.4 km/s and the lower crust with a velocity of 6.6 - 6.9 km/s are observed on profile P2. The velocities of the crustal layers are generally higher than in P1 by about 100 m/s and the upper crust shows a steeper gradient. The Moho drops from 22 to 26 km. The uppermost mantle exhibits a velocity of 7.8 to 7.9 km/s.

All layers show a uniform velocity distribution, only in the upper section of the Pre-Messinian sediments a variation in the velocity gradient is observed at 95 km. A very small velocity variation is observed at 75 km in the carbonate layer, accompanied by an unevenness along the boundaries of carbonates and upper crust. Unlike the model of P1, a significant thickening of the crust towards the shelf can be seen. This thickening takes place mainly in the lower crust, but also the upper crust increases its thickness from 4 km in the basin to 6 km near the edge of the model.

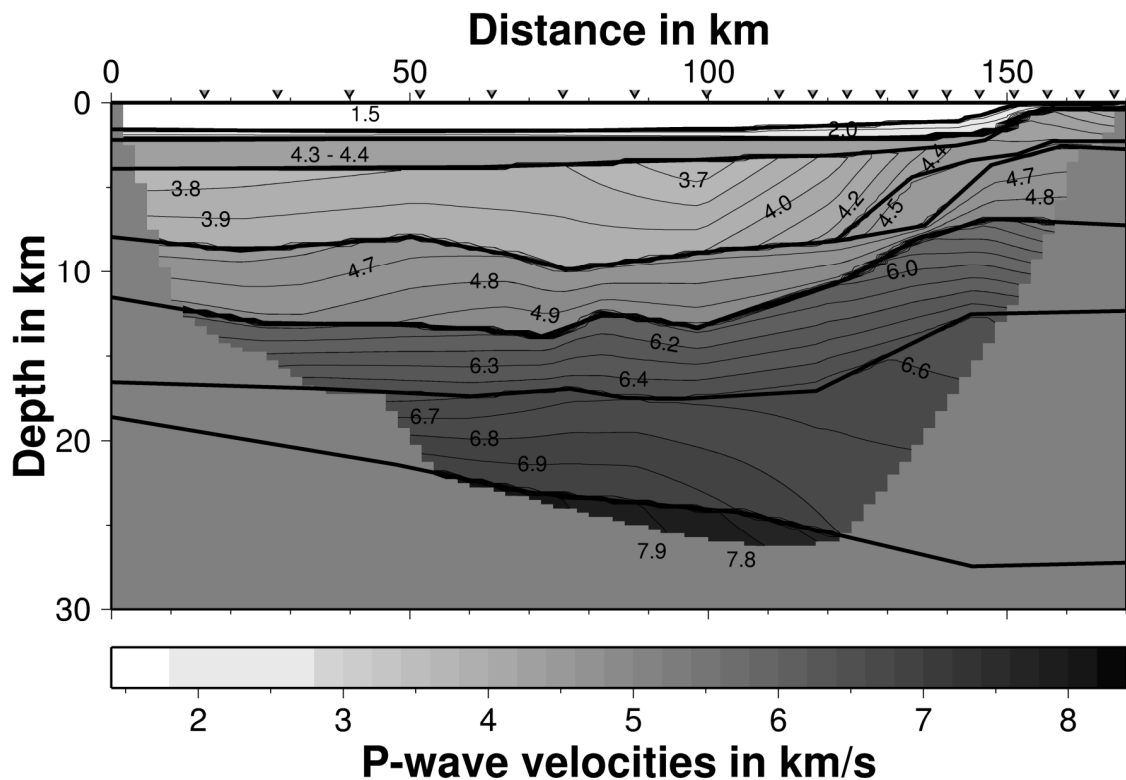


Figure 4.12 Final velocity model of line P2. Velocities (in km/s) are indicated by greyshades and contour lines where constrained by ray coverage. Thick black lines represent layer boundaries. Triangles mark positions of the OBH.

4.6.3 Gravity models

In order to provide a further constraint on the crustal structure free air gravity modelling was carried out along both lines, P1 and P2. The deduced density models are based on the results of the velocity models using common velocity-density relationships (e.g. Nafe and Drake 1963). The modelling was carried out using a 2-D modelling program based on Talwani et al. (1959). For both models the layer boundaries were kept fixed where constrained by seismic data. The misfit between observed and modelled free air anomaly is less than 10 mGal. This maximum misfit might seem large, but a look at a free air anomaly map of the Levantine Basin, based on satellite data by Sandwell and Smith (1997) shows that large anomalies lie off the lines P1 and P2 or run obliquely to the profiles (Fig. 4.13). Therefore a 2D-approach in gravity modelling can only yield limited accuracy. The density model of P1 (Fig. 4.14) confirms the velocity model. In order to fit the local minimum at 60 km an additional sediment block had to be modelled. Because of the short wavelength of this minimum it cannot be caused by a deeper body, e.g. in the crust. Towards the end of the line the thickness of both upper and lower crust has to increase to match the observed gravity values and compensate the effects of the shelf. On line P2 (Fig. 4.15), in comparison, free air gravity significantly increases at the end of the model and follows the bathymetry. On this line crustal thickening already occurs in the centre of the model, also visible in the velocity model. The additional sediment body in the velocity model near the shelf was modelled

together with the other Pre-Messinian sediments as one layer, since the best gravity fit was obtained with the same densities of both bodies.

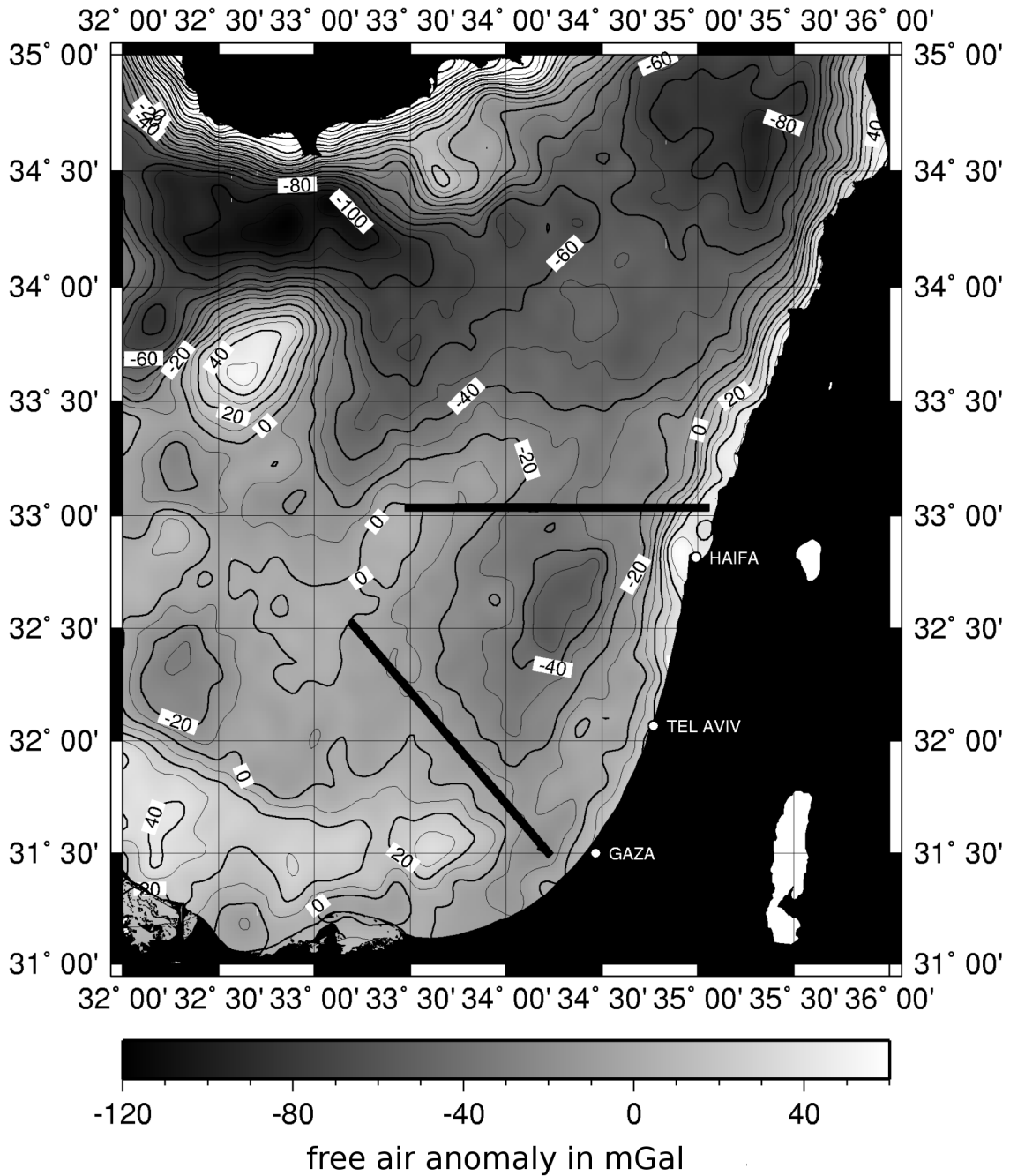


Figure 4.13 Free air anomaly map of the Levantine Basin, based on satellite data of Sandwell and Smith (1997). Solid lines mark the positions of profiles P1 and P2.

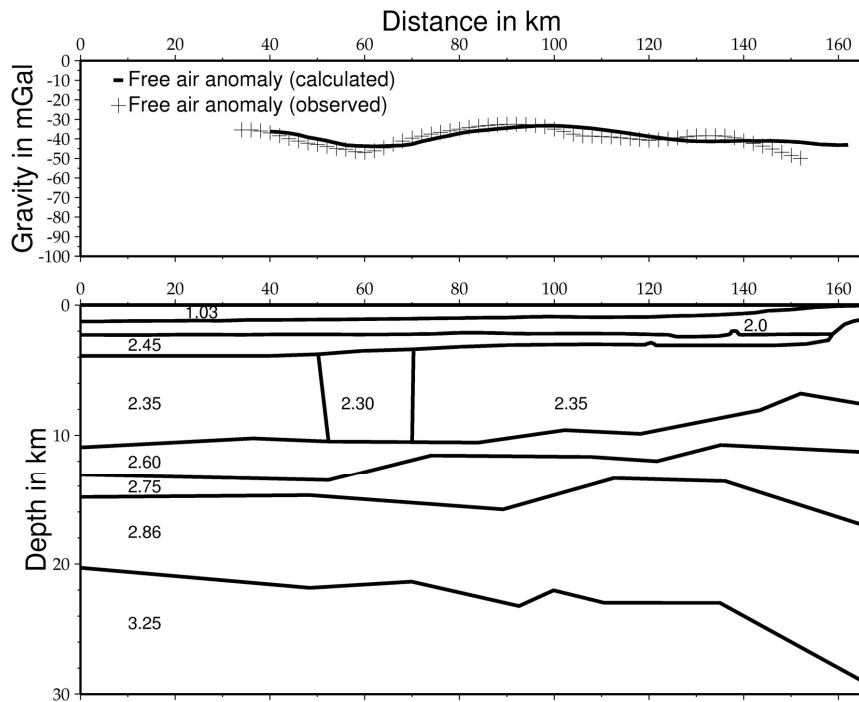


Figure 4.14 The upper part shows observed (+) and calculated (-) free air anomaly, based on the final 2D-density model of P1 shown in the lower part. Layer boundaries were retained from the velocity model where constrained by ray coverage. Maximum misfit is < 10 mGal.

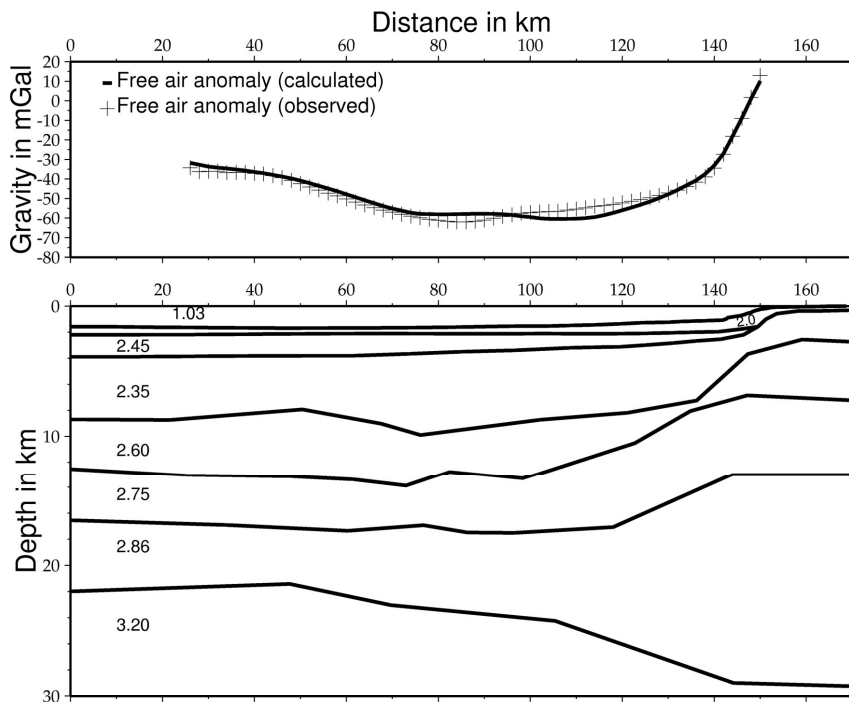


Figure 4.15 The upper part shows observed (+) and calculated (-) free air anomaly, based on the final 2D-density model of P2 shown in the lower part. Layer boundaries were retained from the velocity model where constrained by ray coverage. Maximum misfit is < 10 mGal.

4.7 Discussion

4.7.1 Velocity distribution and crustal structure

On line P1 lateral changes in the velocity gradient in the Pre-Messinian sediments are observed at 25 km, 90 km, and at 110 km. The change at 90 km, which also appears in the crust, coincides with the projection of the Pelusium Line on P1, and the change at 25 km coincides with the location of the Damietta-Latakia Line. The variation in the velocity structure at 110 km is not clearly associated with any known fault line or other structure.

On line P2 only one distinct change in the velocity gradient appears at 95 km. On the map of Neev et al. (1976) the Damietta-Latakia Line would meet the profile at approx. 75 km. An earthquake lineament runs along this line starting from about 33° N and continuing towards the Cyprus Arc (Fig. 4.1). At 75 km, only small velocity and boundary undulations are observed. These undulations are likely to be an effect of the Damietta-Latakia Line.

The Pelusium Line is projected to meet line P2 between 130 and 140 km. Here no velocity effects are visible. But at 120 km, the slope of the deeper sediment layers begins, so any velocity variation owing to the Pelusium Line might be masked by the slope and its steep layer boundaries. To sum up, indications of the known shear zones, Pelusium and Damietta-Latakia Line, are observed on both lines, although they are more pronounced on line P1. We also found evidence of shearing in yet unpublished industrial MCS data of the Levantine Basin. Since shear zones are much more common in continental than in oceanic crust, this is a first indication of continental crust in the Levantine Basin.

In general, the velocities of the lower crust cannot be classified as either typical of oceanic or continental crust, but with 6.4 - 6.9 km/s they would be remarkably low for oceanic crust, especially if the - for oceanic crust - anomalously great depth and resulting pressure is considered. In theory, increased heat flux and higher crustal temperature might decrease the velocities in the lower crust. Heat flow maps of the Eastern Mediterranean Sea (Makris and Stobbe 1984, Jiménez-Munt et al. 2003) do not show increased heat flow values in the Levantine Basin. Heat flow values range between 40 and 60 mW/m² (Jiménez-Munt et al. 2003) and 38 - 67 mW/m² (Makris and Stobbe 1984). Sediments account for approx. additional 12 mW/m² (Ben-Avraham et al., 2002). This agrees as well with the average heat flow value of 51 - 62 mW/m² given for oceanic crust of Late Jurassic to Late Cretaceous age (Pollack et al. 1993), as expected for the Levantine Basin. But it agrees just as well with the average heat flow value of 65 mW/m² of continental crust (Pollack et al. 1993). Hence the heat flow values are not specific of either type of crust, but a decrease of velocity in the lower crust due to thermal sources and increased crustal temperature can be excluded and no correction of the velocity of the lower crust is necessary. Therefore the velocity of the

lower crust rather supports the assumption of continental crust.

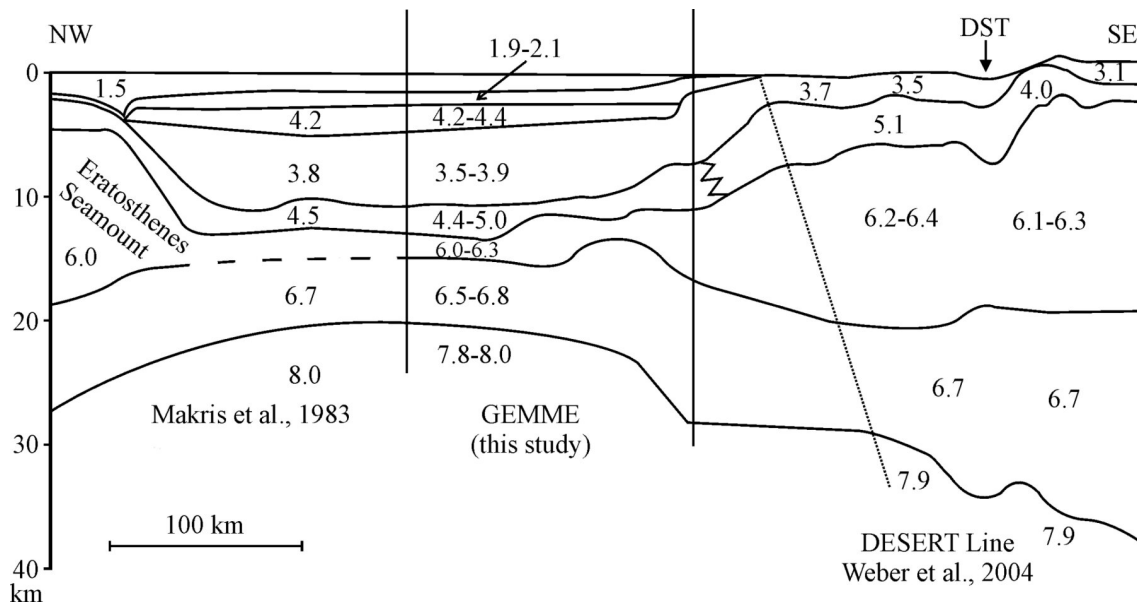


Figure 4.16 Compilation model from Eratosthenes Seamount over Levantine Basin into Jordan, based on the previous velocity model of Makris et al. (1983), the crustal model of the DESERT2000-line and line P1 of this study (see Fig. 4.1 for location). Dashed line marks suggested continuation of intercrustal layer boundary observed on P1 and DESERT2000-line, but not in the model of Makris et al. (1983). Dotted lines mark the limits of each survey, vertical zigzag indicates transition from marine carbonates to sandstone.

The crustal velocities found onshore by Ben-Avraham et al. (2002) only slightly south of line P2 and the crustal velocities of line P2 are in good agreement. Ben-Avraham et al. (2002) find an average P-wave velocity of 6.3 km/s in the upper and 6.7 km/s in the lower crust, which match the 6.0 - 6.4 km/s in the upper crust of line P2 and the 6.6 - 6.9 km/s in the lower crust. A compilation of the results of the DESERT2000-project (Weber et al., 2004), profile III of the study of Ben-Avraham et al. (2002) and our line P1 (Fig. 4.16), which are almost in line (Fig. 4.1) reveals a very good correspondence between the crustal structure and velocities under Israel and Jordan and the model of P1. The continuation with profile III of Ben-Avraham et al. (2002) shows a matching Moho depth, but there only one crustal layer was detected. Since the study of Ben-Avraham et al. (2002) was based on fewer receivers and a greater receiver spacing, the velocity models obtained from our study should be considered as more reliable. Figure 4.4 shows the ray coverage of the upper crust on line P2. It shows not only reflections from the boundary between the upper and the lower crust, but also rays which are refracted within the upper crust. The arrivals corresponding with these rays are directly related to the p-wave velocity in the upper crust and confirm the presence of a layer of another p-wave velocity than that in the lower crust. Therefore a velocity model with 2 crustal layers fits our data much better than a model with only 1 crustal layer.

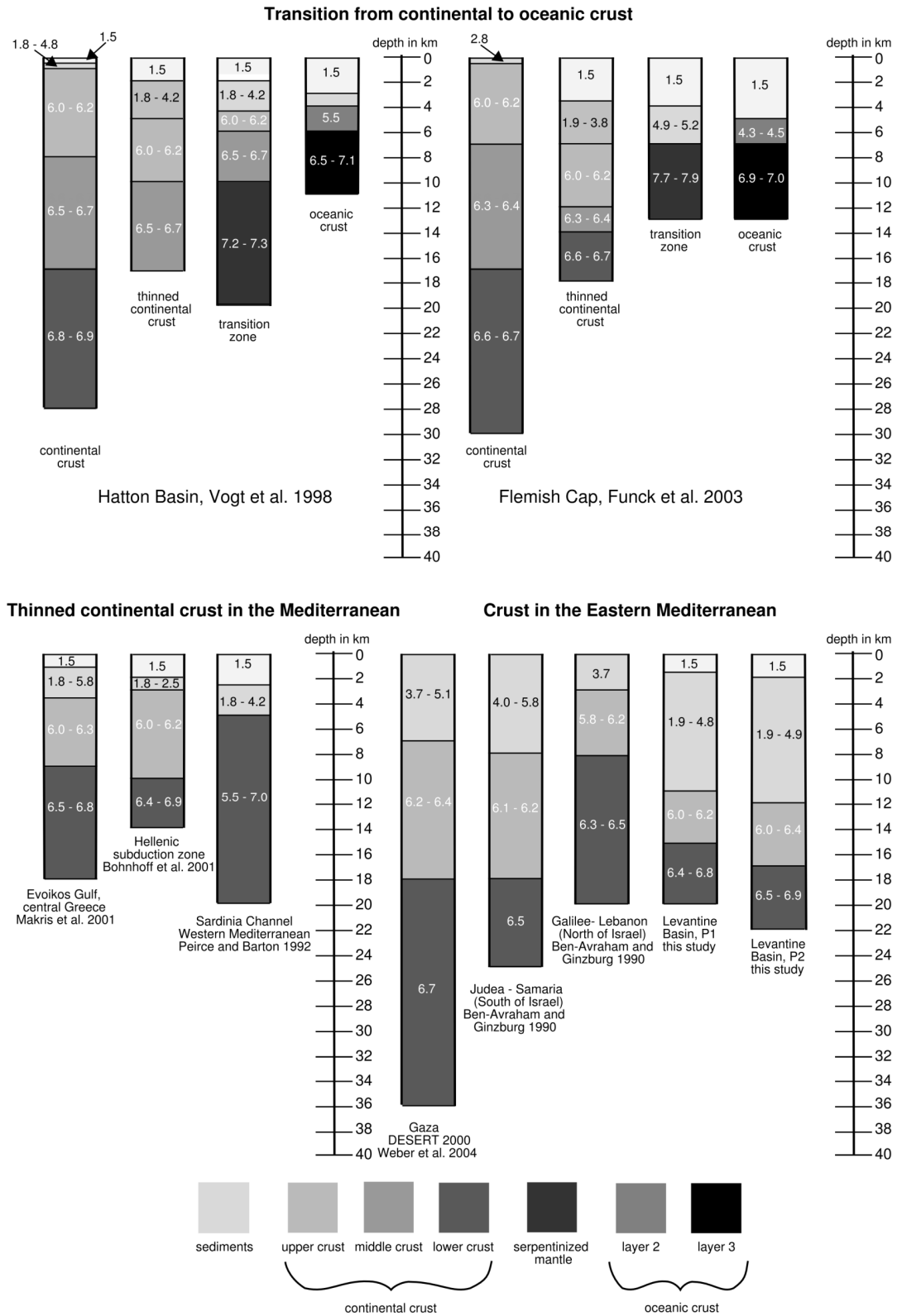


Figure 4.17 Compilation of 1d velocity-depth profiles. The numbers denote p-wave velocities in km/s. Top: Examples of transitions from continental to oceanic crust. Bottom left: Examples of thinned continental crust in the Mediterranean Sea. Bottom right: velocity-depth profiles of the Levantine Basin and adjacent areas.

The crustal velocities found on the DESERT2000-line are 6.1 - 6.4 km/s in the upper crust and 6.7 km/s in the lower crust. These are slightly higher than the velocities on line P1 with 6.0 - 6.2 km/s and 6.5 - 6.8 km/s, respectively, and slightly lower than on line P2 with up to 6.4 km/s in the upper and 6.6 - 6.9 km/s in the lower crust, which can be considered a good match and further supports the hypothesis of continental crust extending into the Levantine Basin.

The thickness ratio of upper crust to lower crust varies between 1:3 and 2:5 on line P1 and 1:2 and 2:3 on line P2. However, with an uncertainty of 0.5 km and thicknesses of 2 - 4 km in the upper crust and 6 - 9 km in the lower crust the uncertainty in the thickness ratio can reach 70 %. Considering this, and taking into account that the resolution values in the crust of line P1 is relatively low, any considerations of changes in the thickness ratio and crustal flow are futile.

The Moho depth lies between 22 and 26 km and the combined thickness of both layers varies between 8 and 18 km. Although in the seismic survey of Makris et al. (1983) and Ben-Avraham et al. (2002) only one crustal layer could be detected, the same Moho depths were found. On the basis of 1-D velocity-depth profiles yielding different Moho depths under Judea-Samaria and Galilee-Lebanon (Fig. 4.17), different velocities in the upper crust with 6.0 km/s and a Moho depth of 20 km and 6.3 km/s and 25 km, respectively, Ben-Avraham and Ginzburg (1990) suggested those were different terrains. In our study the average velocities of the upper crust are about 6.1 and 6.2 km/s on P1 and P2, respectively. This small difference does not point to the existence of different crustal blocks or terrains in the basin.

Although the model of the crustal structure resulting from this study can neither be classified as typically oceanic nor as typically continental, it is comparable with those of other areas of thinned continental crust in the Mediterranean Sea (Fig. 4.17). Bohnhoff et al. (2001) analysed three seismic refraction profiles in the southern Aegean across Crete and found continental crust under Santorini and further south, with a Moho depth between 15 and 33 km and a crustal thickness of approx. 13 km. The crust under Santorini consists of two layers with velocities between 6.0 - 6.4 km/s in the upper crust and 6.5 - 6.9 km/s in the lower crust, which is comparable to our results. A seismic refraction survey of Makris et al. (2001) in central Greece has yielded a similar crustal structure, i.e. they also find thinned continental crust with a Moho depth as low as 18 km, a crustal thickness of 13 km, overlain by sediment layers of several km thickness. The specific velocities of the upper and lower crust are given as 6.0 - 6.3 km/s and 6.5 - 6.8 km/s, respectively, and the ratio in thickness of upper to lower crust varies between 2:3 and 2:5. Peirce and Barton (1992) analysed a refraction seismic profile in the Sardinia Channel as part of the European Geotraverse program. They found only one crustal layer between Sardinia and Tunisia thinning from 24 to 10 km in thickness with a central Moho depth of 18 km and identified it as thinned continental crust. In general, the continental crust in the Mediterranean Sea seems to consist of not more than two layers. Outside the Mediterranean Sea, in the Galicia Interior Basin offshore Portugal, at a rifted non-volcanic margin, Pérez-Gussinyé et al. (2003) find thinned continental crust

which exhibits a transition in crustal structure from three layers to two layers. They interpret this transition as a suture separating two terrains with different crustal characteristics. Hauser et al. (1995) find such a transition from a three-layer to a two-layer crust in the Rockall Trough and offer another explanation for the disappearance of a third crustal layer. They postulate that the stretching of the crust modifies it and causes amalgamation of the upper and the middle crust into only one seismically detectable layer. Since throughout the Mediterranean Sea considerably attenuated continental crust is found, it is conceivable that this crust had been structured in three layers, but has been modified by thinning into a crustal composition of two layers.

The assumption of oceanic crust requires a transition from continental to oceanic crust. An abrupt transition is not observed on either line, but the rise of the Moho from 26 to 22 km on line P2 and from 27 km (Weber et al. 2004) near Gaza to 22 km on line P1 could mark a zone of a gradual transition from continental to oceanic crust. Such a transition zone has been observed elsewhere, e.g. at the Hatton margin offshore Ireland (Vogt et al., 1998), at the Flemish Cap off New Foundland (Funck et al. 2003) and in Nova Scotia (Funck et al. 2004). In Nova Scotia and at the Flemish Cap the transition zones are characterized by an extremely thinned crust of 2 - 3 km overlying serpentinized mantle of 7.2 - 7.6 km/s (Nova Scotia) or 7.7 - 7.9 km/s (Flemish Cap). This layer is significantly faster than the lower continental crust with 6.6 to 6.9 km/s. A strong decrease of Moho depth from 30 to 10 km (Flemish Cap) and 37 to 13 km (Nova Scotia) is also observed. At the Hatton margin crustal thinning from 20 to 5 km is observed along with a decrease in Moho depth from 22 to 12 km (Fig. 4.17). Under the extremely thinned crust, magmatic underplating has taken place, and the underplated body has a velocity of 7.2 - 7.3 km/s compared to 6.8 - 6.9 km/s of the lower crust. Common features of these three transition zones from continental to oceanic crust are extremely thinned crust of only a few km above a layer of a velocity > 7.0 km/s, which is higher than the velocity of the adjacent lower continental crust and a distinct decrease in Moho depth. In both the models of P1 and P2, neither a body with a velocity > 7.0 km/s, nor extremely thinned crust of 5 km or less are observed. The comparatively gentle rise of the Moho from 27 to 22 km, the decrease in thickness from 18 to 8 km and the stable velocity gradient from 6.4 - 6.8 km/s (P1) and 6.5 - 6.9 km/s (P2) show little similarity to the transition zones seen at Nova Scotia, at the Flemish Cap or at the Hatton margin. They rather suggest continuous, thinned continental crust in the Levantine Basin. A comparison with the Galicia Interior Basin (Pérez-Gussinyé et al., 2003) where the Moho depth decreases from 22 to 14 km, and the crustal thickness from 18 to 8 km, but the velocity stays constant at 6.6- 6.9 km/s reveals much more similarity with the Levantine Basin and suggests that in the Levantine Basin, similar to the Galicia Interior Basin, rifting took place, but the stage of continental break-up and seafloor spreading was not reached.

4.7.2 β -factor

The stretching factor (β -factor) is defined as the ratio between the crustal thickness before and after stretching. On both lines P1 and P2 the crust thins to a thickness of 8 km, but the β -factor strongly depends on the initial thickness. Taking the present crustal thickness of 18 km under Galilee or Judea-Samaria as initial (Ben-Avraham et al. 2002), the resulting β -factor would be 2.25, but according to Weber et al. (2004) the crustal thickness increases continuously from Israel into Jordan to almost 40 km (Fig. 4.17). Considering 40 km as the initial thickness and assuming that the crust under Galilee is already thinned, the β -factor would increase to 5. A β -factor of > 2 is found in several regions in the Mediterranean Sea. Peirce and Barton (1992) find a decrease in crustal thickness in the Sardinia Channel from 24 to 10 km, which would yield a β -factor of 2.4. Bohnhoff et al (2001) find the crust near Crete thinning from 28 to 13 km, yielding a β -factor of 2.2, and according to Makris et al. (2001) the crustal thickness in the Evoikos Gulf in Central Greece decreases from 27 to 13 km, which results in a β -factor of 2.1. Comparing these results with the Levantine Basin a β -factor of 2.25 seems reasonable and not unusual.

A β -factor as high as 5 can also be found in other regions. E.g. Hauser et al. (1995) find a β -factor of 4 - 6 in the Rockall Trough offshore Ireland, assuming an initial crustal thickness of 30 km. Funck et al. (2004) calculate a β -factor of 4.4 with an initial thickness of 35 km in Nova Scotia, and Pérez-Gussinyé et al. (2003) find a β -factor of even 5.3 in the Galicia Interior Basin. These comparisons show that even an assumption of 40 km initial crustal thickness and the resulting β -factor of 5 in the Levantine Basin do not rule out the possibility of thinned continental crust. Taking the present 18 km crustal thickness under Galilee as the initial thickness, the resulting β -factor of 2.25 could even be classified as typical of thinned continental crust in the Mediterranean region.

4.7.3 Implications

The assumption of continental crust in the Levantine Basin allows the following consideration: According to Buck (1991) continental lithospheric extension can be divided into 3 modes, the narrow rift mode, the wide rift mode, and the core complex mode. The narrow rift mode is characterized by a narrow region (< 100 km) of extensional faulting, a large lateral gradient in crustal thickness, a low initial heat flow of approx. 60 mW/m^2 , and a Moho temperature of $< 750 \text{ }^\circ\text{C}$. In the wide rift mode, the region of extension can be as large as 800 km, the lateral gradient in crustal thickness is small, the initial heat flow approx. 80 mW/m^2 , and the Moho temperature is $> 750 \text{ }^\circ\text{C}$. The core complex mode results from extension at a high strain rate over a narrow (< 100 km) region and a high initial heat flow of 100 mW/m^2 , accompanied by a very high Moho temperature.

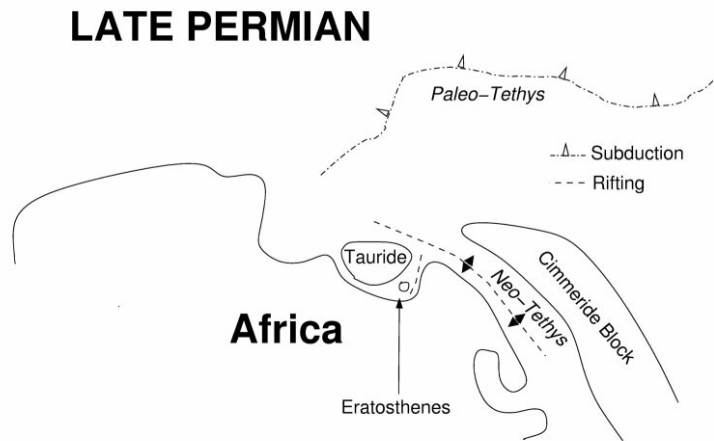


Figure 4.18 a) Reconstruction, modified after Garfunkel (1998). In the onset of the opening of the Neo-Tethys many rifting axes existed, and an extensional regime moved the Eratosthenes Seamount north-west.

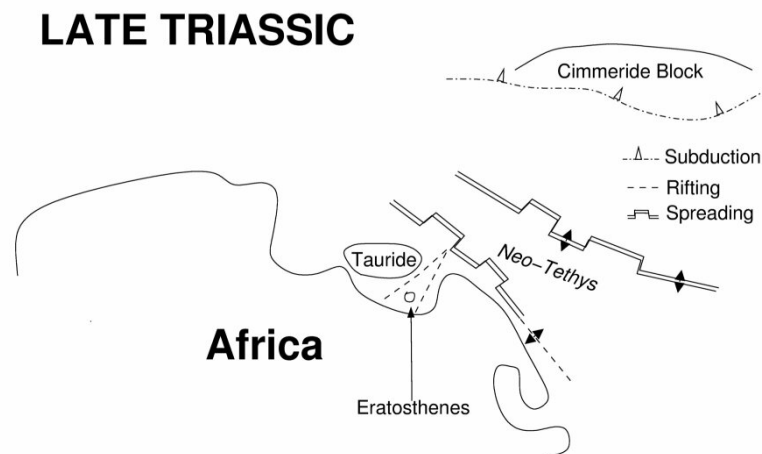


Figure 4.19 b) Continuation of the reconstruction into the Trias, likewise modified after Garfunkel (1998). The rifting axis south of the Cimmeride block has become a spreading axis, and Garfunkel also postulates a second spreading axis further north. The rift south-east of the Eratosthenes is still active, but does not reach the stage of seafloor spreading. The crust is significantly thinned, but still continental.

Considering the distance of max. 250 km between the continental fragment of the Eratosthenes Seamount and the Israeli margin, the region of the rifting in the Levantine Basin must have been narrow. Extensional faults are not resolved in the velocity models and are masked by salt tectonics in MCS lines, but Hirsch et al. (1995) show extensional faults over a range of ≈ 110 km. Although on both P1 and P2 rather small lateral gradients in crustal thickness are observed, these findings support the assumption of extension in the narrow rift mode in the Levantine Basin. Thus the heat flow at the time of extension was probably not significantly higher than presently, viz 50 - 60 mW/m².

Pérez-Gussinyé et al. (2003) suggest a deformation model for the Galicia Interior Basin with an initially cold and thin crust, where at the beginning of the rifting, the upper rocks deformed brittlely and the lower crustal rocks ductily without significant lower crustal flow. With $\beta < 2$ the ratio in thickness of upper to lower crust stays constant, the extension occurred by pure shear. With increasing extension lower crustal rocks cooled, changed from plastic to brittle deformation, and at $\beta > 3.5$ faults began to reach into the crust and on a small scale lower crustal flow started in the direction opposite to fault dip. The extrapolation of $\beta > 5$ yields purely brittle deformation of the crust, faults reaching into the mantle and leading to serpentinization. In order to explain the faults in the crust observed by Hirsch et al. (1995), an intermediate β -factor of ~ 3 would be required according to Pérez-Gussinyé et al. (2003), corresponding with an initial crustal thickness of 24 km. Since we do not have any further constraints, e.g. on the rheology of the crust, a detailed analysis of the rifting process is left to speculation. However, based on our interpretation of continental crust in the Levantine Basin we suggest a modification of the paleo-reconstruction of Garfunkel (1998) (Fig. 4.18a,b). The Paleo-Tethys is subducted in the Late Permian (Fig. 4.18a). Two stages of rifting follow, the first from Late Permian to Early Triassic, the second from Late Triassic to Early Jurassic (Walley 1998). In the late Triassic the rifting axis running E-W develops into a seafloor spreading axis opening the Neo-Tethys and thus oceanic crust is generated. The N-S rifting south-east of the Eratosthenes Seamount does not reach the stage of spreading, and the Levantine Basin develops as a continental basin above stretched continental crust.

According to Walley (1998), extensional faults in both trends, E-W and NNE-SSW, represent zones of weakness during the compressional Syrian Arc events from the Late Cretaceous to the Early Miocene and develop into fold chains. We find only weak evidence of the NNE-SSW trending Pelusium and Damietta-Latakia Lines. Where those lines cross our profiles, a little crustal thickening is observed.

4.8 Conclusions

Velocity distribution and structure of the crust along both profiles neither exhibit typical features of oceanic nor of continental crust, but resemble those of thinned continental crust found in other parts of the Mediterranean Sea. Comparison with the results of the DESERT2000-group (Weber et al., 2004) shows similarities in both structure and velocity distribution and confirms the hypothesis of continental crust in the Levantine Basin. The β -factor can only be estimated at a value between 2.25 and 5, depending on the choice of initial crustal thickness between 18 km under Galilee or 40 km under Jordan, but an assumption of 24 km yielding a β -factor of 3 seems reasonable. A comparison of the models of P1 and P2 with models of known ocean-continent-transition zones and a rifted continental margin that did not reach the stage of seafloor-spreading has revealed more similarities to the merely rifted margin than with the ocean-continent transition, which further confirmed our postulation of continental crust

in the Levantine Basin.

Acknowledgements

We would like to thank the crew and scientific staff of RV Meteor for the excellent support. Thanks to Lea Scharff for carrying out the depth migration, to Hillel Wust-Bloch for setting up the onshore station, and to Jan Grobys for intense discussions and countless helpful tips. Figures 4.1, 4.7, 4.8, 4.9, 4.10, 4.11, 4.12, 4.13, 4.14, and 4.15 were created with GMT (Wessel and Smith 1998). The GEMME project was funded by DFG grant HU698/07.

5 The structural evolution of the Messinian Evaporites in the Levantine Basin

(G. L. Netzeband, C. P. Hübscher, D. Gajewski, submitted to *Marine Geology*, December 2005)

Abstract

The Levantine Basin in the South-eastern Mediterranean Sea is a world class site for studying the initial stages of salt tectonics driven by differential sediment load, because the Messinian evaporites are comparatively young, the sediment load varies along the basin margin, they are hardly tectonically overprinted, and the geometry of the basin and the overburden is well-defined. In this study we analyse depositional phases of the evaporites and their structural evolution by means of high-resolution multi-channel seismic data. The basinal evaporites have a maximum thickness of about 2 km, precipitated during the Messinian Salinity Crisis, 5.3 - 5.9 Ma ago. The evaporite body is characterized by 5 transparent sequences bounded by four internal reflections. We suggest that each of the internal reflections indicate brittle evaporites, possibly interbedded clastic sediments, which were deposited during temporal sea-level rises. All of these internal reflections are differently folded and distorted, proving that the deformation was syn-depositional. Thrust angles up to 14 degrees are observed. Backstripping of the Plio-Quaternary reveals that salt tectonic is mainly driven by the sediment load of the Nile Cone. The direction of lateral salt displacement is mainly SSW - NNE and parallel to the bathymetric trend. Apparent rollback anticlines off Israel result rather from differential subsidence than from lateral salt displacement. In the south-eastern basin margin slumps are observed, which are coeval to a number contractional faults, providing a link between slumping processes and salt tectonics.

The superposition of 'thin-skinned' tectonics and 'thick-skinned' tectonics becomes apparent in several locations: The fold belt off the Israeli Mediterranean slope mainly results from active strike-slip tectonics, which becomes evident in faults which reach from the seafloor well below the base of the evaporites. Owing to the wrenching of the crustal segments which are bounded by deep-rooted fault lines like the Damietta-Latakia, Pelusium and Shelf Edge Hinge line the setting is transpressional south of 32°N, where the fault lines bend further towards the west. This adds a component of 'thick-skinned' transpression to the generally 'thin-skinned' compressional regime in the basin. Above 1.5 km of evaporites, a mud volcano is observed with the mud source seemingly within the evaporite layer. At the eastern Cyprus Arc, the convergence zone

of the African and the Anatolian plates, deep-rooted compression heavily deformed the base of the evaporites, whereas at the Eratosthenes Seamount mainly superficial compression affecting the Post-Messinian sediments and the top of the evaporites is observed.

Key words: Levantine Basin, salt tectonics, Messinian evaporites, slump, mud volcano, reflection seismic data

5.1 Introduction

During the Messinian Salinity Crisis, 5.9 - 5.3 Ma ago, thick evaporite layers were deposited in the main basins of the entire Mediterranean Sea (Hsü et al. 1973). The Messinian evaporites were the target of two DSDP legs (Hsü et al. 1973, 1978) and a number of other studies (e.g. Cohen 1993, Clauzon et al. 1996, Gradmann et al. 2005). The evaporite facies are differentiated in basinal and marginal evaporites (Garfunkel and Almagor 1984, Cohen 1993, Gradmann et al. 2005). The marginal evaporites, mainly consisting of gypsum, anhydrite, carbonates and intercalated shales, are known from offshore and onshore drillings in Messinian and Pre-Messinian drainage channels (Gvirtzman and Buchbinder 1978, Garfunkel et al. 1989, Druckmann et al. 1995). The basinal evaporites presumably consist mainly of halite (e.g. Cohen 1993). Drilling in these basinal facies did not reach the halite layer, but only an upper evaporitic layer with several tens of meters of carbonates and gypsum interspersed with Nile sediments. The reflection marking the bottom of the Messinian evaporites has been termed N-reflection and that marking the bottom of the Plio-Quaternary overburden has been termed M-reflection (Ryan et al. 1970). The M-reflection constitutes an erosional unconformity in the entire Mediterranean Sea (Hsü et al. 1973, Almagor 1984).

Salt tectonics as described by e.g. Letouzy et al. (1995) and Waltham (1997) can be studied at the initial stages, because of the comparatively young age of the evaporites and because of little tectonic overprint. Gradmann et al. (2005) have investigated Post-Messinian deformation in the basin in E - W direction off northern Israel. In this study we analyse the interrelation between thick-skinned tectonics, differential sediment load and subsidence, and salt tectonics in the entire Levantine Basin. This includes a discussion of the impact of the sediment load of the Nile Fan on north-south directed gravity gliding and of the importance of the Eratosthenes Seamount as a potential backstop.

5.2 Regional setting

The Levantine Basin lies in the south-eastern Mediterranean Sea and is considered to be a relic of the Mesozoic Neo-Tethys Ocean (Robertson and Dixon 1984, Garfunkel 2004). It opened during several rifting stages in the Triassic (Garfunkel 1998, Robertson 1998). Whether the crust underneath the basin is of oceanic origin or stretched continental crust has been a matter of debate for many decades (e.g. Woodside 1977, Makris et al. 1983, Dercourt et al. 1986, Hirsch et al. 1995, Ben-Avraham et al. 2002), but recent studies indicate that the crust in the Levantine Basin is of continental origin (Vidal et al. 2000a, Gardosh and Druckman 2006, Netzeband et al. *accepted January 2006*).

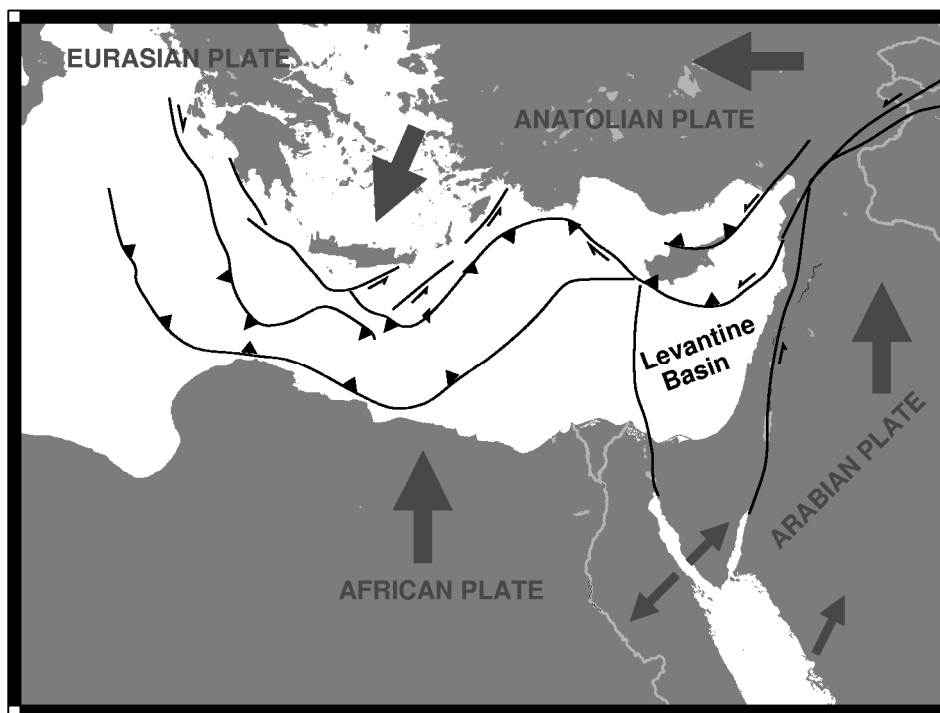


Figure 5.1 Simplified tectonic map of the Eastern Mediterranean Sea. Arrows indicate the sense of plate motion, half arrows indicate transform/strike-slip faults.

This area represents a very complex tectonic environment, which includes the northward moving African plate, the postulated Sinai-sub-plate (Almagor 1993, Mascle et al. 2000), the N - NW moving Arabian plate, and the westward moving Anatolian plate (Fig. 5.1). The rotational movement of the Anatolian plate is accommodated by dextral strike-slip along the North Anatolian Transform Fault and corresponding sinistral strike-slip on the East Anatolian Transform Fault (Hall et al. 2005). The convergence rate of the African and the Eurasian plates in the Levantine Basin is approx. 1 cm/yr (Jiménez-Munt et al. 2003, Kempler and Garfunkel 1994). According to Vidal et al. (2000b) the Cyprian Arc represents the current plate boundary between the African and Anatolian plates. They find that the African-Anatolian plate boundary is not a sharp boundary but a wide zone bounded by two strike slip fault systems. The lack

of strong earthquakes of intermediate depth at the Cyprus Arc indicates that subduction stopped there, and the plate movement supposedly has a large transverse component (Papazachos and Papaioannou 1999). Woodside (1977) and Hall et al. (2005) suggest that subduction at the Cyprus Arc has relatively recently and has been replaced by a more complex deformation process, because all oceanic crust has been subducted and the continental part of the African plate now meets the Anatolian Plate. According to Hall et al. (2005) the deformation at the Cyprus Arc changed from compression to strike-slip after the Messinian.

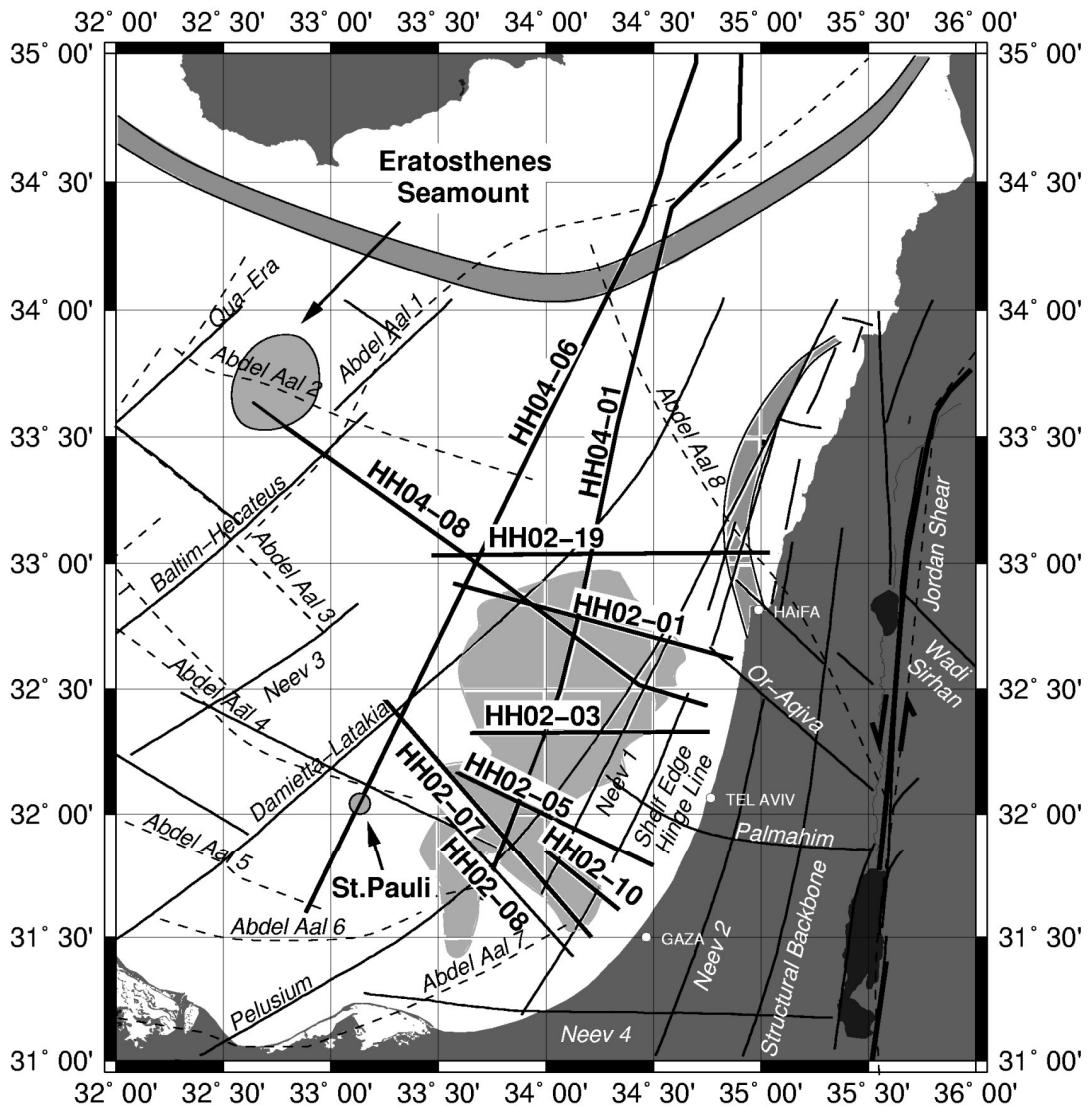


Figure 5.2 Map of the study area. The Eratosthenes Seamount and the St. Pauli mud volcano are marked. Thick, solid lines indicate main seismic profiles. Thin solid lines and dashed lines represent fault lines postulated by Neev (1975, 1977), Neev et al. (1976), and Abdel Aal et al. (2000), respectively. Fault lines are labelled with their names, unnamed faults are numbered. The fault zone off Haifa after Schattner et al. (submitted) and the Cyprus Arc are indicated by grey shaded arcs. The area shaded in a lighter grey corresponds to the slump complex delineated by Frey-Martinez et al. (2005).

Apart from the Cyprus Arc, which marks the plate boundary between the Anatolian and the African, and the Dead Sea Transform fault, which divides the Arabian and the African plates, a number of smaller fault zones has been identified in the Levantine Basin (Fig. 5.2). Several SW - NE striking shear zones converge towards the north, e.g., the Pelusium Line, the Hinge Line and the Damietta-Latakia Line (Neev 1975, 1977, Neev et al. 1976, Abdel Aal et al. 2000). These authors also depicted NW - SE trending fault lines. Mart (1984) confirms these findings and suggests that the NNE - SSW directed faults are normal faults, and the NW - SE oriented faults are strike-slip faults and possibly originate in the crust. According to Neev (1975), the north-eastward wedging compressional features originate in the south-eastern corner of the Mediterranean, although no evidences have been presented. Abdel Aal et al. (2000) also show faults trending NNE - SSW and NW - SE which more or less coincide with the fault lines depicted by Neev et al. (1976) (Fig. 5.2).

The Pelusium line represents the western edge of the Syrian Arc fold belt. According to Gardosh and Druckmann (2006) the evolution of this regional compressional tectonic feature started in the Late Cretaceous and persisted until the Early-Middle Miocene. Its evolution was related to the closure of the Neo-Tethys (see Garfunkel 1998 and 2004 for comprehensive summaries). Gradmann et al. (2005) interpreted seismic data off northern Israel and suggested tectonic activity along the shear-zones also in the Plio-Quaternary. North of Haifa, the converging shear zones merge with the seismically active Carmel fault zone, which continues along the central Levantine continental margin, viz from the Carmel Structure in the south until south of Beirut (Schattner et al., submitted) (Fig. 5.2). In the following discussions, we consider the Pelusium line as a regional tectonic feature in the south-eastern Mediterranean and not as a transcontinental shear as proposed by Neev (1977).

The sediment fill of the Levantine Basin reaches a thickness of up to 14 km (Ben-Avraham 2002 et al., Netzeband et al. submitted). It is composed of a carbonate layer of possibly Cretaceous to Jurassic age with a thickness of 1 - 3 km, followed by several km of Paleogene-Neogene pelagic sediments, a layer of Messinian evaporites of up to 2 km thickness, and a Plio-Quaternary cover, which mainly consists of Nile sediments (Druckman 1995, Vidal et al. 2000b, Ben-Avraham et al. 2002, Ben-Gai et al. 2005). The Messinian evaporites were deposited during the Messinian Salinity Crisis, when the evolving Mediterranean Sea lost its connection to the Atlantic, mainly because of the collision of the African and Eurasian plates (Hsü et al, 1973, 1978). The blocked water exchange and the high evaporation rate caused a drop in sea level, an increase in salt concentration and finally precipitation of evaporites. Druckman et al. (1995) estimate the fall of the sea level to approx. 660 - 820 m, Ben-Gai et al. (2005) find evidence of a sea level fall of 800 - 1300 m. As a consequence, the Mediterranean Sea was a succession of more or less separate basins with different rates of sedimentation and different depositional environments (Montadert et al. 1978). According to Hsü et al. (1973), the reflooding was a very rapid event, lasting only 1000 - 2000 years. Rouchy and Saint Martin (1992) estimate that about 25 cycles of refill and subsequent

drawdown or a semi-permanent inflow of fresh water or a combination of both are required to deposit the amount of evaporites found in the basins in the Mediterranean Sea. Whereas Hsü et al. (1978) only acknowledge one single transparent evaporite layer, Rouchy and Saint Martin (1992) assess from borehole analysis in the Western Mediterranean Sea that basinal evaporites generally consist of 2 successive units, one consisting of massive chloride salt and the other of calcium sulphate - marlstone interbedded with rare chloride salts. Polonia et al. (2002) observe even 4 subunits of Messinian evaporites in the Herodotus Abyssal Plain southwest of Cyprus. Bridge et al. (2005) find probably non-halitic units within the evaporite succession in the Cilicia Basin north-east of Cyprus, and Gradmann et al. (2005) also find prominent internal reflections within the evaporite layer in the Levantine Basin. Garfunkel and Almagor (1984) and Garfunkel (1984) offer an interpretation of such internal reflections as embeddings of overpressurized clastic sediments between evaporites. According to Abdel Aal et al. (2001), the Nile Scarp, an up to 600 m high escarpment south and east of the Eratosthenes Seamount, is considered to be the backstop of the compressed Messinian evaporites.

The deposition of the Plio-Quaternary sediments above the Messinian evaporites is determined by the sediment supply of the Nile River (e.g. Mart and Ben-Gai 1982). The thickness of the sediment cover and the sedimentation rate decrease accordingly to the north, a sedimentation rate of 162 m/my in Echo-1 (near HH02-05, < 50 m water depth) and 111 m/my in borehole Delta-1 (near line HH02-03 (Fig. 5.2) in about 120 m water depth) are given for the Pleistocene by Tibor et al. (1992). According to Tibor and Ben-Avraham (2005), the Levantine Basin becomes shallower, because sedimentation exceeds subsidence. After anomalously high subsidence rates in the Pliocene (123 m/my in Echo-1) as a flexural response to the rapid deposition of Messinian evaporites, the subsidence was significantly reduced (7 m/my in Holocene in Echo-1) (Tibor et al. 1992, Ben-Gai et al. 2005). The entire subsidence of the top of the Messinian amounts to 500 m in the basin (Tibor et al. 1992).

Several slumping complexes were found offshore Israel (Garfunkel 1984, Mart 1987, Almagor 1993, Frey-Martinez et al. 2005). Almagor (1984, 1993) finds seismic evidence of displaced sediments along the entire slope offshore Israel, and classifies earthquake triggered slumping as the most important agent of downslope sediment transport. Based on the analysis of an extensive 3D dataset, Frey-Martinez et al. (2005) find over 40 slump complexes within the Post-Messinian, seismically characterized by a zone of chaotic or weak reflections appearing almost transparent. Three stratigraphic units are identified, which show different slumping behaviour. The Holocene shows numerous (about 25) small slump bodies, with no more than 80 km³, in the Pleistocene approx. 15 slump bodies have been found with a size of 400 km³, and in the Pliocene one single slump complex has been detected, the Israeli Slump Complex (ISC). According to Frey-Martinez et al. (2005), the ISC consists of at least 3 major slumps accounting for 1000 km³, effecting an area of 4800 km², which places the ISC in the dimension of the Storegga Slide offshore Norway.

Mud volcanoes are found in several places in the Eastern Mediterranean Sea, mainly on the Mediterranean Ridge (Huguen et al. 2005), at the Anaximander Seamount (Dimitrov and Woodside 2003) and in the Nile Deep Sea Fan (Loncke et al. 2004). They usually occur in clusters, accompanied by pockmarks (Dimitrov and Woodside 2003). Pockmark fields without neighbouring mud volcanoes are furthermore found on the top of the Eratosthenes Seamount (Dimitrov and Woodside 2003) and in the southeastern Levantine Basin (Coleman and Ballard 2001).

5.3 Materials and methods

The data of this study were collected during the GEMME cruise M52/2 (HH02-lines) with the German research vessel RV METEOR in 2002 (Pätzold et al. 2003) and during the SAGA expedition (cruise PE228; HH04-lines) with the Dutch research vessel RV PELAGIA. 44 multichannel seismic reflection lines were recorded during the cruise M52/2, and another 12 reflection lines were recorded during the cruise PE228 (Figs. 5.2 and 5.3a). All were recorded with a streamer of 600 m active length profiles HH02-01, HH02-03, HH02-05, and HH02-08 were also recorded with a second streamer of 150 m active length. Both streamers comprised 24 channels with a group distance of 6.25 m and 25 m, and a maximum offset of 190 m, and 700 m, respectively. Both recorded with a sampling rate of 1 ms. For HH02-07 and HH02-19 the source consisted of two airgun small clusters: one with two GI-Guns, each with a volume of 105 in³ operated in the harmonic mode, and the other cluster consisting of one GI-Gun with 205/105 in³ operated in the airgun mode and a G-Gun of 380 in³ (6 l). For HH02-01, HH02-03, and HH02-05 only the GI-Gun cluster (2 x 205/105 in³) was used, and for HH04-01, HH04-06, and HH04-08 the source consisted of 2 G-Guns with 380 in³ (6 l) each. The shot spacing was 25 m (10 s).

The recordings of both streamers were CMP-sorted with a CMP spacing of 6.25 m and 12.5 m, then stacked and bandpass filtered with passing frequencies between 10 and 150 Hz. On lines HH02-07, HH02-19, HH04-06, and HH04-08 further processing was applied on the recording of the longer streamer:

- a stacking velocity analysis on every 100th CMP in supergathers of 5 - 9 CMPs. The deeper the analysed horizon, the more CMPs in the supergather.

- smoothing of the resulting velocity field
- time-migration and stacking
- interval velocity analysis
- model based pre-stack depth migration

Interval velocities of Post-Messinian sediments and evaporite layers were 2.0 ± 0.2 km/s and 4.2 ± 0.3 km/s. With a maximum offset of 800 m and the base of the

evaporites at ~ 4 km, the interval velocity of the evaporite layer was difficult to determine, and it was impossible to find any reliable interval velocity from below.

We carried out an Airy-backstripping of the Plio-Quaternary sediments after Allen and Allen (1990). We simply removed the sediment load, not taking into account any effect of compaction of either evaporites or Pre-Messinian sediments. The relation of the depth of the present seafloor and the seafloor after backstripping is given in equation 1.

$$d_{\text{seafloor}} = d_w + d_{\text{sed}} (\rho_{\text{mantle}} - \rho_{\text{sed}}) / (\rho_{\text{mantle}} - \rho_w) \quad (\text{Eq. 1})$$

Here, d_{seafloor} denotes the depth of the seafloor after backstripping, d_w denotes the present water depth and d_{sed} the thickness of the sediment layer that is removed. ρ_{sed} marks the density of the sediment layer, ρ_w the density of the water column and ρ_{mantle} the density of the mantle. For ρ_w , ρ_{sed} , and ρ_{mantle} we assumed densities of 1.03 g/cm^3 , 2.0 g/cm^3 and 3.3 g/cm^3 , respectively, for the evaporites 2.2 g/cm^3 . (Ben-Avraham et al. 2002, Netzeband et al. *accepted January 2006*). We also applied this method with the same parameters to intra-evaporite layers.

5.4 Results

Top (M) and base (N) of the evaporite layer are clearly visible on all seismic lines. As an overview, a rough map of Plio-Quaternary sediment thickness and evaporite thickness in the southern portion of the Levantine Basin is shown in Fig. 5.3b and 5.3c, line drawings of depth migrated lines HH04-06 and HH04-08 are shown in Fig. 5.4a - d. On the southern slope of the Nile Delta the Plio-Quaternary sediment thickness reaches thicknesses of almost 3 km, while in the centre of the basin the thickness is less than 500 m. The sedimentary cover is also reduced around the Eratosthenes Seamount (Fig. 5.3b).

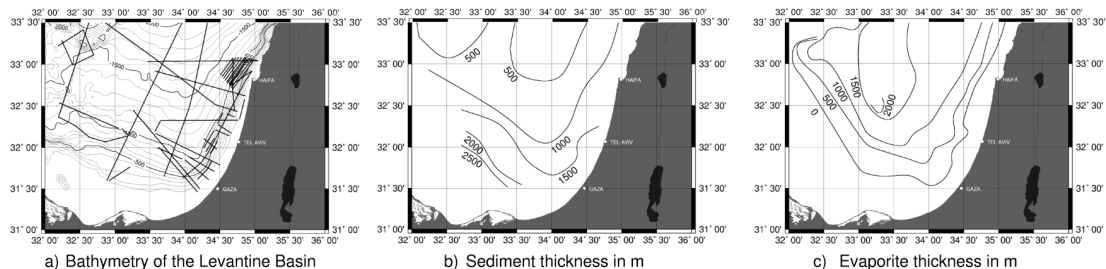


Figure 5.3 Maps of study area: a) bathymetry of the Levantine Basin, numbers correspond to depth in m. All the seismic lines this study is based on are shown for reference. Note the Eratosthenes Seamount south of Cyprus. b) isolines indicating the sediment thickness in the Levantine Basin. c) isolines indicating the thickness of the evaporite body in the Levantine Basin.

The thickness of the Messinian evaporites, in contrast, increases towards the centre of the basin to over 2 km (Fig. 5.3c). The evaporites extend to about 30 km off the Israeli coast, the boundary runs more or less parallel to the coast. This distribution reveals the NNE - SSW orientation of the Levantine Basin, which is also indicated by the bathymetry (Fig. 5.3a).

5.4.1 Post-Messinian subsidence

All seismic lines show a thinning of the basinal evaporites towards the eastern and southern margin of the basin (Fig. 5.4a, b). The top of the evaporites, the M-reflection, declines towards the pinchout and forms an apparent rollback anticline. A typical example of such a rollback on W - E striking lines is presented in Fig. 5.5. Besides the rollback, these lines show a group of faults close to the pinchout. The subsidence analysis aims at the explanation of the rollback in terms of lateral gravity gliding or differential subsidence. After backstripping of the Plio-Quaternary sediment layer, the top of the evaporites is basically flat and horizontal, except for some small-scale undulations (Fig. 5.6). This result is in accordance with the results of Tibor and Ben-Avraham (2005), who performed 2D-backstripping including decompaction. Line HH02-01 south of Haifa is the only significant exception. Here, the presence of salt rollers and salt welds proves lateral salt withdrawal (see Gradmann et al., 2005, for a comprehensive discussion).

The removed Plio-Quaternary sediment layer is of more or less constant thickness along the Israeli margin, with about 500 m in the basin and 1.1 km at the shelf (Fig. 5.6). The calculated subsidence in the basin amounts to 200 m. Differential sediment load and subsidence occurred between the upper slope and the central basin. It should also be mentioned that on the northern W - E striking lines the pinchout of the evaporites lies basinwards from shelf break, whereas in the south of HH04-06 and HH04-01 the evaporites extend under the shelf.

At the Nile Fan, in the south of line HH04-06, which is N - S oriented, nearly 3 km of sediments overlie the evaporites due to the proximity to the Nile delta. Here, the M-reflection is clearly planer after the backstripping, but the depth still varies between 1.8 and 2.4 km. Near the southern rollback, the depth of the M-reflection is about 2.1 km, going north we see forebulging with the M-reflection rising for approx. 80 km to only 1.8 km depth and then declining again towards the centre of the basin to 2.4 km.

5.4.2 Internal reflections

Up to 4 internal reflections (E1 - E4) are observed within the evaporite layer with varying reflection and deformation patterns (Figs. 5.4, 5.7). These mostly well pronounced reflections separate seismically transparent sequences. E1 shows similar

reflection characteristics as the N-reflection, and the reflection characteristics of E2 and E3 also resemble each other and those of E4 and the M-reflection as well. The thickness of the internal sequences is more or less constant with 0.2 - 0.4 km in the basin, leading to a total evaporite thickness of approx. 1.6 km.

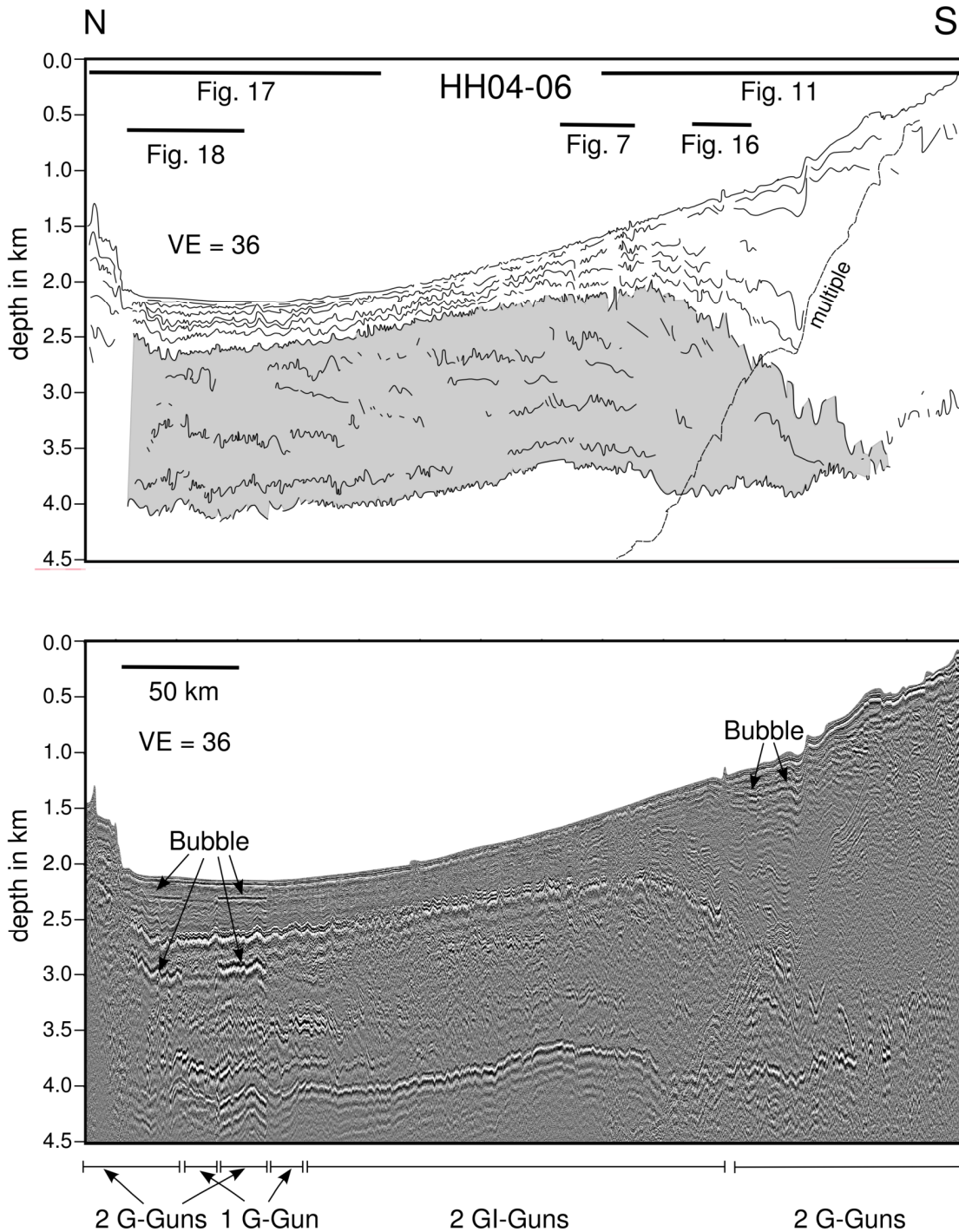


Figure 5.4 a. Depth migrated seismic line (below) and line drawing (above) of line HH04-06. The seafloor multiple is marked by the dashed line, the grey shaded area indicates the evaporite layer. Internal reflections within the evaporite layer are observed. The forebulging of the evaporite body is clearly visible.

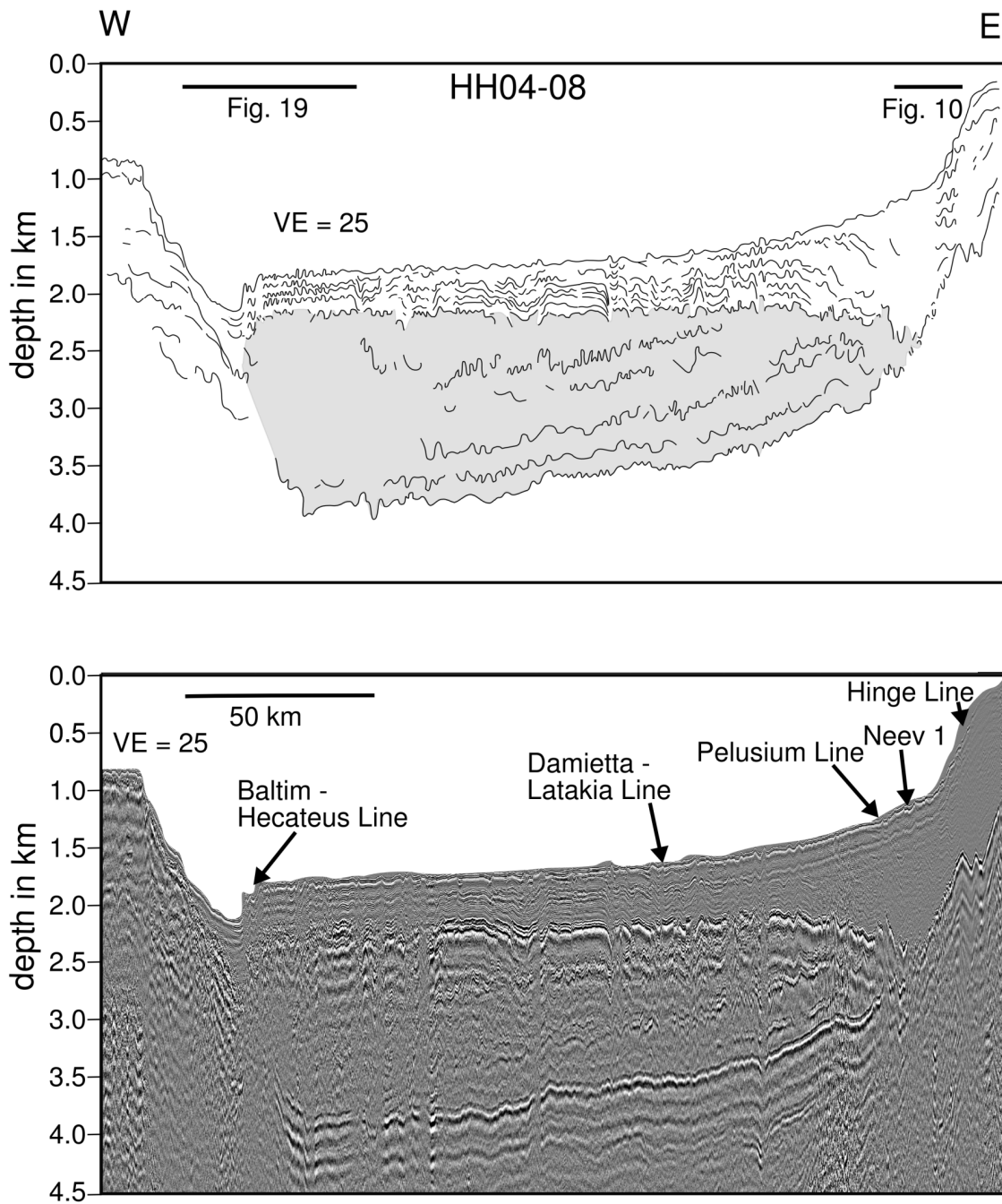


Figure 5.4 b. Depth migrated seismic line (below) and line drawing (above) of line HH04-08, analogue to 5.4a. The grey shaded area indicates the evaporite layer. Internal reflections within the evaporite layer are observed. The positions of the major fault lines (Baltim-Hecateus, Damietta-Latakia, Pelusium, Neev 1 fault line, and the Shelf Edge Hinge line) are marked.

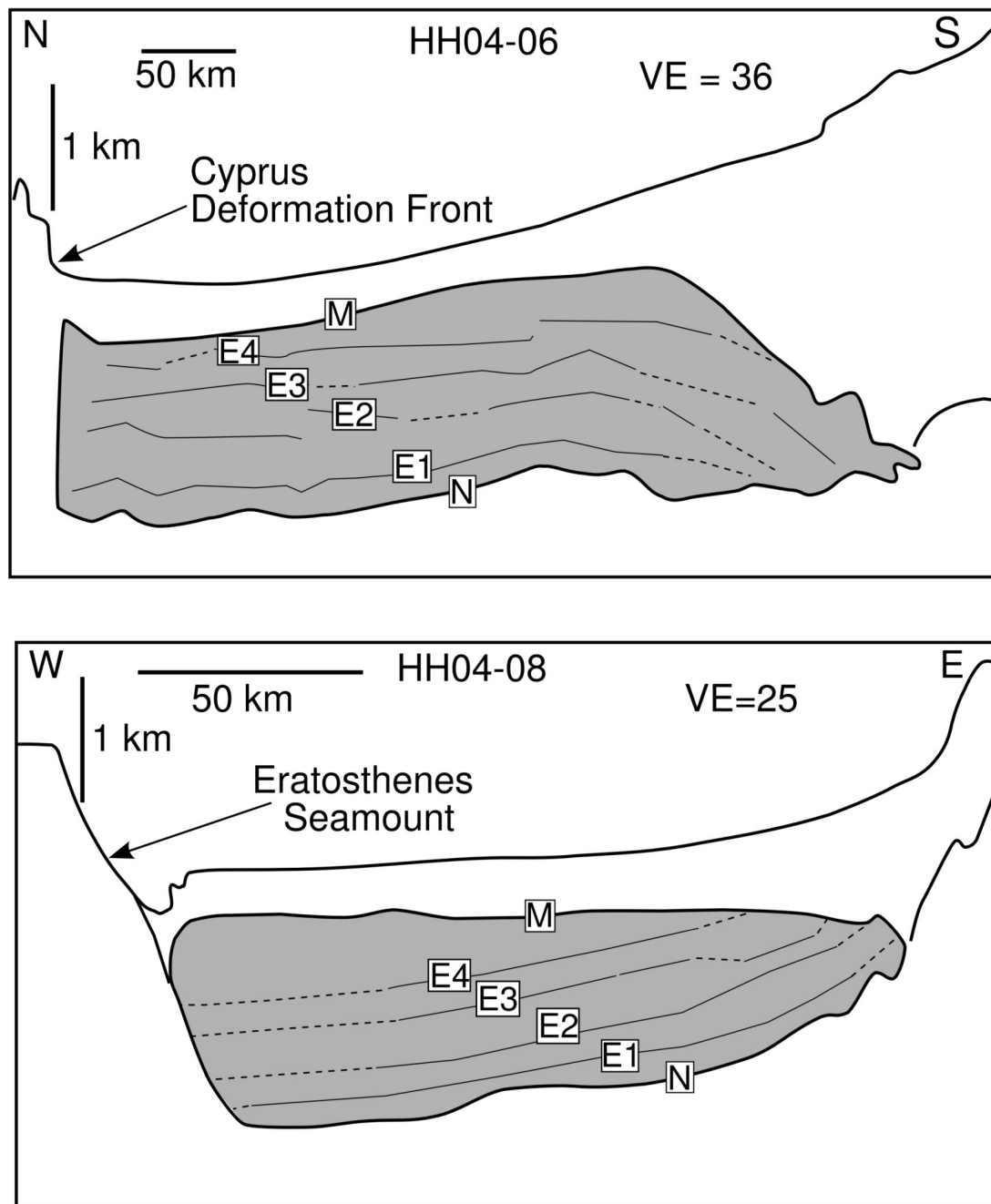


Figure 5.4 c (above) and d (below). Simplified line drawings of lines HH04-06 and HH04-08. The grey areas mark the evaporite body, M and N correspond to top and bottom of the evaporites, respectively. The solid lines labelled E1 - E4 indicate the observed internal reflections, the dashed lines indicate extrapolation, where the internal reflections are not clearly visible.

On the N - S profiles, e.g. HH04-06 (Fig. 5.4a, 7), the deformations of these internal reflections and of the M- and N-reflections do not necessarily correspond with each other. Different kinds of deformations can be observed at the same location in different layers (Fig. 5.7, CMP 23200, CMP 23600, CMP 24100). One of the steepest thrusts observed in E4 is visible at CMP 23500 on line HH04-06 (Fig. 5.7), while the M-reflection and the seafloor above are not affected and the overburden overlies the M-

reflection concordantly. The maximum thrust angle of the internal reflections is highest in E4 and decreases with depth. In E4 on line HH04-06 thrust angles of 8° are observed, up to 14° are reached at the tip of the thrusts (Fig. 5.7). On N - S lines, the general orientation of thrust faults and oblique folds within the evaporites is northward, i.e. basinwards, on line HH04-01 and HH04-06 (Fig. 5.2, 5.4a, 5.7). On N - S lines, E1 - E4 are only parallel to the basal N-reflection in the northern part, but they seem to downlap onto the N-reflection beneath the Nile Fan and near the pinchout of the evaporites (Fig. 5.4a, c).

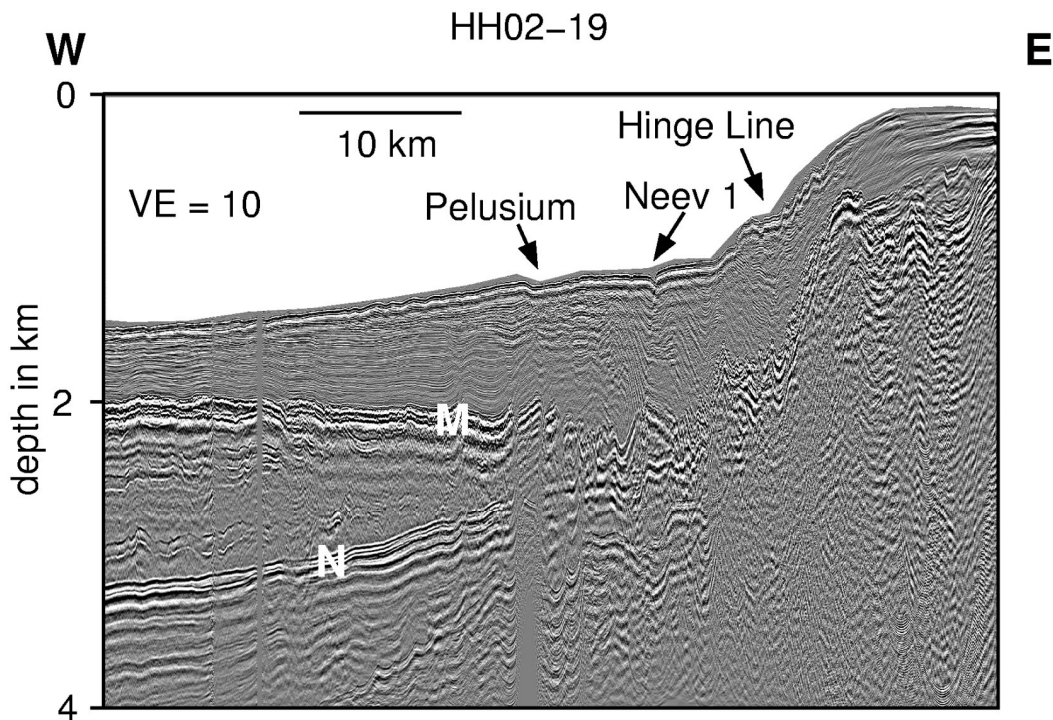


Figure 5.5 Section of seismic lines HH02-19, showing the pinchout of the evaporite layer and the apparent rollback. Top and bottom of the evaporites are marked M and N, respectively. Note the decline of the M-reflection towards the pinchout. The position of the major fault lines (Pelusium, Neev 1 fault line, and the Shelf Edge Hinge line) are marked.

Typically, on E - W lines all internal reflections dip basinward and run parallel to basal N-reflection (Fig. 5.4b, d). Here, the evaporite thrusts are only observed in the top of the evaporites and E4, e.g. in lines HH02-01 (Fig. 5.2, 5.8), HH02-03 and HH04-08 (Fig. 5.2, 5.4b). Both eastward and westward oriented thrusts and also pop-up structures are observed (Fig. 5.8). Strongly folded intra-evaporite reflections are also present. In general, on the lines running E - W thrusting is less pronounced within the evaporites than on those running N - S.

In order to explain the basinward dipping internal reflections we performed backstripping of the internal sequences from top to bottom of line HH04-08 (Fig. 5.9a - g). The tops of the individual evaporitic sequences are not horizontal after backstripping

the overburden, but still dipping westwards. No basinal evaporites are deposited at a depth less than 1800 m. At the eastern edge, the evaporites prograde towards the basin. After removal of the lowermost layer, the basin remains asymmetric. On the assumption that each layer was horizontally deposited, we removed the tilt of the basin at 180 km after backstripping the Plio-Quaternary and the uppermost evaporitic sequence until the top of the evaporites was horizontal (Fig. 5.9h). Consequently, the deeper sequences became also almost horizontal (Fig. 5.9 h) - l). After backstripping the remaining evaporitic sequences the basin is approx. symmetric between Eratosthenes Seamount and the Israeli slope.

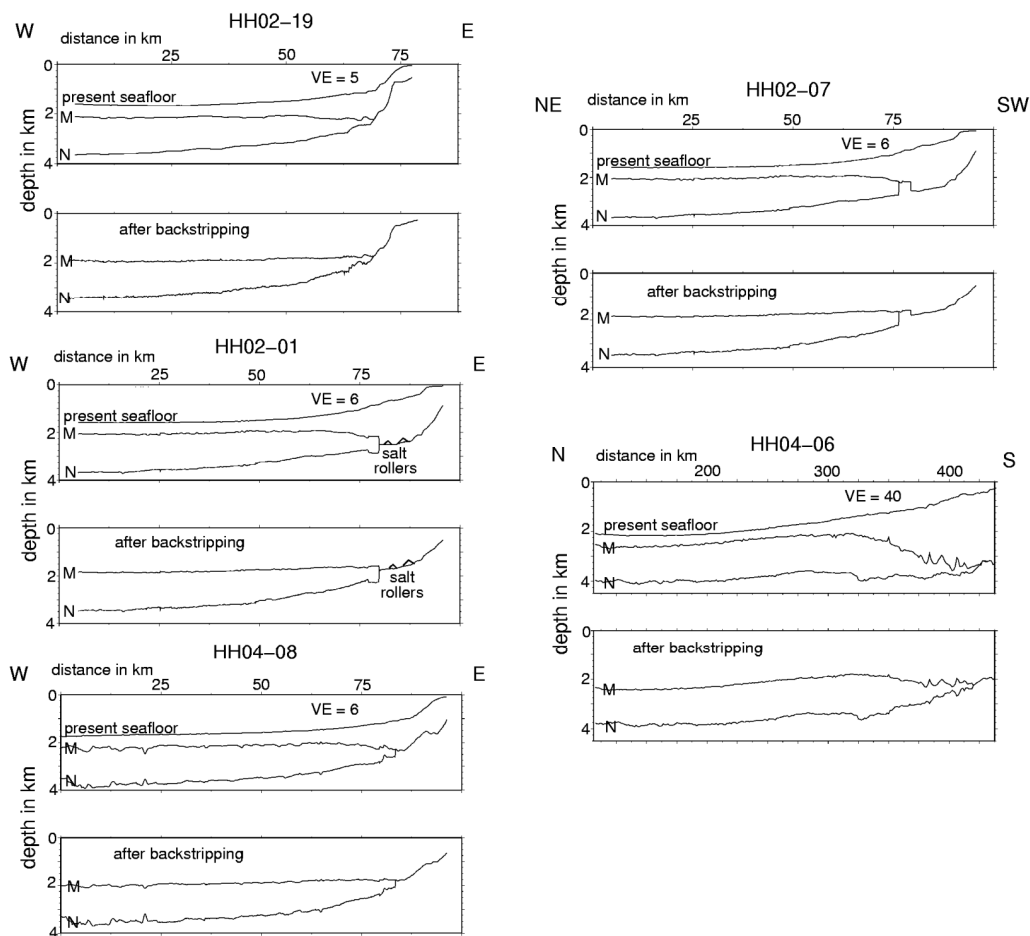


Figure 5.6 Examples of Airy backstripping. Sketches of several profiles split into two parts: the present seafloor, top and bottom of the evaporites in the upper part, and top and bottom of the evaporite layer after backstripping of the Plio-Quaternary sediments in the lower part. Vertical exaggeration (VE) varies. Note how the M-reflection, the top of the evaporites, is almost flat after the backstripping, except for line HH04-06. Also note the change in thickness of the sediment prism and thus the varying differential load. On line HH02-01 salt rollers are observed.

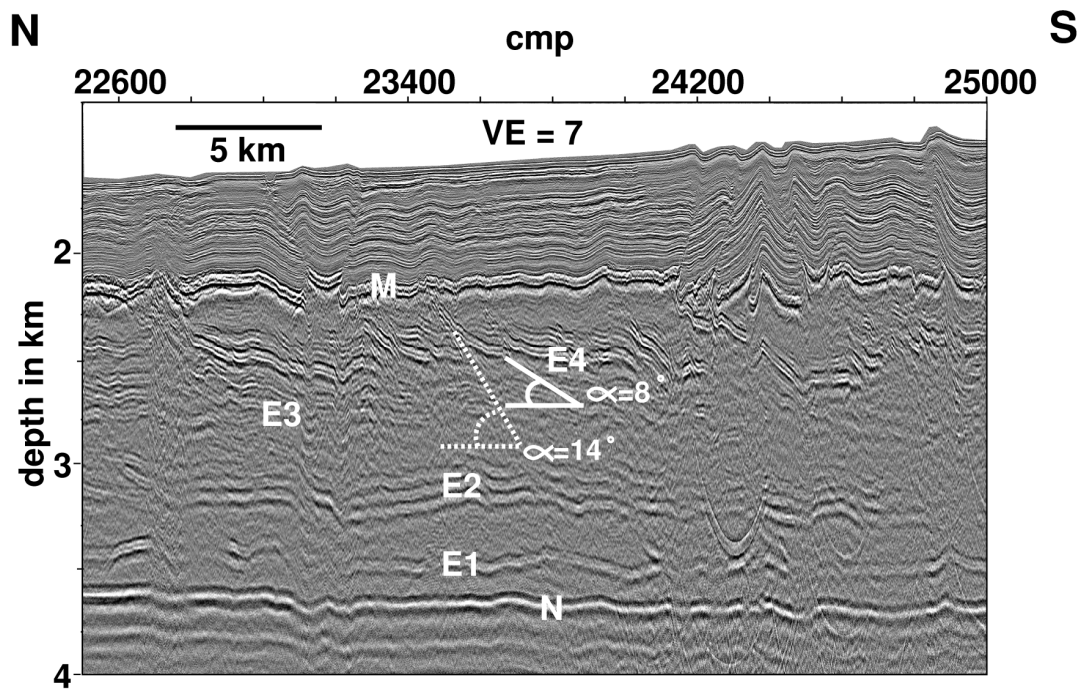


Figure 5.7 Section of seismic line HH04-06, depth migrated. Top and bottom of evaporite layer are indicated by M, and N, respectively. E1 - E4 mark the internal evaporite reflections. Note the large angles of thrust within the internal reflections, particularly in E4. Two angles (the solid angle corresponding to 8° , the dashed one to 14° , the vertical exaggeration is 7) are drawn for reference.

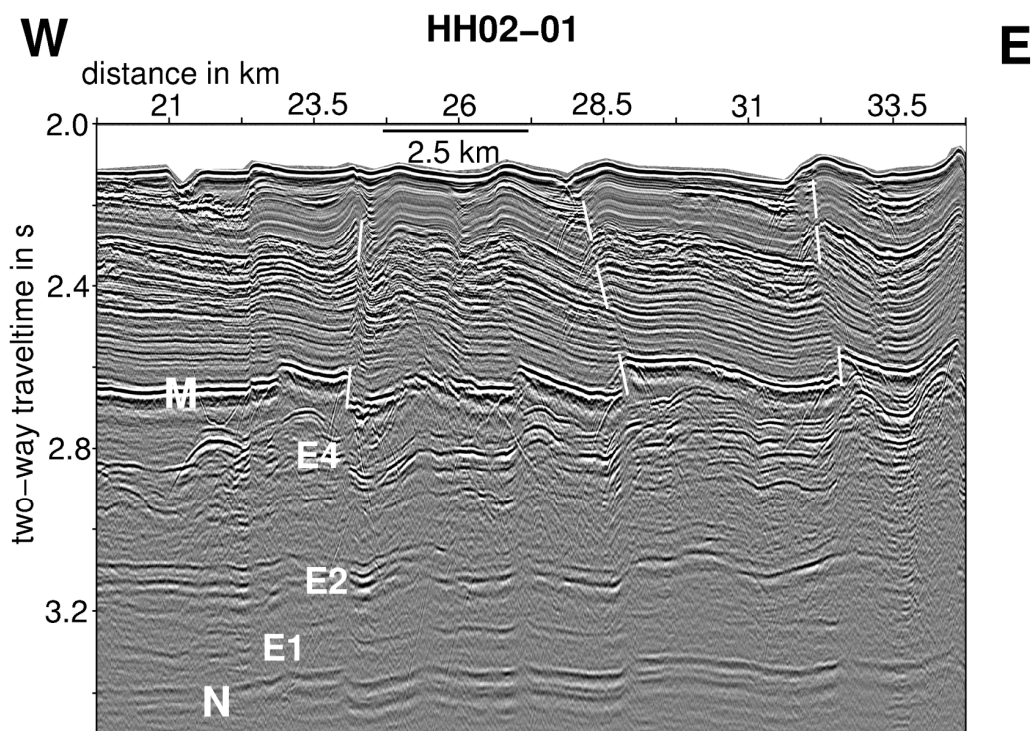


Figure 5.8 Section of seismic line HH02-01, time migrated. Top and bottom of evaporite layer are indicated by M, and N, respectively. E1 - E4 mark the internal evaporite reflections. Note the constant throw of the thrusts up to a certain level, indicating that these thrusts are an episodic phenomenon rather than slowly developing growth faults, as already described by Gradmann et al. (2005).

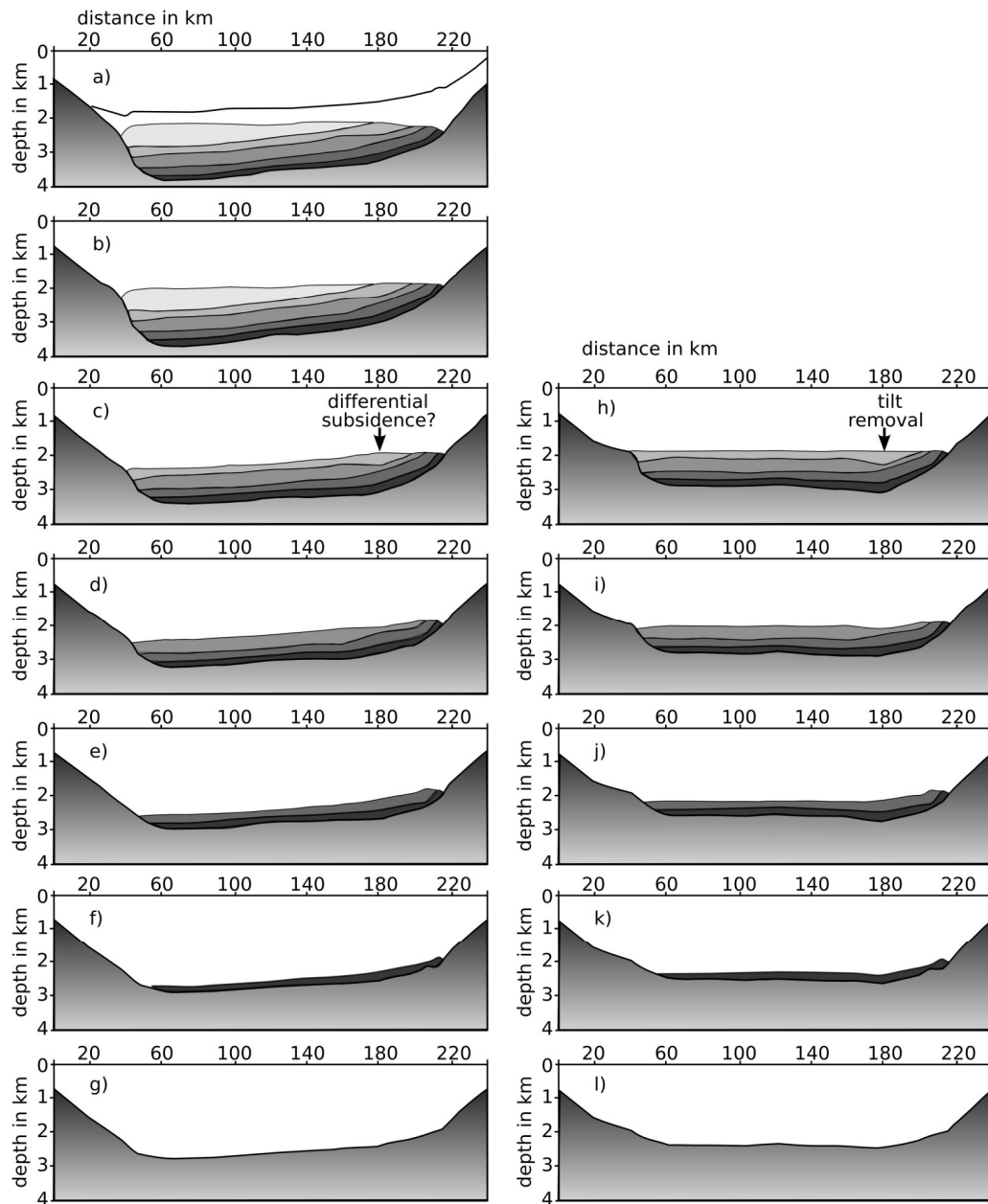


Figure 5.9 Airy backstripping of line HH04-08, including the internal salt reflections. The left column, a - g represents the backstripping results, as one layer at a time is removed. The right column, h - l, shows a modification of the backstripping: After removal of the Plio-Quaternary and the uppermost salt layer, the basin is partially uplifted, basinwards from km 180, until the top of salt is horizontal. Then backstripping is continued. Note that the thickness of the internal salt layers is more or less constant, apart from the uppermost layer. Also note how in Fig. h-l the tops of the internal reflections stay almost horizontal.

5.4.3 Marginal structures

The eastern basin margin off Israel is characterized by extensional faulting. Listric and antithetic growth faults, sometimes forming keystone grabens, are observed along the entire slope (Figs. 5.10, 5.11, 5.14, 5.15). Some of these faults can be traced from the seafloor to the top of the evaporites, some even penetrate the base of the evaporites. They occur where the thickness of the evaporite layer decreases towards the slope to less than 1 km. In these locations the top and the base of the evaporites are heavily faulted and folded and difficult to trace. Active extensional faults which are piercing the seafloor are also observed on the Nile Fan (Fig. 5.11). Mapping these faults and keystone grabens as extensional features reveals that the extensional regime prevails in a narrow corridor parallel to the coastlines (Fig. 5.12).

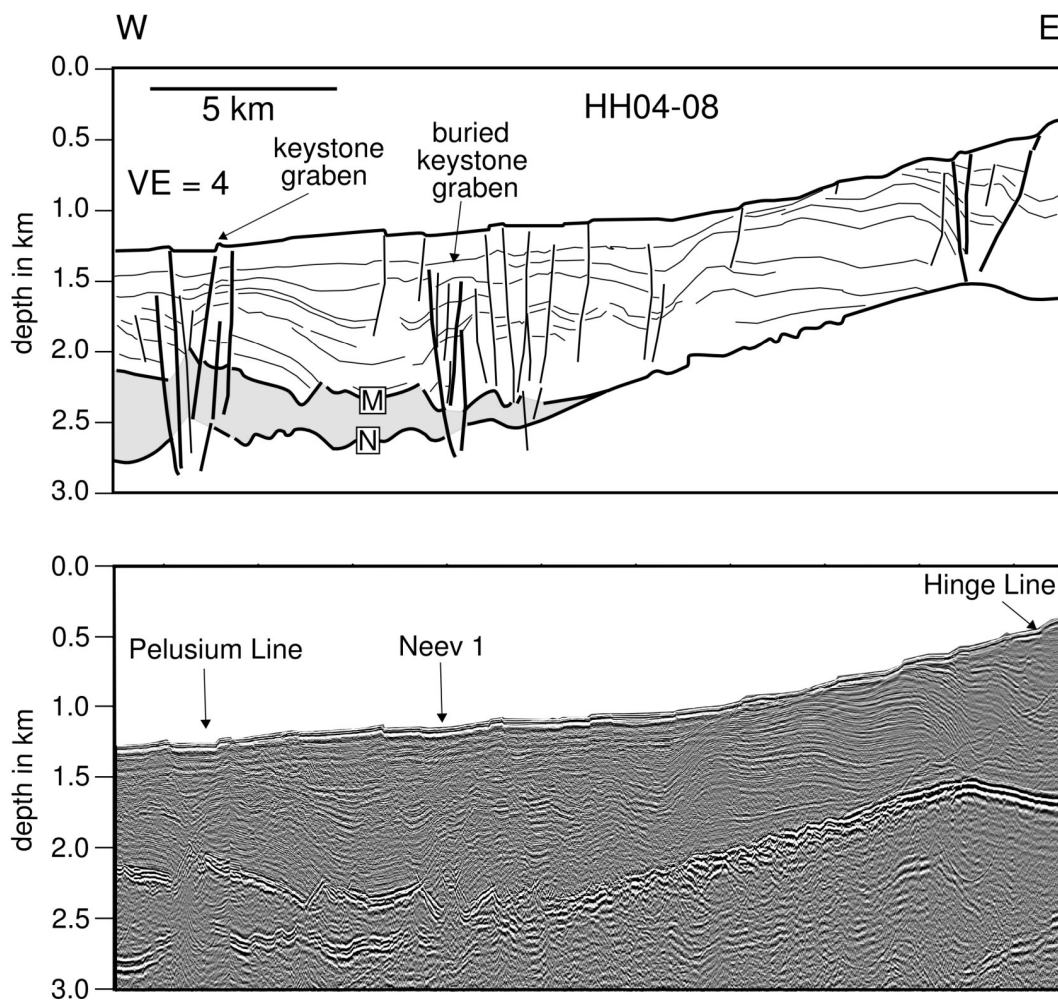


Figure 5.10 Section of depth migrated seismic line (below) and line drawing (above) of profile HH04-08. The grey shaded area indicates the evaporite body. Top and bottom of the evaporite layer are indicated by M, and N, respectively. Extensional faulting in the Plio-Quaternary sediments is observed, in some places even piercing the evaporite layer. Listric and antithetic growth faults from keystone grabens occur. The position of major fault lines (Pelusium, Neev 1 fault line, and the Shelf Edge Hinge line) are marked.

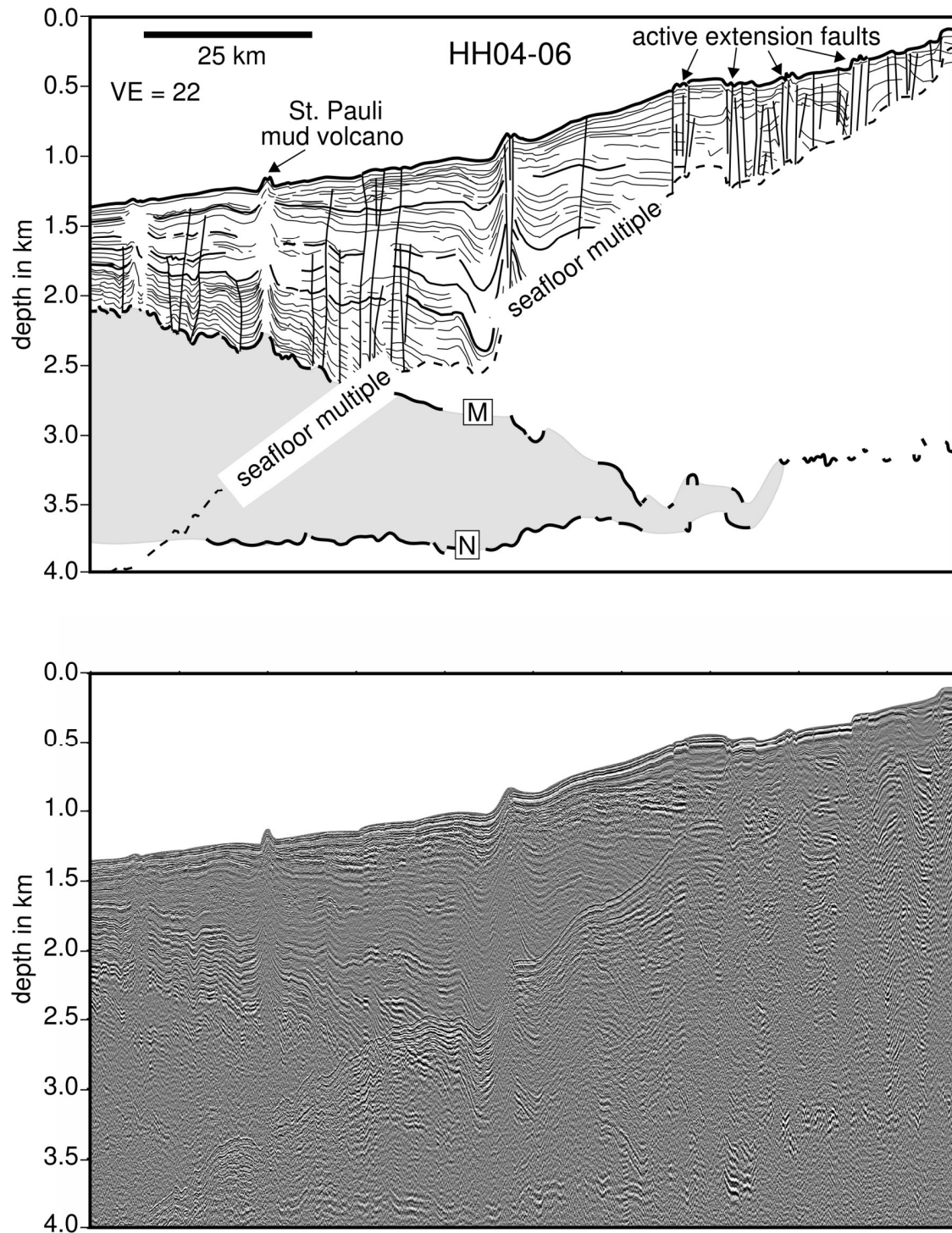


Figure 5.11 Section of depth migrated seismic line (below) and line drawing (above) of profile HH04-06. The grey shaded area indicates the evaporite body. Top and bottom of the evaporite layer are indicated by M, and N, respectively. The seafloor multiple is marked by the dashed line. Extensional faulting in the Plio-Quaternary sediments is observed. Note the increased sediment thickness compared to Fig. 5.10. The M-reflection and the N-reflection are heavily ruptured, but faults in the Plio-Quaternary cannot be traced through the evaporites. Note the mud volcano 'St. Pauli', located above a 1.5 km thick evaporite layer.

According to the tectonic maps of Neev (e.g. 1975), several shear-zones termed Pelusium, Neev1 and Shelf Edge Hinge Lines narrow towards the north. On line HH02-03 both the entire evaporitic succession and the overburden are disrupted and the associated faults within the PQ pierce the seafloor (Fig. 5.13). The location of the Hinge Line is also accompanied by seafloor piercing faults and a significant change in the slope angle of the Pre-Messinian. Further south, the Shelf Edge Hinge Line is represented by the divergent reflection pattern of a divergent growth fault within the PQ, which is covered by mass waste deposits (Fig. 5.14). Displacements of individual growth faults reach values of up to 300 ms TWT (> 220 m). The evaporitic succession is dissected. However, there is no indication of differential subsidence at both sides of the fault or of lateral salt withdrawal and creep. Since the slope angle decreases from north to south, the impact of the Hinge Line is less pronounced in the Plio-Quaternary sediment layer south of 32°.

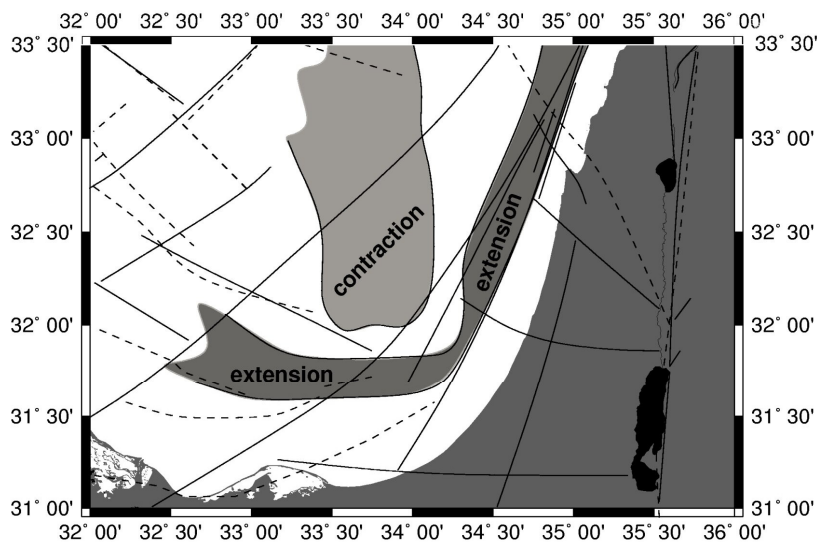


Figure 5.12 Map of extensional and compressional features observed in the Plio-Quaternary, based on seismic lines of this study (Fig. 3a). No distinction between deep-rooted and salt-related structures has been made in this map. Between the 'belt of extension' and the zone of contraction, a corridor of comparatively low deformation is observed. Solid lines and dashed lines represent fault lines postulated by Neev (1975, 1977), Neev et al. (1976) and Abdel Aal et al. (2000), respectively. See fig. 2 for labels. Note how the eastward boundary of the belt of extension corresponds to the course of Shelf Edge Hinge line, and the southern boundary to the Abdel Aal 5 - fault.

The Pelusium Line and the Syrian Arc change their striking directions from NNE to NE south of 32°N. Here, the Pelusium- and Neev1 Lines are characterized by an intricate fault system. On line HH02-08 (Fig. 5.15), the M- and N-reflections are pretty much blurred by the multiple, especially on the western half. However, an apparently 10 km wide and at least 400 m high (500 ms TWT, $V_p > 1.6$ km/s) anticline can be clearly identified at the top of the Pre-Messinian. Basinwards, this unconformity forms 10 km wide and south-eastward tilted terraces. Above the dominant anticline the Plio-Quaternary shows a vertical succession of sequences, some of which are of laterally

equal thickness and some are thinned above the crest. On the north-western flank a segment with divergent reflections (listric growth faults) follows. An uplifted horst is framed by two graben-like features. Most of the faults pierce the seafloor. In accordance with Neev (1975), the anticline corresponds to the Neev1 line, while the horst and the western graben correlate with the Pelusium Line. In general, all major fault lines can be identified in the available seismic data off Israel.

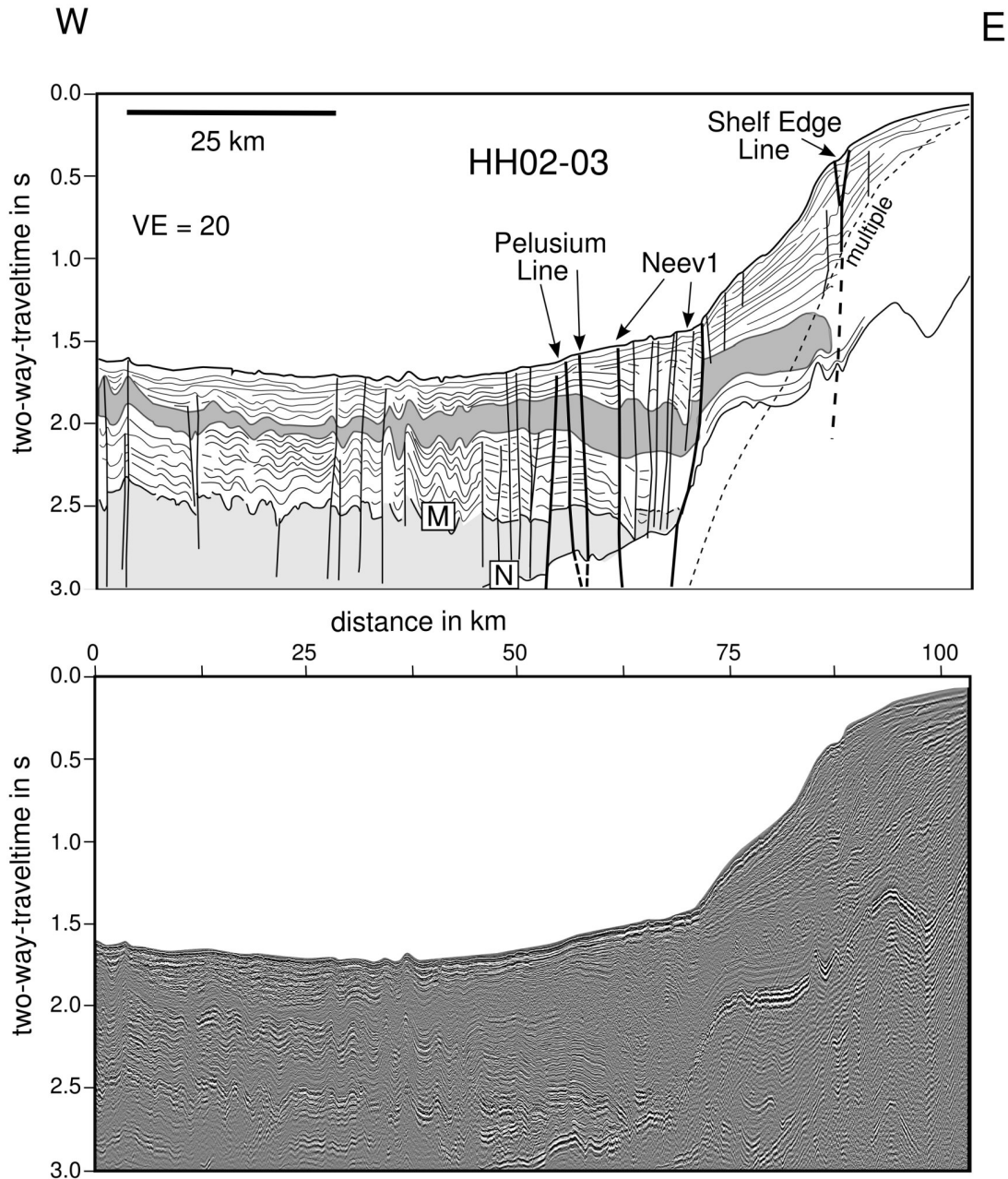


Figure 5.13 Section of time migrated seismic line (below) and line drawing (above) of profile HH02-03. Top and bottom of the evaporite layer are indicated by M, and N, respectively, and the sea floor multiple is marked by the dashed line. Faults penetrating the evaporite layer coincide with the position of the Pelusium Line and the Neev 1 fault. The Shelf Edge Hinge Line is also well expressed. The area shaded in light grey corresponds to the evaporite body. The area shaded in darker grey indicates the slump body. A transition of the slump body into a transparent layer is observed, this layer can be traced well into the basin.

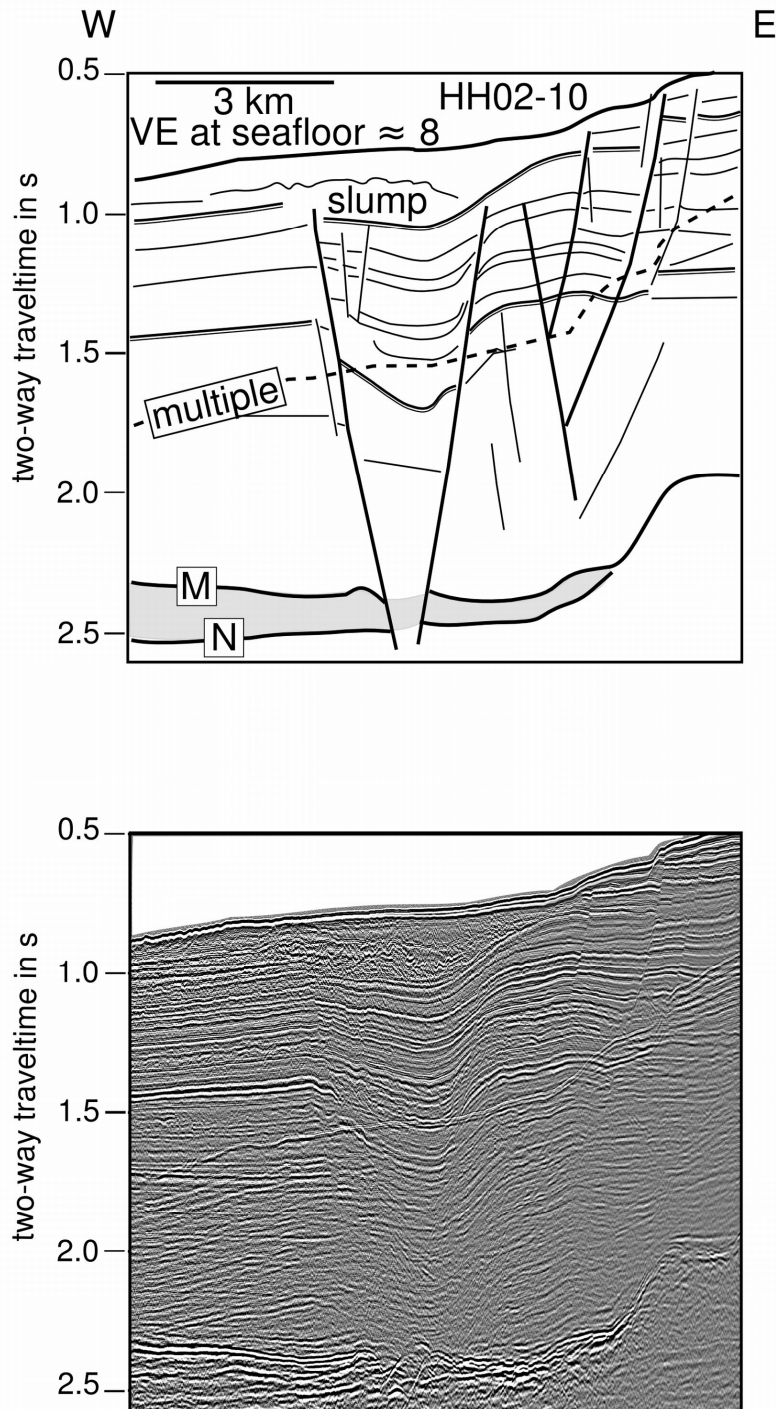


Figure 5.14 Section of time migrated seismic line (below) and line drawing (above) of profile HH02-10, showing the location of the Shelf Edge Hinge line. Top and bottom of the evaporite layer are indicated by M, and N, respectively, and the seafloor multiple is marked by the dashed line. Major faults penetrate the evaporite layer, and further upslope a flower structure is expressed. Also, evidence of a slump is observed.

5.4.4 Israeli Slump Complex

The ISC can be identified on lines HH02-03, HH02-05, HH02-01, HH02-19, HH02-07, and HH04-08 (e.g. Fig. 5.13, 5.14). This zone of heavily disturbed sediments is

almost seismically transparent, whereas the sediments above and below are well stratified. The ISC is prominent on the slope where it reaches a thickness of up to 200 m at a depth of 150 - 250 m below seafloor (bsf), and then thins towards the basin. There it can be correlated with a seismically transparent sequence that can be traced throughout the basin, also in the Nile Fan and serves as an isochrone. This transparent sequence shows a more or less constant thickness of approx. 50 m in the basin, whereas the zone of disturbed sediments near the shelf significantly varies in thickness.

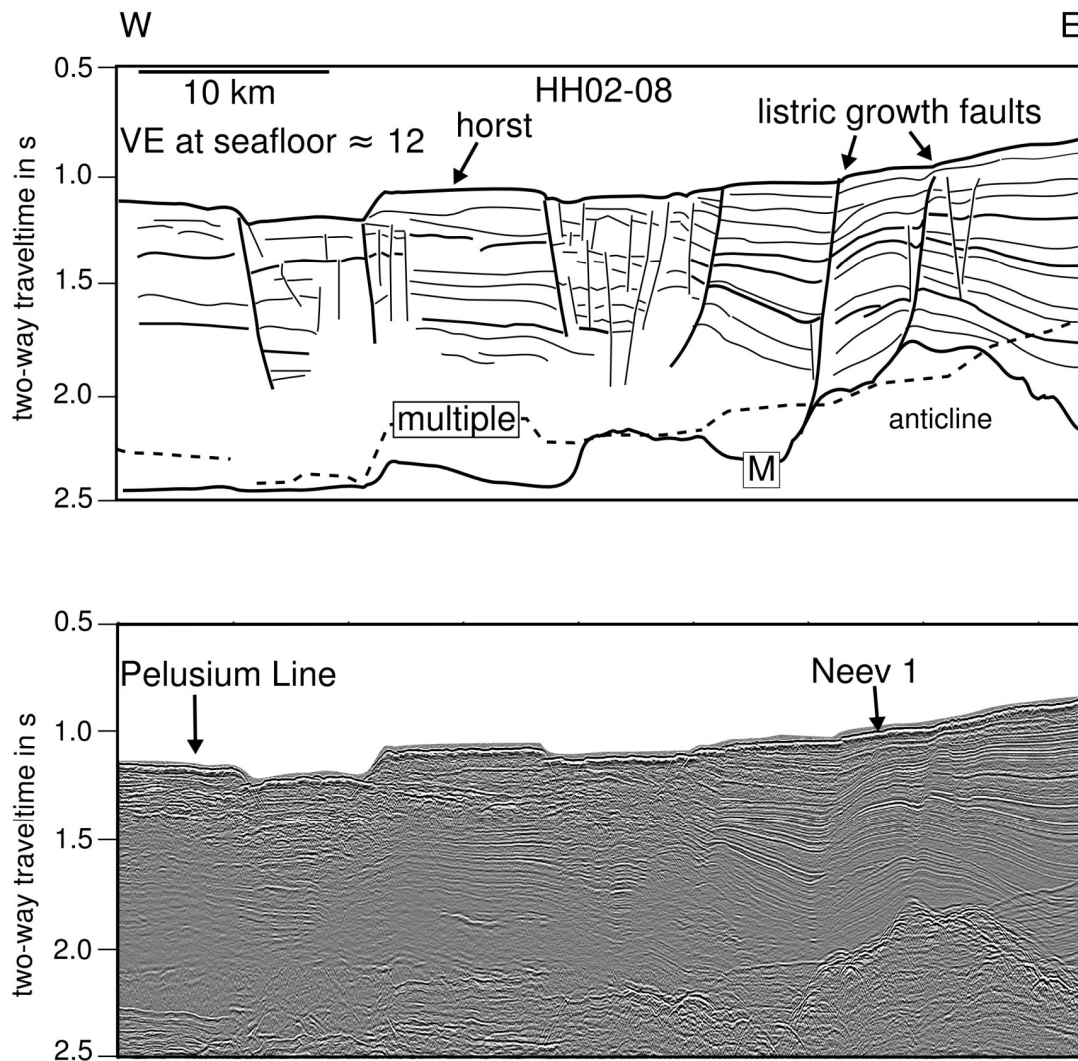


Figure 5.15 Section of time migrated seismic line (below) and line drawing (above) of profile HH02-08. The top of the evaporite layer is indicated by M, and the seafloor multiple is marked by the dashed line. Note the anticline and the horst - graben structure.

5.4.5 Mud Volcano

A mud volcano is observed at CMP 28000 (33°20 E/32°20 N) on the southern part of Line HH04-06 (see Fig. 5.2), which we named 'St.Pauli' (Fig. 5.16). This mud volcano lies at a water depth of 1.2 km, approx. 150 km offshore Egypt. It rises to 120 m above

the seafloor and has an apparent width of over 1.5 km. Several strong intra-salinar reflections pinch out against this cone. The overburden beneath is severely distorted and a caldera-like feature underlies the mud volcano approx. 300m beneath the seafloor.

The uppermost evaporitic sequence beneath forms a cone-like structure with an apparent width of 4 km. It is unclear to which extent deeper reflections are affected, because they are partly concealed by the seafloor multiple. However, the continuous base of the evaporites, the N-reflection, can be clearly identified. The entire evaporitic sequence beneath St. Pauli is still about 1.5 km thick. There is no evidence for any significant extension, faulting or folding, nor for salt welds.

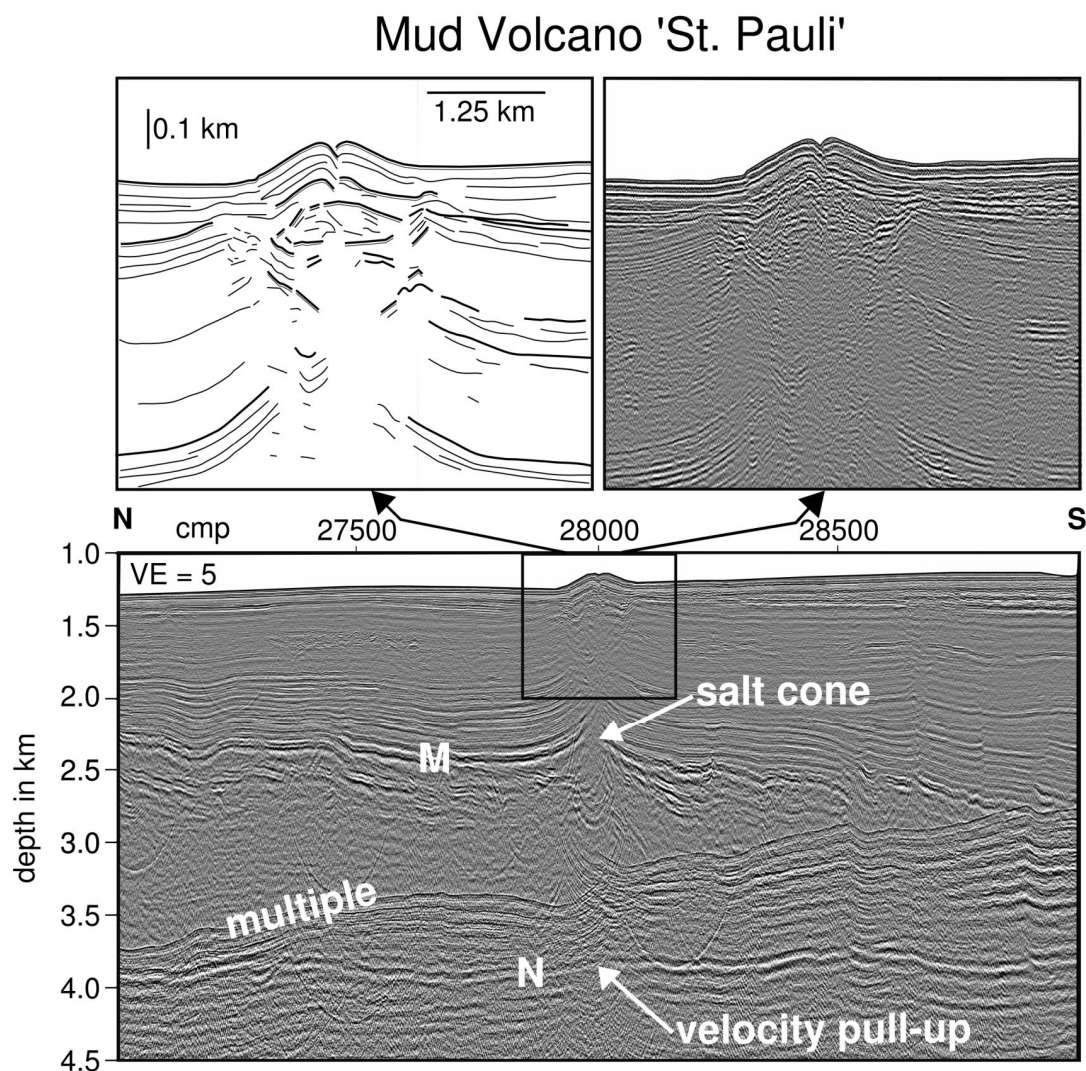


Figure 5.16 Mud Volcano 'St. Pauli'. Upper left: Line drawing of a close-up of the mud volcano. Upper right: Seismic image, depth migrated, of the mud volcano. Both flanks are almost symmetric. Reflections underneath the mud volcano are bent upwards. Bottom: Depth migrated seismic section of line HH04-06, showing the position and surroundings of the mud volcano and the salt cone. Top and bottom of the evaporite layer are indicated by M, and N, respectively. While the M-reflection is clearly affected by the mud volcano, the N-reflection is smooth and appears continuous.

5.4.6 The basin

Compressional features such as folding, thrusting and pop-up-structures in the basin are observed on all profiles (Fig. 5.12). In N - S direction thrusting prevails which is directed northwards, while in E - W direction the deformation is more symmetrical, pop-up structures are found, and thrusts are as common in eastward as in westward direction. The degree of compression varies within the evaporite layers as well as within the Plio-Quaternary cover (Fig. 5.7 and 5.8, 5.12).

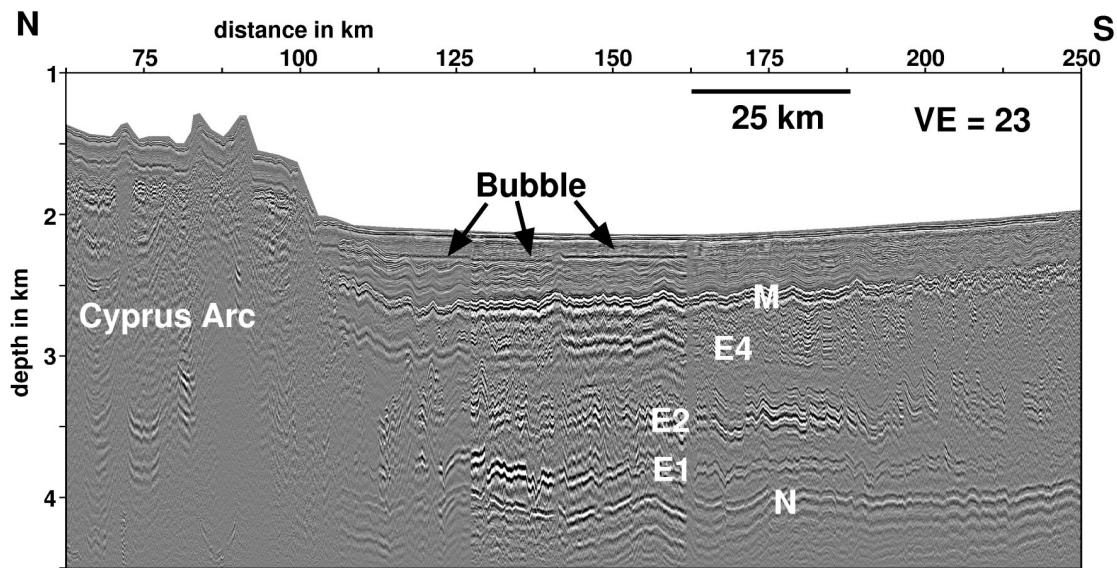


Figure 5.17 Section of seismic line HH04-06, depth migrated, showing the Cyprus Arc. Top and bottom of evaporite layer are indicated by M, and N, respectively. E1 - E4 mark the internal evaporite reflections. E3 is not marked, because it is not well visible. Note the increase in compression in the N-reflection, the M-reflection, and E1 - E4 near the Cyprus Arc, while the seafloor is almost flat. For a close-up of the Plio-Quaternary, see Fig. 5.18.

There is an abundant number of compressional faults within the basin which reach from the upper evaporites to the transparent sequence mentioned above (e.g., Figs. 5.8, 5.13). In contrast to the growth faults observed at the margin, these faults show a constant displacement. They can be found as far into the basin as 140 km off the ISC. Consequently, slumping and faulting are coeval processes.

The fold height and compression increase towards the Cyprus Arc (Fig. 5.17). Up to 50 km south of the Cyprus Arc the base of the evaporites and the internal reflections E1 and E2 are deformed much more heavily than in the basin. The M-reflection and E4, in contrast, show accented deformation compared to the basin only for approx. 25 km, whereas the seafloor looks flat and undisturbed. A close-up of the Plio-Quaternary reveals that the lower part of the Post-Messinian sediments, a complex of constant thickness of about 220 m shows the same deformation patterns as the M-reflection, indicating pre-kinematic deposition (Fig. 5.18). Above this pre-kinematic sediment

package the deformation in the sediments decreases to about 50 - 100 m below the seafloor. These upper 50 - 100 m of sediments show no deformation at all, indicating post-kinematic deposition.

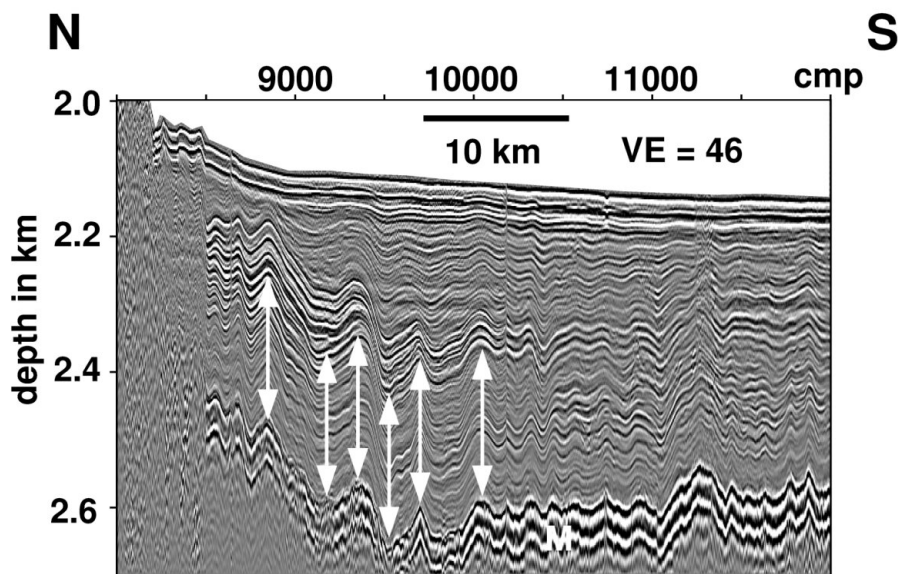


Figure 5.18 A depth migrated section of seismic line HH04-06, showing a close-up of the Plio-Quaternary near the Cyprus Arc. The lower part of the Post-Messinian sediments of roughly 220 m shows the same deformation patterns as the M-reflection (indicated by the white M). The sediment package above shows a decrease in deformation up to about 50 - 100 m below the seafloor. The uppermost sediments appear almost undisturbed.

At the Eratosthenes Seamount the seafloor is heavily deformed, almost parallel to the top of the evaporites, which pinch out near CMP 3000 at the very steep angle of 23° (Fig. 5.19). Here the M-reflection is heavily distorted and disrupted, much in contrast to the N-reflection, which appears smooth until it begins to rise at an angle of about 4° near CMP 4300 and disappears approx. 10 km off the flank of the seamount. Internal reflections are not continuously observed, therefore it is not possible to determine down to which depths the evaporites are affected by compression. Nevertheless, the N-reflection does not seem to be affected. Faults, pop-ups or heavy folding are observed at the locations of the fault lines or shear zones postulated by Abdel Aal et al. (2000) and Neev et al. (1976) (Fig. 5.20), which confirms the existence of these fault lines and shear zones in the basin.

5.5 Discussion

5.5.1 Origin of the internal reflections

Up to 4 internal reflections within the evaporites are observed in the Levantine Basin (Figs. 5.4, 5.7, 5.8, 5.17). Internal reflections and layering of evaporites in the Mediterranean Sea have been described by other authors (e.g. Réhault et al. 1984, Garfunkel, 1984, Rouchy and Saint Martin 1992, Polonia et al. 2002, Gradmann et al. 2005, dos Reis et al. 2005). Three explanations have been given for these reflections: a) interbedded shales, b) layers of different evaporites, and c) several depositional cycles.

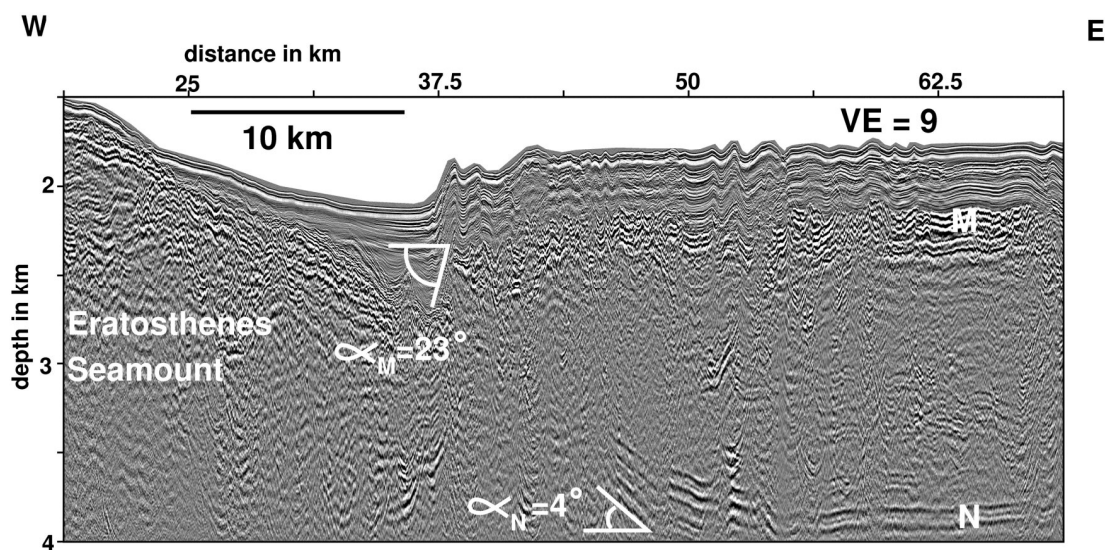


Figure 5.19 Section of seismic line HH04-08, depth migrated, showing the Eratosthenes Seamount. Top and bottom of evaporite layer are indicated by M, and N, respectively. The M-reflection is severely distorted, whereas the N-reflection is comparatively smooth, rising at an angle of about 4° , which matches the slope of the seamount. Note the steep decline of M near the seamount, importing an angle of 23° (vertical exaggeration is 9) of the top of the evaporite body.

a) Garfunkel (1984) and Garfunkel and Almagor (1984) postulate overpressured shales interbedded within the impervious evaporites. This explanation can not be ruled out. However, it does not explain the different deformation pattern of the individual evaporitic sequences nor their different rheology.

b) Réhault et al. (1984) identify three layers within the evaporite succession in the Western Mediterranean: upper evaporites (composed of halite, gypsum and marls), salt (halite), and lower evaporites (possibly of the same composition as the upper evaporites). Dos Reis et al. (2005) find these three layers also in the Gulf of Lions. Polonia et al. (2002) detect two units within the Messinian in the Eastern Mediterranean Sea. They interpret the upper unit, which is characterised by folded high-amplitude

reflections, as upper evaporites composed of marls and gypsum, and the lower unit, which is almost transparent and reflection-free, as halite. These observations and interpretations delineate a single cycle of evaporite deposition.

c) Cohen (1993) describes a typical depositional cycle of Messinian evaporites in the Levantine Basin as marine clay → gypsum → halite, although he finds from well measurements that quite often one of the evaporitic members is missing and cycles become a couplet of either clay → gypsum or clay → halite. Our observation of 4 internal reflections, i.e. 5 including the M-reflection, with 5 transparent layers in between leads to the assumption of 5 cycles of evaporite deposition. Cohen (1993) also observes several cycles of evaporites in boreholes offshore Israel. Consequently, we suggest that the single intra-salinar reflections mark the boundaries between 5 cycles of evaporite deposition. This explains also the brittle deformation of the uppermost evaporites, as already described by Gradmann et al. (2005), owing to the presence of, e.g., anhydrite or gypsum at the top of each sequence.

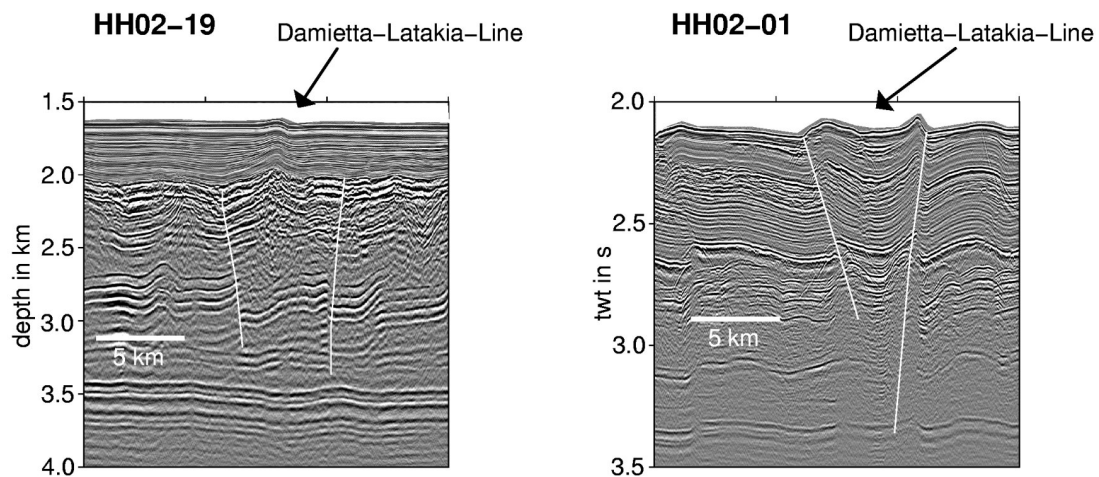


Figure 5.20 Seismic sections showing the effects of the Damietta-Latakia Line. Left: Hump in the seafloor above thrusts in the M-reflection and internal reflections and a depression in the N-reflection on HH02-19 where the Damietta-Latakia Line crosses. Right: Pop-up structure which developed above the Damietta-Latakia Line on HH02-01.

5.5.2 Syn-depositional evaporite deformation

The vertical variation of the distortion patterns of each intra-salinar reflection and evaporitic sequence, respectively, can be interpreted by syn-depositional deformation before the next sequence was deposited. The orientation of the internal reflections in N - S direction differs significantly from their orientation in E - W direction (Figs. 5.4c and 4d). The remarkable N – S directed thrusts of reflection E4 (Fig. 5.7), which do not occur in E3 and which do not affect the uppermost evaporitic sequence, can be explained by a northbound displacement during the Messinian, caused, e.g., by gravity

gliding that forced the young and 'wet' evaporites to creep downslope towards the basin centre. Such young and wet evaporites are supposed to have very low internal shear strength. On the other hand, numerical models of salt tectonics driven by sediment load show that post-depositional gravity gliding of salt occurs with vertically different gliding velocities depending on the assumed flow dynamics (Gemmer et al., 2004). Consequently, if Poiseuille or combined Poiseuille-Couette dominated salt flow is assumed, the highest gliding velocities occur in the middle of the salt body. If this model applies to the evaporites in the Levantine Basin, the northbound contraction of intra-salinar sequences observed in the centre of the basin can be also explained by Post-Messinian deformation. However, since the thrusts did not penetrate or even affect the uppermost evaporitic sequence, we rule out this possibility.

In E - W direction the intra-salinar reflections run subparallel to the N-reflection. They dip basinward and top lap the M-reflection in the landward direction. The subsidence analysis indicates that in E - W direction little lateral displacement took place. Therefore, the geometry of the basinal evaporites can be restored by removing this sediment load (Fig. 5.6). Consequently, the E - W lines gives the better picture of the status of the evaporites after the Messinian (Fig. 5.4a).

The backstripping analysis of the evaporites gives an idea how the individual evaporitic sequences were deposited. Assuming simple isostatic compensation of the evaporite load, i.e. without crustal flexure response or additional differential subsidence, the lower 4 sequences were deposited parallel to the slope with a westward dipping upper boundary (Fig. 5.9a-g). The question arises whether salt can be deposited with a non-horizontal surface or not. A horizontal deposition seems to be more likely since the salt precipitates from a brine with a high salt concentration. If we assume a westward tilt of the basin after a horizontal deposition of the lower 4 sequences, the uppermost sequence was also horizontally deposited, which also explains its westward increasing thickness (Fig. 5.9h - l). The westward tilt of the Levantine Basin in the Late-Messinian could be related to major geodynamic changes in that realm like the transition from contraction to strike-slip tectonics along the eastern Cyprus Arc (Hall et al., 2005) or the onset of seafloor spreading in the Red Sea (Bosworth et al., 2005).

On the eastern basin margin, the sequences reveal a basinwards prograding pattern. No basinal evaporites are present at a depth of less than 1800-1900 m after the backstripping of the Plio-Quaternary sediment prism. In general, several explanations are possible, e.g., by a sea level drop of almost this amount. However, this contradicts the results of two-dimensional stratigraphic simulations which led to the assumption of a sea level drop by 800-1300 m (Ben-Gai et al., 2005). Another explanation is erosion of the evaporites during the Post-Messinian transgression event or by currents parallel to the coast. Finally, a syn-depositional and basinward creep might also be considered.

5.5.3 Post-Messinian Deformation

For the discussion of the post-Messinian deformation we divide our study area into five regions: the eastern and southern basin margin, the central basin, the Cyprus Arc and the Nile Scarp around the Eratosthenes Seamount. We further discuss the basinal shear zones, the Israeli Slump Complex and the St. Pauli mud volcano.

Eastern Margin

Extensional features such as normal and listric growth faults and keystone grabens are observed at the margin, forming a corridor of extension parallel to the coastline (Fig. 5.12). Both thin-skinned and thick-skinned tectonics have to be considered. As it is discussed by Gradmann et al. (2005) and as it is confirmed by the backstripping analysis in this study, some lateral displacement of the basinal evaporites occurs southwest of Haifa along line HH02-01 (Fig. 5.6). The N-reflection represents the detachment fault. Salt rollers and salt welds evolved where the evaporites have been withdrawn. The presence of brittle upper evaporites and the observed turtle structures led to an adapted model of Letouzey et al. (1995) (Fig. 13 of Gradmann et al., 2005). Further south a lateral displacement did not occur and no salt welds evolved (e.g., Figs. 5.6, 5.10, 5.13). The extension of the upper basinal evaporites and the overburden probably represent an earlier stage of salt tectonics, because the thickness of the overburden is less than in the north. Compared to line HH02-01, the pinchout of the evaporites beneath the overburden occurs further downslope where the differential load is less significant. The evaporites are distorted but not withdrawn. This is in accordance to the numerical models of Gemmer et al. (2004), which show similar extensional features after 5 Ma in similar settings.

However, purely salt tectonic models do neither explain the faults that pierce the N-reflection nor the growth faults that are above disturbed, but laterally continuous basinal evaporites as on line HH02-10 (Fig. 5.14). Since the M-reflection is at the same depth level on both sides of the faults, extension owing to differential subsidence can be ruled out. Faults that cut through the entire basinal evaporites without affecting the N-reflection can also not be explained by accompanied rollover folding or antithetic normal faults, since salt tectonic should cause mainly ductile deformation.

Active transform or transcurrent faults represent an explanation of thick-skinned tectonics as suggested by other authors (Abdel Aal et al. 2000, Neev et al. 1976, Neev 1975, 1977) (Fig. 5.2). The strongest evidence of active thick-skinned tectonics is found in the southernmost survey area. South of 32° the Syrian Arc and Pelusium Line bends further to the west, which represent a right stepover. The dominant anticline and the horst (Fig. 5.15) can be considered as contractional ramps. As already proposed by Neev (1975), the transpression is a direct consequence of northward wedging of the crustal segments bounded to the east and west by the Dead Sea Transform Fault, the Pelusium Line and the Damietta-Latakia Line, respectively. Seafloor piercings of the

main faults represent compelling evidence of neotectonic activity, which is not surprising because the DST is also an active fault. Contrary to the Pelusium and Neev Line, the Shelf Edge Hinge Line runs subparallel to the DST and it reveals extension. The growth fault in Fig. 5.14 is right above the Hinge Line and can be also explained by transtension or block rotating.

Consequently, we suggest that those folds and faults which affect the upper Pre-Messinian as well as the basinal evaporites and the Plio-Quaternary cover sequences are the consequence of active strike-slip tectonics. Northwest of Haifa, the strike-slip faults (Fig. 5.5) merge with the fault zone that reaches from the Carmel structure to south of Beirut (Schattner et al., submitted).

Southern Margin

The thick layer of Plio-Quaternary sediments of the Nile Fan reveal extensional faults in the overburden. The subsidence estimations suggest a northbound displacement of the basinal evaporites. No salt diapirism could be detected, although the landward extension should give accommodation space for rising diapirs (Vendeville et al., 1992). According to the models of Gemmer et al. (2004), salt diapirism can be suppressed by continued sediment filling of extensional basins. The forebulging is also a feature that has been predicted by Gemmer et al. (2004). However, Gemmer et al. did not consider differential subsidence in their models.

Basinal contraction

There is an abundance of contractional folds, faults and thrusts in the basin (Figs. 5.7, 5.8, 5.19). In E - W direction, Gradmann et al. (2005) have also observed extensional structures near the shelf and pop-up-structures and overthrusting in the basin, which complies with the models of Letouzy et al. (1995) of moving salt. However, the backstripping analysis suggests that little westward salt flux occurred in the Levantine Basin except directly southwest of Haifa. In N - S direction, however, on line HH04-06, the backstripping of the sediment load reveals that the evaporite body is first reduced by about 200 m near the pinchout and then thickened by about 200 m. The orientations of the thrusts within the evaporites are also different depending on the orientation of the seismic profile. While the thrusts are oriented basinwards on the S - N profiles, no specific orientation is observed on the E - W profiles. This suggests that the evaporites have been squeezed northwards by the sediment load and accumulated approx. 50 km to the north. The northbound creep of the evaporites can be explained by the particularly thick sediment load near the Nile Fan of almost 3 km compared to about 1 km on the shelf off Israel. The pop-up structures and overthrusting observed on the E - W profiles represent probably out-of-plane movement. At the Eratosthenes Seamount the basin is narrower than north or south of it, like a bottleneck for the S - N flow of the evaporites. However, since the orientation of the bathymetry and the evaporite thickness in the Levantine Basin is not exactly S - N, but SSW - NNE (Figs. 5.3a and c), it seems

plausible that SSW - NNE is actually the main direction of salt movement (Fig. 5.21).

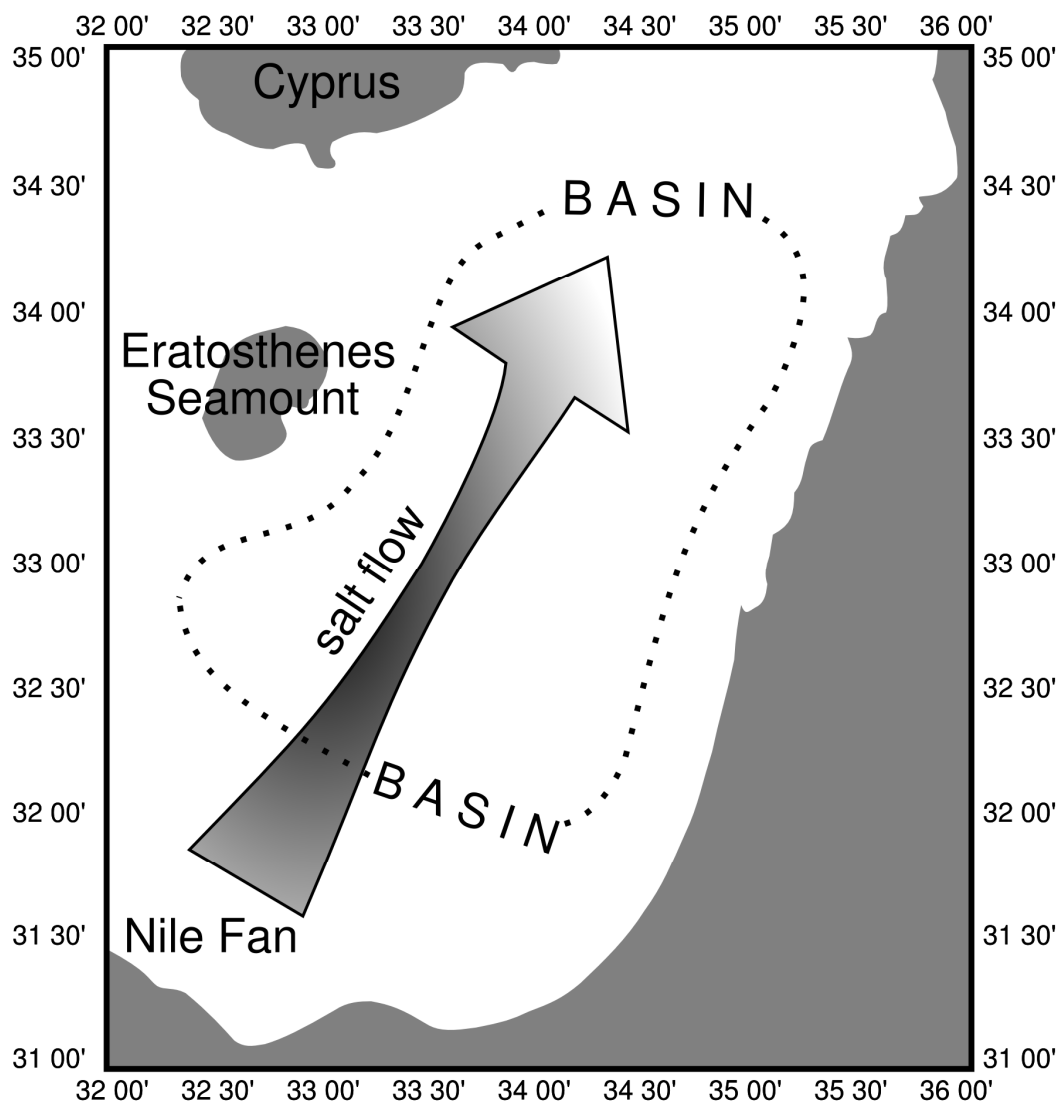


Figure 5.21 Sketch visualising the postulated NNW - SSE salt flow in the Levantine Basin towards the Cyprus Arc. The thinning of the arrow represents the bottleneck effect of the Eratosthenes Seamount on the salt flow.

Israeli Slump Complex

Slump masses have been found on several lines, and slumps in the south of the Levantine Basin have been described by Frey-Martinez et al. (2005). On our lines, these slump masses can be correlated with a transparent layer that is present throughout the entire basin (Fig. 5.13). A significant number of faults which have developed isochronously to the slump bodies are found up to 140 km offshore. It is possible that these faults are associated with mass wasting. Slumping causes the relocation of large

amounts of sediments, which then leads to a sudden change in sediment load on the evaporites at the lower slope. It is well conceivable that in order to compensate the increased differential load after the slumping, abrupt movements in the evaporites are triggered. In this case, the salt movement in the Levantine Basin would be an episodic process, a reaction to the slumping.

Cyprus Arc

While evidence of compression is found throughout the basin, enhanced compression occurs at the Cyprus Arc. The N-reflection is severely distorted, which proves that the observed compression at the arc is a result of thick-skinned tectonics.

The N-reflection is exceedingly deformed over a distance of 50 km and the M-reflection over a distance of 25 km. The seafloor, however, is flat. This indicates that compression abated since the Messinian and has now ceased completely. The sediments down to 50 to 100 mbsf are undisturbed, with the rough estimate of a constant sedimentation rate since the Messinian. This means that the contraction at the Cyprus Arc stopped at least 1 Ma ago. A comparison with bathymetric data of Benkhelil et al. (2005) reveals that the seafloor is not entirely flat along the Cyprus Arc. Our line HH04-06 runs through an area of recent quiescence, but to the east and west of it the seafloor is folded. Two models may explain the contraction here: 1) Thick-skinned (plate tectonic) basin shortening due to the subduction at the Cyprus Arc and 2) Thin-skinned tectonics (salt tectonics) owing to the northward creep. According to the models of Gemmer et al. (2004), an increased deformation is expected far in the north after some 10 Ma only. Hall et al. (2005) date the transition from a compressional to a transpressional regime at the Cyprus Arc to early-middle Pliocene, which is much earlier than the observations on line HH04-06 indicate. Consequently, we assume that the increased but partly ceased deformation at the Cyprus Arc is a consequence of thick-skinned tectonics.

Eratosthenes Seamount

Near the Eratosthenes Seamount, the situation is entirely different. The N-reflection appears comparatively flat and smooth until it merges into the flank of the seamount, while the M-reflection and the seafloor are strongly distorted. Hence, the deformation observed there has probably been caused by thin-skinned tectonics. Since there is no significant E - W movement of the evaporites, the E - W contraction observed at the Eratosthenes has probably been caused by the northward creep through the bottleneck between seamount and the Levantine margin. It is a remarkable fact that no salt glaciers or salt tongues escaped from the evaporites into the Nile Scarp.

Basinal shear zones

At the Nile Scarp, the evaporites and the overburden might be overprinted by the Baltim-Hecateus Shear Zone, which runs along its south-eastern flank. Where the Damietta-Latakia Line (Abdel Aal et al., 2000; Neev, 1975, 1977; Neev et al., 1976) is crossed by the seismic lines (Fig. 5.2), thrusting, folding, and pop-up structures are observed (Fig. 5.20). The observed faults are clearly contractional. It is likely that faults in the crust do not only affect the sediments immediately above, but have an impact on a wider range of the overlying sediments of up to several km. Considering the tectonic regime with the rotational movements of the African and the Anatolian plates the shear zones cannot be purely strike-slip, but must have a transpressional component. This component of transpression could partly account for the compression observed in the evaporites and Plio-Quaternary sediments in the Levantine Basin, along with effects of salt tectonics. Generally, the compressional regime in the basin is probably generated by a superposition of thick-skinned and thin-skinned tectonics.

St. Pauli mud volcano

Mud volcanoes and cold seeps are common features in the Mediterranean Sea (see Huguen et al. 2005, Kopf et al. 1998, Limonov et al. 1996, Loncke et al. 2004, Coleman and Ballard 2001). Loncke et al. (2004) find mud volcanoes on the Nile Deep Sea Fan in an extensive regime, where salt is absent as a result of gravity gliding or above growth faults, which act as fluid paths from deeply buried mud sources, i.e. well below the salt. However, since the evaporites are 1.5 km thick beneath the St. Pauli mud volcano and since there is no trace of faults cutting through them, this mud volcano does not seem to fall under this category.

The presence of the seismically transparent cone on the upper evaporites and beneath the mud volcano suggests a correlation between these two features, which implies a fluid escape from the evaporites. In most settings salt represents an impermeable and sealing sequence. On the other hand, salt is permeable for fluids if the fluid pressure is above the lithostatic pressure, because the tensile strength of salt is negligible (J. Urai, pers. comm.). Fluid migration through a solid sequence of Messinian evaporites has already been proposed by Gradmann et al. (2005). Further, we hypothesise that the cone atop the M-reflection and beneath the mud volcano consists of salt which has precipitated from fluids that escape from the evaporites and which feed the mud volcano. This interpretation and the observed sediment thickness of less than 1000 m above the salt cone suggest a fluid reservoir within or beneath the evaporites.

Murton and Biggs (2003) present a simple model for assessing the depth of the mud source from the height of a mud volcano above the seafloor and the density of the underlying sediments (Eq. 2).

$$h_{s2} = (h_v(\rho_{mud} - \rho_w) - h_{s1}(\rho_{s1} - \rho_{mud})) / (\rho_{s2} - \rho_{mud}) \quad (\text{Eq. 2})$$

Here, ρ_{mud} denotes the density of the mud, ρ_w the density of water, ρ_{s1} the density of

the upper sediments, and ρ_{s2} the density of the lower sediment (in this case evaporites). The height of the mud volcano is h_v , the water depth is h_w , the thickness of the upper sediment layer is denoted by h_{s1} , and the thickness of the lower sediment layer from the top to the mud source is represented by h_{s2} .

We assumed densities of 1.8 - 2.0 kg/m³ for the upper sediments, and 2.2 kg/m³ as an average for the evaporites. These densities have been used for gravity modelling in the Levantine Basin (Ben-Avraham et al. 2002, Netzeband et al., submitted). The sediment density also corresponds with borehole measurements at the Napoli mud volcano on the Eastern Mediterranean Ridge (Kopf et al. 1998). The density of the mud must be greater than the density of the upper sediments but not the same as the density of the evaporites as required by the equation of Murton and Biggs (2003). A mud density 0.1 - 0.2 kg/m³ greater than the sediment density, i.e. e. 1.9 - 2.1 kg/m³ yields a depth of the mud source within the evaporite layer. If the mud source were deeper than the base of the evaporites, the sediment density would have to be lower, e.g. 1.7 kg/m³, and the mud density at least 0.3 or the mud kg/m³ greater than the sediment density.

These estimates corroborate our interpretation of fluid sources beneath the top of the evaporites. An overpressurized fluid source within the evaporites can be explained by dewatering of young and wet salt, by gypsum-anhydrite conversion, or by the presence of intercalated water bearing sediments. Fluid pressure above the lithostatic pressure may also result from undercompacted and heated subsalt sediments. Overpressuring from plate-tectonics could result from transpressional strike-slip faulting along the Pelusium Line.

5.6 Conclusions

The Messinian evaporitic succession reveals five evaporitic sequences, separated by four internal reflections traceable throughout the entire Levantine Basin. The interpretation of the sequences as deposited during five depositional cycles is consistent with onshore drillings. The 4 internal reflections and M represent 4 temporal sea level rises, during which thick halite layers were deposited, interbedded with rigid evaporites or clastic sediments or both. Each sequence was independently folded and faulted in a northern direction. We conclude that syn-depositional deformation occurred, e.g., lateral basinward creep caused by gravity forcing.

W - E striking seismic lines show basinward dipping internal reflections. However, the top of the evaporites, the M-reflection, runs horizontally and the uppermost sequence thickens to the west. This depositional pattern can be explained by horizontally deposited evaporitic sequences and a basinward tilt of the Levantine Basin during the Late Messinian, before the last and upper sequence precipitated. This tectonic event might be correlated with the overall changes of the geodynamic setting in the

Middle East during that time.

Off Israel and from south to north the sediment load on the edge of the basinal evaporites increases, since the marginal pinchout has been shifted from beneath the lower slope to beneath the shelf. The apparent rollback folding, however, is a consequence mainly of differential subsidence and not of lateral displacement of the evaporites and thin-skinned extension, respectively.

The northward increasing differential sediment load allows the study of initial salt tectonics in succeeding evolutionary stages. Off southern Israel, only the Plio-Quaternary sediment cover shows extensional faults and the upper evaporites are little deformed. In general, very little basinward displacement occurred to the west. Off northern Israel and right south of Haifa the presence of salt welds and salt rollers gives evidence of the displacement of the entire basinal evaporites.

After backstripping the Plio-Quaternary and the evaporite layer, the Pre-Messinian seafloor is 1800 - 1900 m deep. This suggests that the sea level drop during the Messinian Salinity Crisis might have been greater than the previously assumed maximum of 1300 m. Alternatively, the evaporites could have been eroded or displaced during or directly after deposition, before they were covered by Pliocene sediments.

The load of the Nile Fan sediments squeezes the evaporites into an NNE direction parallel to the bathymetric gradient of the basin. In front of the lower fan, the evaporites are thickened due to forebulging. However, even here the rollback folding is mainly a seeming feature. The decline of the top of the evaporites beneath the Nile Fan is caused by differential subsidence.

The remobilization and depositing of the sediments from the Israeli Slump Complex on the edge of the evaporites coincides with the episodic contractional faulting of upper evaporites and overburden up to 140 km away from the slumps, which has been observed by Gradmann et al. (2005). We therefore suggest a causative correlation.

A seismically transparent cone on the top of the evaporites and beneath the St. Pauli mud volcano is interpreted as salt which has precipitated from fluids escaping from the evaporites. Since the thickness of the evaporites is about 1500 m, the fluid reservoir must lie within the evaporites, or the fluids migrate through the entire evaporitic succession.

Several strike-slip faults like the Pelusium, Shelf Edge Hinge and Neev1 Lines, which run subparallel to the Israeli slope, as well as the Damietta-Latakia Line are tectonically active. The faults overprint the entire succession of evaporites and overburden. Where the Pelusium Line bends further to the West, transpression occurs resulting in uplifted horsts and anticlinal folding.

Acknowledgements

We would like to thank the masters, crews and scientific staff of RV Meteor and RV Pelagia for the excellent support during the surveys. Thanks to Zvi Ben-Avraham, Zvi Garfunkel and Janos Urai for initial ideas. Special thanks to Lea Scharff for carrying out the depth migration. Figures 5.1, 5.2, 5.3, and 5.6 were created with GMT (Wessel and Smith 1998). The GEMME project was funded by DFG grant HU698/07. The SAGA cruise was funded by the University of Hamburg.

6 Conclusions

In my thesis I have analysed the crust in the Levantine Basin. I have shown that the Moho lies in a depth between 20 km and 28 km. The thickness of the crystalline basement varies between 20 km at the southern Israeli margin and 8 km in the centre of the basin. I have also proved that the crust in the Levantine basin is thinned continental crust, stretched with a β -factor of approx. 3.

The existence of fault lines in the crust, postulated by Neev et al. (1976), Neev (1975, 1977) and Abdel Aal (2000), e.g. the Pelusium Line, the Shelf Edge Hinge Line, and the Damietta-Latakia Line has been confirmed. Some of these fault lines indicate an extensional regime, some a compressional one, but all are active. According to Walley (1998) these fault lines developed during the rifting phases from the Late Permian to the Early Jurassic along a N – S axis parallel to the present margin. They were later reactivated in the Cretaceous by the compressional regime of the Syrian Arc. I have shown that since the Messinian the Pelusium Line, and the Shelf Edge Hinge Line, and other fault lines between these two have been active as extensional fault lines, whereas the Damietta-Latakia Line has been influenced by a compressional setting.

These are major findings which have to be included in future geodynamic reconstructions of the Tethys and the Mediterranean. Rifting took place along a N – S axis, accompanied by extensional faulting. The rifting did not reach the stage of seafloor spreading. Compression during the Syrian Arc event in the Cretaceous took place in the basin, while the margin was predominantly influenced by extension. This coexistence of both regimes is still active and has been so for at least 5 Ma. These discoveries are the result of both parts of my investigation, the modelling of the refraction seismic data and the analysis of the multichannel seismic data. The inference that the crust is continental has been the key to the interpretation of the active deep-rooted faults.

The analysis of the evaporite layer and the Plio-Quaternary has yielded new insights into salt tectonics. A clear distinction between plate tectonic and salt tectonic phenomena is possible, because the base of the evaporite is well expressed in the data. The evaporite body has been found to consist of 5 distinct layers, probably representing just as many cycles of evaporites, possibly interbedded with sediments. From the varying deformation patterns of the evaporite layers and the Plio-Quaternary it was possible to deduce the change in the plate tectonic regime from compression to transpression at the Cyprus Arc. The position of the tops of the internal evaporite layers indicates that initially, these layers were deposited horizontally. Differential subsidence of the basin possibly occurred towards the end of the Messinian, before deposition of the last evaporite layer. The direction of the Post-Messinian evaporite movement is not

radial towards the centre of the Levantine Basin, but has been identified as NNE, following the orientation of the basin. Running northwards along the margin, the pinchout of the evaporites moves from the lower slope to the shelf, which leads to a higher sediment load near the pinchout in the north than in the south. Hence, different stages of salt tectonics can be observed along the margin. Nevertheless, even near Haifa, where the salt movement is most advanced and salt rollers have been observed by Gradmann et al. (2005), only very early stages of salt tectonics are involved.

A slump body, which Frey-Martinez (2005) named the ISC, was observed on several seismic lines of the study area. A series of faults are coeval, which suggests a causative relation, the slump possibly triggering sudden salt movement. A mud volcano was found in the south of the Levantine Basin. It is located above a thick evaporite layer and there is evidence that the mud source lies within this evaporite layer.

All these results are important for the understanding of the regional setting and contribute to our knowledge of the Mediterranean. But some findings, viz. the mud volcano above a thick evaporite layer, the possible relation of slumps and salt tectonic faulting, the deposition pattern of the evaporites and the inhomogeneity of the evaporite body, are of global significance, because they present new information regarding salt tectonics and related fluid flow. Fluid paths through thick halite layers were considered impossible until recently. Therefore the mud volcano St. Pauli represents important new evidence of the permeability of halite by fluids. The conditions under which halite becomes permeable for fluids have yet to be investigated.

The 'bull's eye' pattern of evaporite deposition (e.g. Einsele 2000) implies that the top of the evaporites extends upwards the pre-evaporite slope. However, the Airy backstripping analysis gives evidence of a horizontal evaporite deposition. This presents a new detail in the comprehension of salt layers. The partition into several evaporite layers which are attributed to different depositional cycles does not contradict our understanding of evaporite deposition, but it has never been observed so clearly. The various stages of salt tectonics along the margin constitute an excellent site for a refinement of our understanding of salt tectonics. Gradmann et al. (2005) have already suggested a modification of Letouzey's (1995) models. In consequence of this thesis, these models can be further improved. We now know e.g. that the sediment load induces differential subsidence resembling a rollback, which can be mistaken for a lateral salt movement. It can also be stated, that for an analysis of salt tectonics it is indispensable to properly image the base of the evaporite layer. Contrary to the general presumption that a salt layer decouples tectonic processes in the basement from the sediment overburden, I have proved that deep-rooted faults in the basement can pierce an evaporite layer and even create a significant throw. Without a thorough study of the plate tectonic processes it may not be possible to decide whether a fault originates in the crust. Otherwise it may be mistaken for a salt tectonic feature.

The possibility of slumping as a possible trigger for salt movement far into the basin represents a valuable addition to the present knowledge of salt tectonic processes. An evaporite body which reacts over several tens of km to stress strongly deviates from our

image of salt as a generally viscous, primarily ductile body.

In summary, I have found that the crust in the Levantine Basin is thinned continental crust and adjusted the geodynamic reconstructions of the Tethys and the Mediterranean Sea accordingly. This result also supports the hypothesis of the transition from subduction to continent collision at the Cyprus Arc in the last 5 Ma. I have mapped the evaporites in the basin, and improved the understanding of the salt tectonics in this area. I have found evidence of fluid transport through thick halite in shape of a mud volcano. And finally, I have made several contributions to the general theory of salt tectonics regarding deposition, decoupling, ductility, and trigger mechanisms.

References

- Abdel Aal, A., El Barkooky, A., Gerrits, M., Meyer, H., Schwander, M., Zaki, H., 2000, Tectonic Evolution of the Eastern Mediterranean Basin and its significance for hydrocarbon prospectivity in the ultradeepwater of the Nile Delta. *The Leading Edge*, 19, 1086 - 1102
- Albareello, D., Mantovani, E., Babbucci, D., Tamburelli, C., 1995, Africa-Eurasia kinematics: main constraints and uncertainties. *Tectonophysics*, 243, 25 - 36
- Allen, P. A. and Allen, J. R., 1990. Basin analysis - principles & applications, Blackwell Scientific Publications, Oxford, 463 pp.
- Almagor, G., 1984, Salt controlled slumping on the Mediterranean slope of central Israel. *Mar. Geophys.Res.*, 6, 227 - 243.
- Almagor, G., 1993, Continental slope processes off northern Israel and southernmost Lebanon and their relation to onshore tectonics. *Mar. Geol.*, 112, 151 - 169.
- Ben-Avraham, Z. und Ginzburg, 1990, Displaced terranes and crustal evolution of the Levant and the eastern Mediterranean. *Tectonics*, 9, 613 - 622.
- Ben-Avraham, Z., Kempler, D. & Ginzburg, A., 1988. Plate convergence in the Cyprian Arc. *Tectonophysics*, 146, 231 - 240.
- Ben-Avraham, Z., Tibor, G., Limonov, A.F., Leybov, M.B., Ivanov, M.K., Tokarev, M.Y. et al., 1995. Structure and tectonics of the eastern Cyprean Arc. *Marine and Petroleum Geology*, 12(3), 263 - 271.
- Ben-Avraham, Z. & Ginzburg, A., 1986, Magnetic anomalies over the central Levant continental margin. *Mar. Pet. Geol.*, 3, 220 - 233
- Ben-Avraham, Z., Ginzburg, A., Makris, J. & Eppelbaum, L., 2002. Crustal structure of the Levant Basin, eastern Mediterranean. *Tectonophysics*, 346, 23 - 43.
- Ben-Gai, Y., Ben-Avraham, Z., Buchbinder, B., Kendall, C. G.St.C., 2005. Post-Messinian paleodepth reconstruction of the Levantine margin off Israel. *Mar. Geol.*, 221, 359 - 379
- Benkhelil, J., Bayerly, M., Branchoux, S., Courp, T., Gonthier, E., Hübscher, C., Maillard, A., Tahchi, E., 2005. La branche orientale de l'arc de Chypre. Morphostructure d'une frontière de plaques d'après les résultats de la campagne BLAC (2003). *C. R. Geoscience*, 337, 1075 - 1083
- Berckhemer, H., 1997. Grundlagen der Geophysik. Veröffentlichung der Fachbereichs Geowissenschaften der Johann Wolfgang Goethe Universität. Institut für Meteorologie und Geophysik, Frankfurt

- Bohnhoff, M., Makris, J., Papanikolaou, D., Stavrakakis, G., 2001. Crustal investigation of the Hellenic subduction zone using wide aperture seismic data. *Tectonophysics*, 343, 239 – 262
- Bosworth, W., Huchon, P., McClay, K., 2005. The Red Sea and Gulf of Aden Basins. *Journal of African Earth Sciences*, 43, 334-378
- Bridge, C., Calon, T.J., Hall, J., Aksu, A.E., 2005. Salt tectonics in two convergent-margin basins of the Cyprus Arc, Northeastern Mediterranean. *Mar. Geol.*, 221, 223 - 259
- Buck, W. R., 1991. Modes of continental lithospheric extension. *J. Geophys. Res.*, 96, 20161 – 20178
- Cadek, O. and Martinec, Z., 1991. Spherical harmonic expansion of the Earth's crustal thickness up to degree and order. *Studia Geoph. Geod.*, 35, 151 - 165
- Cobbold, P. & Szamarti, P., 1991. Radial gravitational gliding on passive margins. *Tectonophysics*, 188, 249-289.
- Cohen, A., 1993. Halite-clay interplay in the Israeli Messinian. *Sedimentary Geology*, 86, 211 - 228
- Coleman, D. F., Ballard, R. D., 2001. A highly concentrated region of cold hydrocarbon seeps in the southeastern Mediterranean Sea. *Geo-Mar. Lett.*, 21, 162 – 167
- Crans, W., Mandl, G. & Haremboure, J., 1980. On the theory of growth faulting: a geomechanical delta model based on gravity sliding. *Journal of Petroleum Geology*, 2, 265-307.
- Dercourt, J., Zonenshain, L. P., Ricou, L. E., Kazmin, V. G., Le Pichon, X., Knipper, A. L., Grandjacquet, C., Sbertshikov, I. M., Geysant, J., Lepvrier, C., Pechersky, D. V., Boulin, J., Sibuet, J. C., Savostin, L. P., Sorokhtin, D., Westphal, M., Bazhenov, M. L., Laurer, J. P., Bijou-Duval, B., 1986, Geological evolution of the Tethys belt from the Atlantic to the Pamirs since the Lias. *Tectonophysics*, 123, 241 - 315
- Dimitrov, L. and Woodside, J., 2003. Deep sea pockmark environments in the eastern Mediterranean. *Mar. Geol.*, 195, 263 - 276
- Druckman, Y., Buchbinder, B., Martinotti, G.M., Siman Tov, R., Aharon, P., 1995. The buried Afik Canyon (eastern Mediterranean, Israel): a case study of a Tertiary submarine canyon exposed in Late Messinian times. *Mar. Geol.*, 123, 167 - 185
- Einsele, G., 2000. *Sedimentary basins. Evolution, facies, and sediment budget*. Springer-Verlag Berlin Heidelberg
- El-Isa, Z., Mechie, J., Prodehl, C., Makris, J., Rihm, R., 1987, A crustal structure study of Jordan derived from seismic refraction data. *Tectonophysics*, 138, 235 - 253
- Farris, M.A., Griffiths, M.A., McGrandle, A., 2004. Deep structural lineaments: Influence

- on basin evolution and cenozoic structuration in the East Mediterranean Levant Basin. In: *PETEX 2004, London, 23-25 November 2004, London, Petroleum Exploration Society of Great Britain, 2004*, extended abstracts on CDROM, unpaginated.
- Freund, R., Goldberg, M., Weissbrod, T., Druckman, Y., Derin, B., 1975. The Triassic-Jurassic structure of Israel and its relation to the origin of the Eastern Mediterranean. *Isr. Geol. Surv. Bull.*, 65, 105 - 127.
- Frey-Martinez, J., Cartwright, J., Hall, B., 2005. 3D seismic interpretation of slump complexes: examples from the continental margin of Israel. *Basin Research*, 17, 83 - 108
- Funck, T., Jackson, R., Loudon, K.E., Dehler, S.A., Wu, Y., 2004. Crustal structure of the northern Nova Scotia rifted continental margin (eastern Canada). *J. Geophys. Res.*, 109, doi:10.1029/2004JB003008
- Gardosh, M. and Druckmann, Y., 2006. Stratigraphy and tectonic evolution of the Levantine Basin, offshore Israel. In: A. Robertson (Ed), *Tectonic Development of the Eastern Mediterranean Region*, Geological Society Special Publication. (in press)
- Garfunkel, Z., 1984. Large-scale submarine rotational slumps and growth faults in the Eastern Mediterranean. *Mar. Geol.*, 55, 305 - 324
- Garfunkel, Z. and Almagor, G., 1984. Geology and Structure of the continental margin off northern Israel and the adjacent part of the Levantine Basin. *Mar. Geol.*, 62, 105 - 131
- Garfunkel, Z., 1998. Constraints on the origin and history of the Eastern Mediterranean basin. *Tectonophysics*, 298, 5 - 35.
- Garfunkel, Z., 2004. Origin of the Eastern Mediterranean basin: a reevaluation. *Tectonophysics*, 391, 11 - 34
- Garfunkel, Z., Arad, A. & Almagor, G., 1979. The Palmahim Disturbance and its regional setting. *Geological Survey of Israel Bulletin*, 72, 56.
- Ginzburg, A., Makris, J., Fuchs, K., Prodehl, C., Kaminski, W., Amiti, U., 1979, Seismic study of the crust and upper mantle of the Jordan - Dead Sea Rift and their transition toward the eastern Mediterranean. *J. Geophys. Res.*, 84, 5605 - 5612
- Ginzburg, A. and Ben-Avraham, Z., 1987, The deep structure of the central and southern Levant continental margin. *Ann. Tectonicae*, 1, 105 - 115
- Ginzburg, A., Ben-Avraham, Z., Makris, J., Hubral, P., Rotstein, Y., 1994, Crustal structure in northern Israel. *Mar. Pet. Geol.*, 11, 501 - 506
- Gemmer, L., Ings, S.J., Medvedev, S. & Beaumont, C., 2004. Salt tectonics driven by differential sediment loading: Stability analysis and finite element experiments. *Basin Research*, 16, 199 - 218

- Gradmann, S., Hübscher, C., Ben-Avraham, Z., Gajewski, D., Netzeband, G. L., 2005, Salt tectonics off northern Israel. *Mar. Pet. Geol.*, 22, 597 - 611
- Gvirtzman, G. & Buchbinder, B., 1978. The Late Tertiary of the coastal plain and continental shelf of Israel and its bearing on the history of the Eastern Mediterranean, in: Ross, D.A., Neprochov, Y.P. (Eds.), *Init. Repts. DSDP*, 42 II. U.S Govt. Printing Office, Washington D.C., pp. 1195 - 2220.
- Hall, J. K., Krasheninnikov, V. A., Hirsch, F., Benjamini, C., Flexer (Eds.), A Geological framework of the Levant, Volume II: The Levantine Basin and Israel. Historical Productions-Hall, 2005
- Hall, J., Calon, T.J., Aksu, A.E., Meade, S.R., 2005. Structural evolution of the Latakia Ridge and Cyprus Basin at front of the Cyprus Arc, Eastern Mediterranean Sea. *Mar. Geol.*, 221, 261 – 297
- Hauser, F. O'Reilly, B.M., Jacob, A.W.B., Shannon, P.M., Makris, J., Voigt, U., 1995. The crustal structure of the Rockall Trough: Differential stretching without underplating. *J. Geophys. Res.*, 100, 4097 – 4116
- Hirsch, F., 1984, The Arabian sub-plate during the Mesozoic. In: Dixon, J. E., and Robertson, A. H. F. (Eds.), *Geological Evolution of the Eastern Mediterranean*. Geol. Soc. Spec. Publ. London, 17, 217 - 224
- Hirsch, F., Flexer, A., Rosenfeld, A., Yellin-Dror, A., 1995. Palinspastic and crustal setting of the eastern Mediterranean, *J. Pet. Geol.* , 18, 149 - 170
- Hsü, K.J., Cita, M.B. & Ryan, W.B.F., 1973. The origin of the Mediterranean Evaporites, in: Ryan, W.B.F., Hsü, K.J. (Eds.), *Init. Repts. DSDP*, 13. U.S. Govt. Printing Office, Washington D.C., pp. 1203 - 1232.
- Hsü, K.J., Montadert, L., Bernoulli, D., Cita, B.C., Erickson, A. & Garrison, R.E. et al., 1978. History of the Mediterranean Salinity Crisis, in: Hsü, K.J., Montadert, L. (Eds.), *Init. Repts. DSDP*, 42 I. U.S. Govt. Printing Office, Washington D.C., pp. 1053 - 1078.
- Huguen, C., Mascle, J., Woodside, J., Zitter, T., Foucher, J.-P., 2005. Mud volcanoes and mud domes of the Central Mediterranean Ridge: Near-bottom and in situ observations. *Deep-Sea Research I*, 52, 1911 - 1931
- Humphris Jr., C.C., 1978. Salt movements on continental slope, northern Gulf of Mexico. *American Association of Petroleum Geologists Studies in Geology*, 7, 69-85.
- Jackson, M.P.A., 1995. Retrospective salt tectonics, in: Jackson, M.P.A., Roberts, D.J., Snelson, S. (Eds.), *Salt tectonics: a global perspective*. AAPG Memoir Tulsa, Oklahoma, USA, 65, pp. 1-28.
- Jiménez-Munt, I., Sabadini, R., Gardi, A., Bianco, G., 2003. Active deformation in the

- Mediterranean from Gibraltar to Anatolia inferred from numerical modeling and geodetic and seismological data, *J. Geophys. Res.*, 108, 2006, doi:10.1029/2001JB001544
- Kempler, D., Garfunkel, Z., 1994, Structures and kinematics in the northeastern Mediterranean: A study of an unusual plate boundary. *Tectonophysics*, 234, 19 - 32
- Kopf, A., Clennell, M. B., Camerlenghi, A., 1998. Variations in sediment physical properties and permeability of mud-volcano deposits from Napoli dome and adjacent mud volcanoes. In: Robertson, A.H.F., Emeis, K.-C., Richter, C., Camerlenghi, A. (Eds.), *Proc. ODP, Sci Results*, 160, College Station, TX (Ocean Drilling Program)
- Letouzey, J.B., Coletta, R. & Chermette, J.C., 1995. Evolution of salt-related structures in compressional settings, in: Jackson, M.P.A., Roberts, D.J., Snelson, S. (Eds.), *Salt tectonics: a global perspective*. AAPG Memoir Tulsa, Oklahoma, USA, 65, pp. 41 - 60
- Limonov, A. F., Woodside, J. M., Cita, M. B., Ivanov, M. K., 1996. The Mediterranean Ridge and related mud diapirism: a background. *Mar. Geol.*, 132, 7 - 19
- Loncke, L., Mascle, J., FANIL Scientific Party, 2004. Mud volcanoes, gas chimneys, pockmarks and mounds in the Nile deep-sea fan (Eastern Mediterranean): geological evidences. *Mar. Pet. Geol.*, 21, 669 - 689
- Makris, J., Ben-Avraham, Z., Behle, A., Ginzburg, A., Giese, P., Steinmetz, L. et al., 1983. Seismic reflection profiles between Cyprus and Israel and their interpretation. *Geophys. J. R. Astron. Soc.*, 75, 575 - 591.
- Makris, J. and Stobbe, C., 1984. Physical properties and state of the crust and upper mantle of the Eastern Mediterranean Sea deduced from geophysical data. *Mar. Geol.*, 55, 347 - 363
- Makris, J., Papoulia, J., Papanikolaou, D., Stavrakakis, G., 2001. Thinned continental crust below northern Evoikos Gulf, central Greece, detected from deep seismic soundings. *Tectonophysics*, 341, 225 - 236
- Mart, Y. & Ben-Gai, Y., 1982. Some depositional patterns at the continental margin of the Southeastern Mediterranean Sea. *AAPG Bulletin*, 66, 460 - 470
- Mart, Y., 1982, Quaternary tectonic patterns along the continental margin of the southeastern Mediterranean. *Mar. Geol.*, 1982, 327 - 344
- Mart, Y., 1984, The tectonic regime of the southeastern Mediterranean continental margin. *Mar. Geol.*, 55, 365 - 386
- Mart, Y., 1987. Superpositional tectonic patterns along the continental margin of the southeastern Mediterranean: a review. *Tectonophysics*, 140, 213 - 232
- Martin, R.G., 1978. Northern and eastern gulf of Mexico continental margin: Stratigraphic

- and structural framework. Framework, facies, and oil trapping characteristics of the upper continental margin. *American Association of Petroleum Geologists Studies in Geology*, 7, 21-42.
- Masclé, J., Benkhelil, J., Bellaïche, G., Zitter, T., Woodside, J., Loncke, L. and PRISMED II Scientific Party, 2000, Marine geologic evidence for a Levantine-Sinai plate, a new piece of the Mediterranean puzzle, *Geology*, 28, 779 - 782
- Meissner, R., 1986. *The continental crust*. Academic Press, Inc., Orlando
- Montadert, L., Letouzy, J., Mauffret, A., 1978. Messinian event: seismic evidence. *Init. Repts. DSDP*, 42 I. U.S. Govt. Printing Office, Washington D.C., pp. 1032 - 1050.
- Müller, R. D., Roest, W. R., Royer, J.-Y., Gahagan, L. M., Sclater, J. G., 1997. Digital isochrones of the world's ocean floor. *J. Geophys. Res.*, 102, 3211 - 3214
- Murton, B. J. and Biggs, J., 2003. Numerical modelling of mud volcanoes and their flows using constraints from the Gulf of Cadiz. *Mar. Geol.*, 195, 223 - 236
- Nafe, J. and Drake, C., 1963, Physical properties of marine sediments. In: Hill, M. N. (Ed), *The Sea Vol. 3*, Wiley, New York, pp. 794 - 815
- Neev, D. 1975. Tectonic evolution of the Middle East and the Levantine basin (easternmost Mediterranean). *Geology*, 3, 683 - 686.
- Neev, D. 1977. The Pelusium Line - a major transcontinental shear. *Tectonophysics*, 38, T1 - T8.
- Neev, D., Almagor, G., Arad, A., Ginzburg, A. & Hall, J.K., 1976. The geology of the Southeastern Mediterranean Sea. *Geological Survey of Israel Bulletin*, 68, 1 - 51.
- Netzeband, G. L., Gohl, K., Hübscher, C. P., Ben-Avraham, Z., Dehghani, G. A., Gajewski, D., Liersch, P. The Levantine Basin - crustal structure and origin, *accepted by Tectonophysics (January 2006)*
- Pätzold, J., Bohrmann, G., Hübscher, C., 2003. Black Sea - Mediterranean - Red Sea. METEOR-Berichte 03-2, Leitstelle METEOR
- Papazachos, B. C., Papaioannou, Ch. A., 1999. Lithospheric boundaries and plate motions in the Cyprus area. *Tectonophysics*, 308, 193 - 204
- Peirce, C. and Barton, P.J., 1992. Southern segment of the European Geotraverse - a wide-angle seismic refraction experiment in the Sardinia Channel. *Mar. Geophys. Res.*, 14, 227 - 248
- Pérez-Gussinyé, M., Ranero, C.R., Reston, T.J., Sawyer, D., 2003. Mechanisms of extension at nonvolcanic margins: Evidence from the Galicia interior basin, west of Iberia. *J. Geophys. Res.*, 108, 2245, doi:10.1029/2001JB000901
- Pollack, H.N., Hurter, S.J., Johnson, J.R., 1993. Heat flow from the Earth's interior:

- Analysis of the global data set. *Review of Geophysics*, 31, 267 – 280
- Polonia, A., Camerlenghi, A., Davey, F., Storti, F., 2002. Accretion, structural style and syn-contractional sedimentation in the Eastern Mediterranean Sea. *Mar. Geol.*, 186, 127 - 144
- Press, F. and Siever, R., 1986. *Earth*. W. H. Freeman and Company, New York.
- Réhault, J.P., Boillot, G. & Mauffret, A., 1984. The western Mediterranean Basin, geological evolution. *Mar. Geol.*, 55, 447 - 477
- dos Reis, A. T., Gorini, C., Mauffret, A., 2005. Implications of salt-sediment interactions on the architecture of the Gulf of Lions deep-water sedimentary systems - western mediterranean sea. *Mar. Pet. Geol.*, 22, 713 - 746
- Robertson, A. H. F. & Dixon, J. E., 1984, Introduction: Aspects of the geological evolution of the Eastern Mediterranean. In: Dixon, J. E., and Robertson, A. H. F. (Eds.), *Geological Evolution of the Eastern Mediterranean*. Geol. Soc. Spec. Publ. London, 17, 1 - 74,
- Robertson, A. H. F. 1998a. Mesozoic-Tertiary tectonic evolution of the easternmost Mediterranean area: Integration of marine and land evidence. In: Robertson, A.H.F., Emeis, K.-C., Richter, C., Camerlenghi, A. (eds.). *Proceedings of ODP, Science Results 160*, College Station, TX (Ocean Drilling Program), 723 - 782.
- Robertson, A. H. F., 1998b, Tectonic significance of the Eratosthenes Seamount: a continental fragment in the process of collision with a subduction zone in the eastern Mediterranean (Ocean Drilling Program Leg 160). *Tectonophysics*, 298, 63 - 82
- Rouchy, J.-M., Saint Martin, J.-P., 1992. Late Miocene events in the Mediterranean as recorded by carbonate-evaporite relations. *Geology*, 20, 629 - 632
- Ryan, B.W.F., Stanley, D.J., Hersey, J.B., Fahlquist, D.A. & Allan, T.D., 1970. The tectonics of the Mediterranean Sea, in: Maxwell, A.E. (Eds.), *The Sea*, Wiley, New York, 4 II, pp. 387 – 491
- Rybakov, M. and Segev, A., 2004. Top of the crystalline basement in the Levant. *Geochem. Geophys. Geosyst.*, 5, Q09001, doi:10.1029/2004GC000690
- Sandwell, D. T., Smith, W. H. F., 1997. Marine gravity anomaly from Geosat and ERS 1 satellite altimetry, *J. Geophys. Res.*, 102, 10039 – 10054
- Slater, J. G., Jaupart, C., Galson, D., 1980. The heat flow through oceanic and continental crust and the heat loss of the Earth. *Rev. Geophys.*, 18, 269 – 311
- Schattner U., Ben-Avraham Z., Lazar M. and Hübscher, C.. Tectonic isolation of the Levant basin offshore Galilee-Lebanon - Effects of the Dead Sea fault plate boundary

- on the Levant continental margin, eastern Mediterranean, submitted
- Schultz-Ela, D.D., Jackson, M.P.A. & Vendeville, B.C., 1993. Mechanics of active salt diapirism. *Tectonophysics*, 228, 275-312.
- Stampfli, G. M., Borel, G. D., 2002, A plate tectonic model for the Paleozoic and Mesozoic constrained by dynamic plate boundaries and restored synthetic ocean isochrons, *Earth and Planet. Sci. Lett.*, 196, 17 - 33
- Talwani, M., Worzel, L., Landisman, M., 1959. Rapid gravity computation for two dimensional bodies with application to the Mendocino submarine fracture zone. *J. Geophys. Res.*, 64, 49 - 59
- Tibor, G., Ben-Avraham, Z., Steckler, M. & Fligelmann, H., 1992. Late tertiary subsidence history of the southern Levant Margin, Eastern Mediterranean Sea, and its implications to the understanding of the Messinian Event. *Journal of Geophysical Research*, 97, 17593 - 17614.
- Tibor, G., Ben-Avraham, Z., 2005. Late Tertiary paleodepth reconstruction of the Levantine margin off Israel. *Mar. Geol.*, 221, 261 - 297
- Trusheim, F., 1957. Über Halokinese und ihre Bedeutung für die strukturelle Entwicklung Norddeutschlands. *Zeitschr. Deutsch. Geol. Ges.* 109, 111-151.
- Trusheim, F., 1960. Mechanism of salt migration in Northern Germany. *Am. Assoc. Petr. Geol. Bull.*, 44, 1519-1540.
- Vendeville, B.C. & Cobbold, P.R., 1987. Synsedimentary gravitational sliding and listric normal growth faults: insights from scaled physical models. *Comptes Rendus de l'Académie des Sciences de Paris*, 305 II, 1313-1319.
- Vendeville, B.C. & Jackson, M.P.A., 1992a. The rise of diapirs during thin-skinned extension. *Marine and Petroleum Geology*, 9, 331-353.
- Vendeville, B.C. & Jackson, M.P.A., 1992b. The fall of diapirs during thin-skinned extension. *Marine and Petroleum Geology*, 9, 354-371.
- Vidal, N., Alvarez-Marrón, J. & Klaeschen, D., 2000a. Internal configuration of the Levantine Basin from seismic reflection data (Eastern Mediterranean). *Earth and Planetary Science Letters*, 180, 77 - 89.
- Vidal, N., Klaeschen, D., Kopf, A., Docherty, C., Von Huene, R., Krasheninnikov, V. A., 2000b, Seismic images at the conergence zone from south of Cyprus to the Syrian coast, eastern Mediterranean. *Tectonophysics*, 329, 157 - 170
- Walley, C. D. 1998. Some outstanding issues in the geology of Lebanon and their importance in the tectonic evolution of the Levantine region. *Tectonophysics*, 298, 37 –

- Waltham, D., 1997. Why does salt start to move? *Tectonophysics*, 282, 117 – 128
- Warren, J., 1991. *Evaporites - their evolution and economics*. Blackwell Science.
- Weber, M., Abu-Ayyash, K., Abueladas, A., Agnon, A., Al-Amoush, H., Babeyko, A., Bartov, Y., Baumann, M., Ben-Avraham, Z., Bock, G., Bribach, J., El-Kelani, R., Förster, A., Förster, H.-J., Frieslander, U., Garfunkel, Z., Grunewald, S., Götze, H. J., Haak, V., Haberland, Ch., Hassouneh, M., Helwig, S., Hofstetter, A., Jäckel, K.-H., Kesten, D., Kind, R., Maercklin, N., Mechie, J., Mohsen, A., Neubauer, F. M., Oberhänsli, R., Qabbani, I., Ritter, O., Rümpler, G., Rybakov, M., Ryberg, T., Scherbaum, F., Schmidt, J., Schulze, A., Sobolev, S., Stiller, M., Thoss, H., Weckmann, U., Wylegalla, K., 2004, The crustal structure of the Dead Sea Transform. *Geophys. J. Int.*, 156, 655 - 681
- Wessel, P. and Smith, W., 1998. New, improved version of Generic Mapping Tools released, *EOS, Trans. Am. Geophys. Un.*, 79 (47), 579
- Woodside, J. M., 1977, Tectonics elements and crust of the Eastern Mediterranean Seamount. *Mar. Geophys. Res.*, 3, 317 – 354
- Worrel, D.M. & Snelson, S., 1989. Evolution of the northern Gulf of Mexico, with emphasis on Cenozoic growth faulting and the role of salt, in: Bally, A.W., Palmer, A.R. (Eds.), *The geology of North America - an overview*. Geological Society of America, Boulder, Colorado, USA, A, pp. 97-138.
- Wright, J. and Rothery, D., 2001. *The Ocean Basins: Their structure and evolution*. The Open University, Butterworth-Heinemann, Oxford
- Zelt, C. A., & Smith, R. B., 1992, Seismic traveltime inversion for 2-D crustal velocity structure. *Geophys. J. Int.*, 108, 16 - 34